POLITECNICO DI TORINO

SCUOLA DI DOTTORATO

Dottorato in Ingegneria Meccanica - XXIX ciclo

Tesi di Dottorato

One-dimensional Advanced Beam Models for Marine Structural Applications

Rehan Jamshed

Supervisor: Prof. Erasmo Carrera

Co-supervisor: Alfonso Pagani

August 2017

I would like to dedicate this thesis to my loving parents . . .

Acknowledgements

Foremost of all, I would like to thank my PhD supervisor Prof. Erasmo Carrera. It was him, who believed in my potential and gave me the opportunity to expand my vision and enabled me to pass through challenging stages of research. With his trust, support and guidance, I was able to carry out the research work no matter how difficult it turned out at any moment. Indeed, under his able leadership, the tough objectives were comprehensively achieved and for every success in the work, I am grateful to the Professor.

Dr. Alfonso Pagani, our senior MUL2 colleague, was the first one to welcome me at MUL2 Group. Despite his own committed time for his PhD, he very kindly addressed my issues and enabled me focus on the work. In technical as well as administrative matters, he was always there for my help. I am very much impressed by his teaching style and this proved instrumental in learning the background work. Another, important colleague whom I am thankful is Dr Enrico Zappino. Dr Zappino, was always available to me for discussing new issues. Often, the newly arising challenges in my work were comprehensively addressed after a discussion with him. Mr Stefano Valvano was another nice colleague from our group who always supported and encouraged me during all phases of my research. I am grateful to Mr. Costantino, Tomasso, Andrea, Waqar and other lab fellows for their support and refreshing company.

I would like to thank Politecnico di Torino and MIUR for providing me the scholarship for PhD. I thank Prof. Luiggi Garibaldi for his kind support as PhD Coordinator and addressing all the issues during the work. I especially want to thank Miss Maria Grazia, the department secretary, who provided every possible support.

Indeed, no person can perform in any way without the support of family. I am very much grateful to my wife Munazza Rehan who deserves all credits for supporting me during all phases of my work. She comforted me to her best despite being restless while looking after the whole house. I am thankful to my son Abdur Rehman whose smiling face would refresh me every evening for a new dawn. I am grateful to my brother Shamoon Jamshed who stayed with my parents and provided all support to

all of us. Most importantly, I wish to thank my parents, whose prayers and efforts enabled me avail the opportunity to study at such prestigious institute.

<div align="right">

Rehan Jamshed

August 2017

Torino

</div>

Abstract

At preliminary design stage, the global mechanical behavior of large marine vessels such as container ships has previously been analyzed idealizing them as a classical beam. These structures are complex and a classical beam idealization significantly compromises important structural behavior associated with cross section warping or in-plane displacements. On the other hand, 3D Finite Element (FE) models have been utilized which are accurate in capturing these details but pose high computational cost. In present work, structural analyses of marine vessels with realistic boundary conditions have been presented using well-known Carrera Unified Formulation (CUF). Using CUF, higher order theories can be implemented without the need of ad-hoc formulations. The finite element arrays are written in terms of fundamental nuclei for 1D beam elements that are independent of problem characteristics and the approximation order. Thus, refined models can be developed in an automatic manner. In the present work, the beam cross sections are discretized using elements with Lagrange polynomials and the FE model is regarded as Component-Wise (CW), allowing one to model complex 3D features, such as inclined hull walls, floors and girders in the form of components.

The work is mainly divided in two parts: Hull in vacuo (in absence of water) and Hull with Hydrostatic Stiffness (in presence of water). The former involves static and dynamic structural analyses of hulls with realistic geometries without the effect of water. The later involves static and dynamic analyses of realistic hull geometries that are supported by buoyancy springs. The stiffness of buoyancy springs is made part of the fundamental nuclei and the corresponding FEM matrices for hydrostatic and hydrodynamic loads are obtained. The hydrodynamic loads have been considered in the form of Radiation Wave loads which include damping and added mass effects. Utilization of Component-Wise (CW) model under hydrodynamic loads has afforded an ease in modelling the complex geometrical configurations such as realistic boat shapes and the dynamic response analyses of aircraft carrier due to moving aircraft. All the analyses have been validated with published literature and their computational efficacy is established through their comparison with the results from commercial code.

Contents

I Numerical Results
Hull in Vacuo   29

II Numerical Results
Hull under Hydrostatic and Hydrodynamic Loads   67

List of Figures

List of Tables

Chapter 1

Introduction

1.1 Global Structural Analysis of Ships

Today's ships are large and structurally quite complex than the earlier designs. Many ships such as container ships resemble like beam and it is mainly because of this reason that their global structural response has preferably been modeled as beams at preliminary design stage since long time. Famous classical beam models such as Euler [31] and Timoshenko [89, 90] models have been considerably used for this purpose with the ships's longitudinal dimension considered as beam length. Being simple and suitable for faster computations, these models afford results with inherent simplifying assumptions which limits their scope to demonstrate their robustness in all general scenarios. Such assumptions either result in increased factor of safety thereby resulting in an inefficient and heavy design or the analyst is required to employ ad-hoc relations to capture the detailed kinematics of the global response that classical model alone could not capture. Owing to the particular geometrical form of a ship or a marine vessel in general it may, for instance, exhibit coupling between the bending and torsion and no single classical beam model can capture this behaviour without warranting ad-hoc kinematical relationships.

Together with the ships, numerical methods such as Finite Element Method (FEM) have witnessed considerable advancement owing to the enhanced computational capability of modern computers. Analysts employ 2D shell or 3D solid finite elements from commercial codes that provide fairly accurate results as well as capture all realistic warpage of geometrically complex structure. However, these 2D/3D finite elements often require high computational time and cost which renders their use at preliminary design stage unfeasible.

Figure 1.1 A container ship failure under global loads

Because of the limitation of employing geometrical details at a preliminary design stage, the analysts often rely on earlier designs with similar service profile and loading conditions. This practice does not offer the most optimum structural configuration at preliminary design stage. Catastrophic failures such as shown in Fig.1.1 can be avoided if the global structural behaviour is adequately analysed for which beam models are most suitable. Typical global deformable modes such as "sagging" or "hogging" (shown in Fig.1.2) are satisfactorily captured through the use of classical beam models but in reality ship may be subjected to diverse variety of loads. It may encounter waves at an angle to its longitudinal axis resulting in distributed torsional loads (See Fig.1.3). Since mostly ships have "U" shaped or channel cross section, they have shear center below the keel. Such applied loads result in significant coupling in bending and torsion and the beam cross sections and lateral faces undergo warping. Given the assumptions in classical models, additional kinematical equations are needed to demonstrate the said coupling or warping.
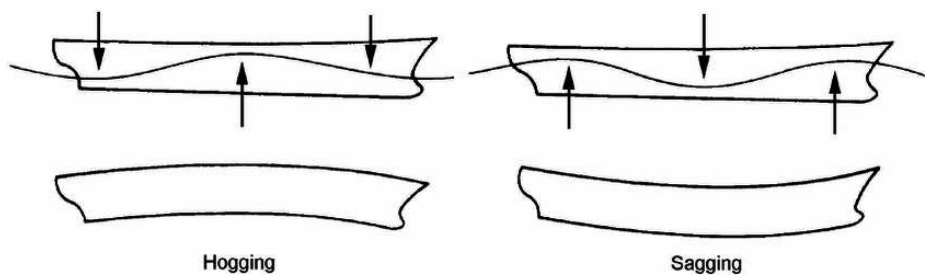
Figure 1.2 Ship under possible global bending modes
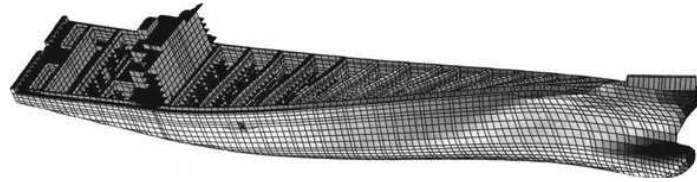
Figure 1.3 Ship under torsional deformation [81]

1.1.1   Some Terminologies for Ships

For the subsequent discussion, various terminologies associated with a typical ship for its geometry and to model its global structural behaviour are considered in the following. Fig.1.4 shows a simplified illustration of important length dimensions of a ship. The overall length is termed as L_{OA} which is between two extreme longitudinal ends of the ship. Length L_{WL} refers to the length of ship measured at water-line and L_{PP} is length between two vertical lines called *Perpendiculars*. The Forward Perpendicular (FP) can be the same as start of L_{WL} whereas the Aft Perpendicular (AP) is usually the rudder axis. The forward part of the ship is called *Bow* and the rear as *Stern*. The upper horizontal surface is called *Deck* and the bottom mid line parallel to ship axis is *Keel*. Ship moving in forward direction while looking from the rear, the right side is called as *starboard* and the left side as *port*.
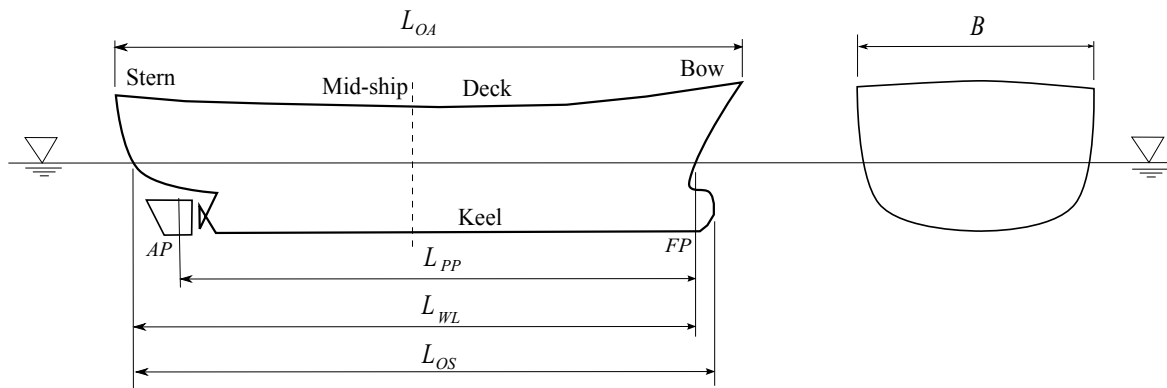
Figure 1.4 Length dimensions in a ship

1.1.2   Ship Motions

Rigid Body Motions

Consider a ship moving in a global cartesian coordinate system as shown in Fig.1.5. The ship length is along y-axis and the z-axis points upwards. A temporary rotation of

ship around $y-$axis is called *Heel* which can be result of temporary external loads such as wind, centrifugal loads or waves. If such rotation is caused by weight distribution of cargo or structure then it is called *List*. Considering the rotation around $x-$axis, a temporary or dynamic rotation is called *Pitch* whereas the one caused by weight distribution is termed as *Trim*. The linear motions along the three global axes x, y and z axes are termed as surge, sway and yaw respectively.
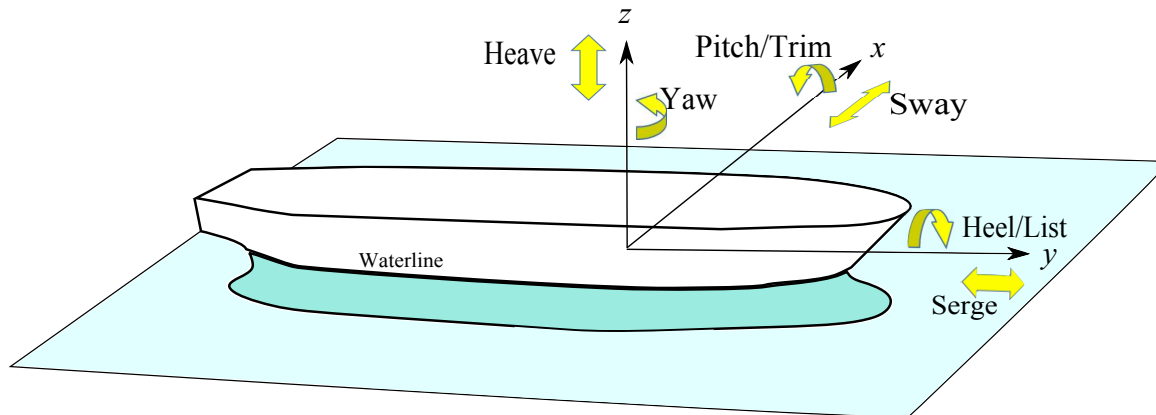
Figure 1.5 Rigid body motions of a ship

Flexible Response

A few global deformation modes of a ship are as follows:

Hogging and sagging

In hogging, the ship bends in a vertical plane in a way that middle region is pushed upwards and the ends are lowered. This situation can arise momentarily or permanently depending the loading on the hull girder. The weight distribution will always bend the structure downwards whereas the buoyancy will resort to push it upwards. This is shown in left sketch in Fig.1.2. Most often, hogging is due to the waves with crest in the middle of the ship. The increased submerged portion increases the buoyancy force and resultantly the middle region is pushed upwards. Sagging is the opposite of hogging where the middle region is pushed downward (Fig.1.2 right). Sagging can be observed even in still water when the weight distribution alone can cause the ship to bend downward in the middle.

Torsion

A ship is subjected to torsion when it encounters loads that are not symmetric about longitudinal vertical plane of symmetry. A ship travelling at an oblique angle to the waves is subjected to such loadings. Since most ships do not have circular cross section, they often develop warping under torsional loads. In fact, the container ships experience high degree of warping compared to others as their "U" shaped or channel shaped cross section offers least resistance to warping.

Racking

A particular mode of deformation occurs is when the forces on the hull tend to distort it in a transverse manner (See Fig.1.6). The transverse section appears to undergo skewing. Racking is more pronounced in container ships owing to their open hatch configuration. The phenomenon is felt greatest when the ship is light or under ballast condition. The transverse bulkheads at reasonable spacing on the side walls resist such loads in collaboration with side walls and strong knees. Ribs joining horizontal bottom and vertical walls resist the bending moments at corner but they interfere with the cargo space.
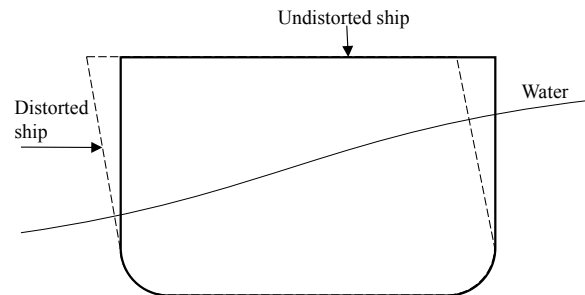
Figure 1.6 Racking

1.2 Literature Review

1.2.1 Beam Models for Ships

Ultimate Hull Girder Strength

In most early works the ships were idealised as Hull Girder owing to their box-like thin-walled section. This idealization often employs famous Euler-Bernouli Beam Model (EBBM) [31]. The EBBM model assumes that in bending, plane cross sections remain

plane as well as perpendicular to the beam axis. This assumption is valid for long beams with simple, solid and homogeneous cross sections. The flexural stress in deck and bottom plating have been predict using EBBM however this model cannot predict the transverse shear stress which is important for side walls of a ship. The Timoshenko Beam Model (TBM) [89, 90] considers the shear effect in addition to bending by allowing beam cross section to rotate about neutral axis. The shear contribution is more pronounced in bending of short beams. An assumption in TBM is constant shear strain distribution over the cross section resulting in non-zero transverse shear stress at the top and bottom beam edges whereas it should be zero. Shear correction factors have been introduced in early works and advanced beam models have overcome this problem.

Hull girder strength has long been considered the most important aspect in ship building and simple beam idealization has greatly facilitated the designers. According to Timoshenko[88], famous British scientist named Thomas Young (*Young's Modulus* named after him) considered ships as beams. In seemingly the earliest attempt of its kind, the curves of weight and buoyancy distribution were obtained whose difference was the load distribution curve applied over the beam length. The stresses thus obtained were experimentally verified.

Ship designers have validated their beam models through experimenting actual or scaled models by subjecting them to bending loads. Rutherford reported in [78] that Sir Isamberd Brunel, in 1850s applied Beam Theory to calculate the flexural stress in the deck and the bottom plating for his ship design which was twice the size of any ship at that time. In a paper by John [95], he considered the ship as a beam and obtained the plate thickness comparing normal stresses with the ultimate strength of the material.

It was not until the failure of "HMS Cobra" in September, 1900 that compressive buckling was considered more important than the tensile failure under bending (sagging or hogging). It was reported by Kell in [67] and [68] that two destroyers "Preston" "Bruce" were tested under sagging and hogging conditions respectively and final collapse was initiated through the buckling of the hull girder in deck or bottom plating. Buckling was followed by overall collapse of the hull girder. During and after the period of World War II, many of the ship failures were investigated with consideration of hull girder strength (See Vasta [44]). In 1949/1950, a collapse of hull girder through buckling of bottom plating was observed while simulating hogging of a destroyer "Albuera" as reported by Lang in [56].

Later literature gives several methodologies to predict progressive failure of metallic hull girders such as Caldwell [45] and Smith [28]. Use of FEM to simulate progressive collapse was first demonstrated in 1983 by ABS group [62]. FEM codes based on Explicit dynamic solver such as LSDYNA [2] have been used to simulate hull girder progressive failure. Most accurate FEM results are obtained by employing 3D solid finite elements. Wall thicknesses being much smaller than the overall ship dimensions ultimately results in a heavy mesh. The need for large computational resources is obvious for such FEM models to analyse complete ship models and is often not justified in the preliminary design stage.

Cross Section Warping

Many ships such as container ships have large hatch opening resulting in mid-ship sections to resemble "U" or channel shape. Since the centroids and shear centers of such sections do not coincide, there exists strong coupling between their horizontal bending and torsion behaviour. This also manifests in the form of out-of-plane warping of cross section under torsional loads. The first solutions to the bending-torsion coupling problem using FEM for ships was proposed by Kawai [86]. Kawai proposed a simplified finite element analysis of a ship structure based on modern beam theory taking into account the coupling of horizontal bending and torsion and cross section warping. In his paper, St. Venant's warping due to torsion was discussed as well as the effect of transverse bulkheads was incorporated in the analysis. Restrained warping has been addressed using Vlasov's thin-walled beam theory in Vlasov [49]. In restrained warping, warping is prevented locally as opposed to St.Venant's free warping. The stresses in the cross section are thus the St. Venant's shear and axial and shear stresses due to restrained warping.

Considerable literature, such as Gunnlaugsson [37], Senjanović [41], Bishop [5], Pedersen [71] and [72], Wu [96], Pittaluga [73] deal with the coupled horizontal bending-torsion response under dynamic conditions such as wave loads. For ships with large hacth openings, Senjanović and his co-workes have implemented advanced theories in beam girder idealization in several papers (See Senjanović [40, 80, 99, 43, 42, 79]). This thesis includes discussion on warping of container ships which was also published in [69].

Advanced Beam Models

The 1D beam models used in early studies of global ship models were based on classical theories by Euler-Bernouli (EBBBM) and Timoshenko (TBM). EBBM did not take in

account the transverse shear whereas TBM assumed a constant shear strain over the cross section. The out-of-plane warping and in-plane deformations of arbitrary cross sections are significant deformations which cannot be captured by these classical models. Well known book by Novozhilov [66] gives many examples to overcome limitations of classical models. Kapania and Raciti [51] and [52] are few of the best reviews on the advanced beam models. Since the problem of warping is pronounced for open section and thin-walled beams, the advanced beam models presented originally for aerospace or other structures are equally well suited for ship structures modelled as beams. The refined beam theories presented over the last century have primarily addressed the issues such as shear correction factor and cross section warping.

An improved shear correction factor for 1D beams has been focus of early investigations in works by Timoshenko and Goodier [91], Sokolnikoff [83], Stephen [84], Hutchinson [39], and much recent work by Nguyen et al. [65]. Nevertheless, the difficulty remains in arriving at a definite solution for shear factor as reported by a review paper by Kaneko [50] and a paper by Dong et al. [30]. Jensen [46] draws a conclusion that very accurate natural frequencies can be achieved if consistent formulation for the shear coefficient, as proposed by Cowper [27] or Stephen [84], is used in the Timoshenko beam model, even for wavelengths of the size of the transverse dimension of the ship hull.

Improvement in displacement kinematics across beam cross-section was introduced by El Fatmi [34] and [33] by introducing non-uniform warping function. This and many other advanced beam models addressing the issue of warping are based on de Saint-Venant solution. In addition to bending-torsion coupling, cross-section warping has been discussed using advanced beam models by ships idealised as thin-walled open/closed section beams by Senjanović in literature cited above.

1.2.2   State-of-the-Art, CUF

This thesis demonstrates the use of 1D beam finite elements based on CUF to model structural response of marine vessels under the buoyancy as boundary condition. CUF provides an automatic procedure to implement any order of cross section refinement for FE beam model. The formulation thus obtained has the cross section and beam discretizations mutually independent. This way, beam geometries with any aspect ratio can be modeled giving structural response close to that of 3D solid elements from a commercial FE code, yet requiring relatively much less DOFs compared to 3D FE models.

CUF was initially demonstrated in the area of structural mechanics for the development of refined plate plate and shell theories [7, 8]. The 1D CUF beam models were then utilized for the study of isotropic, solid and thin-walled sections in [10, 11]. These works employed Taylor polynomials to model cross-sectional displacement field. The adoption of higher order expansion functions led to the accuracy of 3D solid finite elements yet at a much less computational cost [36]. Cross section displacement was modelled with a new class of polynomials, the Lagrange polynomials in [20]. These models had pure displacements as the only unknowns. With Lagrange models, it was easy to involve geometric discontinuities and the local boundary conditions through localised mesh refinement. The free vibration of isotropic structures by Carrera et al. [22] were analysed using CUF where mode shapes with transverse distortions were effectively captured.

1D CUF models have also been used for the investigation of composite structures by Catapano et al. [24] and Carrera and Petrolo [21]. The former employed Taylor expansion functions while latter utilised Lagrange functions for the cross section refinement. The work demonstrated the enhanced capability of 1D CUF models in capturing the 3D stress field requiring much less DOFs.

Recently, the works in [14] and [15] comprehensively demonstrated use of refined 1D beam models based on CUF [12],[9] for structural analysis of marine vessels of complex solid-like 3D geometry.

1.2.3   The Component-Wise (CW) Models

Recently, the CUF has been extended to an approach namely the *Component-Wise* (CW) models [19]. In CW approach, various structural features such as walls, floors or bulkheads of a complex structure may be considered as components (hence the name Component-Wise). Each component is a beam with its own cross section and a length arbitrarily oriented in a 3D global reference system. The approach is effectively modelled employing Lagrange elements in cross sections. Since the CW models are based on CUF, the beam shape-functions and the cross section expansion functions remain uncoupled, allowing the modelling of beams with very large cross section and very small beam length. The interface edges of the components have physical nodes which can be connected by imposing continuity of displacement.

The use of CW has been widely demonstrated for the analysis of aircraft structures where individual structural members (e.g. skin, stringer and longerons) are modelled through 1D CUF. The CW models where employed to carry out the static and vibration analysis of complex aerospace structures by Carrera et al. [16], [17]. These

papers demonstrated that CW models allow actual geometries of different components be connected at common physical nodes and thus no fictitious links are required to connect DOFs of 1D, 2D or 3D components. The CW models were also successfully applied to civil structures by Carrera et al [13] and [18]. In these papers, the industrial and civil structures were analysed.

1.2.4 Beams on Buoyancy Springs

Presently available classical beam models EBBM and TBM and refined beam models can include the effect of buoyancy in the form of employing *winkler founation* (See Hetenyi [38]) but their scope is limited to the few available Degrees of Freedom (DOFs) they offer. These models cannot capture a general 3D warpage of cross section in addition to the gross displacements of the floating structure. Hence, employing 3D solid Finite Elements (FE) remains as next available possibility to capture detailed 3D kinematics but solid FE models are computationally expensive and cannot be employed for preliminary analyses. Ship hulls were modeled as beams in classic works by Bishop and Price [74–76] whereby 2D hydroelasticity theories were developed to model the behaviour of ship hull and the surrounding fluid. These and many early works employed Euler-Bernoulli or Timoshenko beam models to represent ship.

The effect of buoyancy on floating structures is often modeled by elastic foundation. Emil Winkler [55] in 19th century modeled for the first time the beams on elastic foundation. Hetenyi [38] employed winkler model to develop closed form solutions for various cases of beams on elastic foundations which is considered as a series of disconnected springs. Kennard([54]) and Todd [92]) analysed the ship vibrations by considering ship as beam on springs and dampers. Considerable literature deals with general structures supported on elastic foundation. These structures include Very Large Floating Structures (VLFS) such as ice-sheets [60] and floating beams [26] and plates [53] and [87] and jack-up rigs [25] and barges [57] for moving loads and collision problems. Not much literature is seen so far dealing with global structural analysis of ships modelled as beams with buoyancy as boundary condition. Jensen [47] models ship as a rigid body while analysing the effect of hydrostatic forces on ship hull. The vibration problem of hull girder is explained with simply supported boundary conditions. This and works of Shama [81] and Senjenovic [80, 99] involve torsional analysis of container ship with closed ends providing boundary conditions for the analysis. Use of Finite Element Method (FEM) has allowed buoyancy to be modelled as 1D springs attached to the wetted surface [1]. Wu and Sheu [97] have considered ship as a rigid body floating over distributed springs and dampers in their analysis of moving loads on

ships. Jong-Shyong [98] employed uniformly distributed springs to simulate buoyancy for the analysis of floating barge with moving loads. Zhang [101] analysed dynamic behaviour of floating bridges with buoyancy springs as the elastic support. Jer-Fang [48] have considered ship supported on buoyancy springs while analyzing vibration. Getter [70] have analysed hurricane induced barge impact on flood walls with springs attached to the Finite Element model to simulate buoyancy. Recently, the works in [14] and [15] comprehensively demonstrated use of refined 1D beam models based on well-known Carrera Unified Formulation (CUF) [12],[9] for structural analysis of marine vessels of complex solid-like 3D geometry.

Chapter 2

Carrera Unified Formulation

Over the years attempts have been made to address the inconsistencies of classical beam models in capturing the higher-order phenomena such as the bending-shear coupling and restrained warping under torsion. In literature, much focus has remained on Euler-Bernouli and Timoshenko beam models. This chapter introduces the novel approach namely Carrera Unified Formulation (CUF) which unifies the displacement kinematics in compact form. Classical beam theories become special cases through this generic approach which can be automatically extended to any degree of enhancement to include all kind of higher order kinematics.

2.1 Preliminaries

With reference to the coordinate system shown in Fig.2.1, consider a beam of length l which is aligned to global y axis and the cross section area is Ω parallel to xz-plane. Introducing the displacement vector $\mathbf{u}$ as function of global coordinates x, y, z and time t as follows:

$$\mathbf{u}\left(x, y, z; t\right) = \left\{ u_x \quad u_y \quad u_z \right\}^T \tag{2.1}$$

where the superscript T is for transpose of the vector. Similarly, the stress $\boldsymbol{\sigma}$ and strain $\boldsymbol{\epsilon}$ vectors can be written as follows:

$$
\begin{aligned}
\boldsymbol{\sigma} &= \left\{ \sigma_{yy} \quad \sigma_{xx} \quad \sigma_{zz} \quad \sigma_{xz} \quad \sigma_{yz} \quad \sigma_{xy} \right\}^T \\
\boldsymbol{\epsilon} &= \left\{ \epsilon_{yy} \quad \epsilon_{xx} \quad \epsilon_{zz} \quad \epsilon_{xz} \quad \epsilon_{yz} \quad \epsilon_{xy} \right\}^T
\end{aligned}
\tag{2.2}
$$
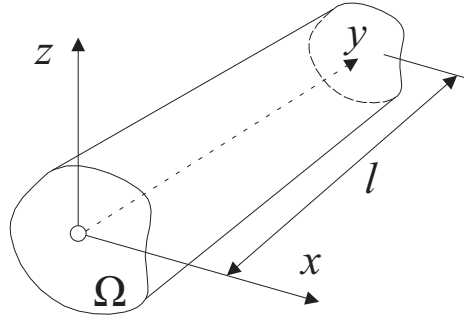
Figure 2.1 Beam aligned with cartesian coordinates

Assuming linear strain-displacement relation for small displacements, strain ϵ is given as:

$$\boldsymbol{\epsilon} = \mathbf{Du} \tag{2.3}$$

where $\mathbf{D}$ is the linear differential operator on $\mathbf{u}$ and it is given as follows:

$$\mathbf{D} = \begin{bmatrix} 0 & \dfrac{\partial}{\partial y} & 0 \\[2mm] \dfrac{\partial}{\partial x} & 0 & 0 \\[2mm] 0 & 0 & \dfrac{\partial}{\partial z} \\[2mm] \dfrac{\partial}{\partial z} & 0 & \dfrac{\partial}{\partial x} \\[2mm] 0 & \dfrac{\partial}{\partial z} & \dfrac{\partial}{\partial y} \\[2mm] \dfrac{\partial}{\partial y} & \dfrac{\partial}{\partial x} & 0 \end{bmatrix} \tag{2.4}$$

The stresses and strains are related through Hook's law as Eq. 2.5:

$$\boldsymbol{\sigma} = C\boldsymbol{\epsilon} \tag{2.5}$$

where C is the stiffness matrix comprising of following terms for an isotropic material:

$$
\begin{bmatrix}
C_{33} & C_{23} & C_{13} & 0 & 0 & 0 \\
C_{23} & C_{22} & C_{12} & 0 & 0 & 0 \\
C_{13} & C_{12} & C_{11} & 0 & 0 & 0 \\
0 & 0 & 0 & C_{44} & 0 & 0 \\
0 & 0 & 0 & 0 & C_{55} & 0 \\
0 & 0 & 0 & 0 & 0 & C_{66}
\end{bmatrix}
\tag{2.6}
$$

where

$$
\begin{aligned}
C_{11} &= C_{22} = C_{33} = \frac{(1-\nu)E}{(1+\nu)(1-2\nu)} = \lambda + 2\mu \\
C_{12} &= C_{13} = C_{23} = \frac{\nu E}{(1+\nu)(1-2\nu)} = \lambda \\
C_{44} &= C_{55} = C_{66} = \frac{E}{2(1+\nu)} = G
\end{aligned}
\tag{2.7}
$$

and λ and μ are the Lamé's parameters and ν, E and G are respectively the poisson's ratio, young's modulus and the shear modulus for the material.

For generally orthotropic composite materials with fiber orientation angle θ, the stiffness matrix becomes as follows:

$$
\begin{bmatrix}
\tilde{C}_{33} & \tilde{C}_{23} & \tilde{C}_{13} & 0 & 0 & \tilde{C}_{36} \\
\tilde{C}_{23} & \tilde{C}_{22} & \tilde{C}_{12} & 0 & 0 & \tilde{C}_{26} \\
\tilde{C}_{13} & \tilde{C}_{12} & \tilde{C}_{11} & 0 & 0 & \tilde{C}_{16} \\
0 & 0 & 0 & \tilde{C}_{44} & \tilde{C}_{45} & 0 \\
0 & 0 & 0 & \tilde{C}_{45} & \tilde{C}_{55} & 0 \\
\tilde{C}_{36} & \tilde{C}_{26} & \tilde{C}_{16} & 0 & 0 & \tilde{C}_{66}
\end{bmatrix}
\tag{2.8}
$$

where the terms of the stiffness matrix can be found in many books for example Reddy [77].

2.1.1 1D Variable Kinematic Modelling

Present 1D finite element formulation is derived in the framework of Carrera Unified Formulation (CUF). According to CUF, the displacement field **u** over the cross section

is assumed to have certain class of expansion function F_τ while along the length it is in terms of interpolation functions, N_i which are function of y-axis. Reader is referred to the book by Carrera [12] for comprehensive detail on the expansion functions and Bathe [3] for the details of the interpolation functions N_i. Referring to Fig. 2.1, the three dimensional displacement field $\mathbf{u}$ can be defined in terms of functions F_τ and nodal displacements $\mathbf{u}_\tau$ as:

$$\mathbf{u}(x, y, z) = F_\tau(x, z)\mathbf{u}_\tau(y), \qquad \tau = 1, 2, ..., M \tag{2.9}$$

where F_τ are the generic expansion functions to approximate displacements in terms of coordinates x and z over the cross-section. M is the number of expansion terms in F_τ. $\mathbf{u}_\tau$ is the vector of the generalized displacements, and the repeated subscript, τ , indicates summation following the Einstein notation. In general, Eq.2.9 represents an axiomatic model to for the three dimensional behaviour of a structure. The order of expansion function allows one to freely increase the accuracy of displacement kinematics surpassing the limits of classical beam theories.

The cross section expansion function can be approximated through different classes of polynomials. In this thesis, Lagrange Expansion (LE) polynomials [13] have been used represented as F_τ. Using LE it was possible to use pure displacements as degrees of freedom for the nodes over beam cross section. The beam cross section can be meshed using 3 noded (L3), 4 noded (L4) or 9 noded (L9) Lagrange elements. An L9 element, for example, has the interpolation function as given in Eq.A.1:

$$F_\tau = \frac{1}{4}(\alpha^2 + \alpha\alpha_\tau)(\beta^2 + \beta\beta_\tau), \qquad\qquad \tau = 1, 3, 5, 7$$

$$F_\tau = \frac{1}{2}\beta_\tau{}^2(\beta^2 + \beta\beta_\tau)(1 - \alpha^2) + \frac{1}{2}\alpha_\tau{}^2(\alpha^2 + \alpha\alpha_\tau)(1 - \beta^2), \quad \tau = 2, 4, 6, 8 \qquad (2.10)$$

$$F_\tau = (1 - \alpha^2)(1 - \beta^2), \qquad\qquad \tau = 9$$

where α and β range from -1 to +1, whereas α_τ and β_τ are the coordinates of the nine points whose numbering and location in the natural coordinate frame are shown in Fig.A.2. The 3D displacement field of the beam model based on L9 polynomial is

Figure 2.2 L9 element in natural coordinates

given as:

$$u_x = F_1 u_{x_1} + F_2 u_{x_2} + F_3 u_{x_3} + F_4 u_{x_4} + F_5 u_{x_5} + F_6 u_{x_6} + F_7 u_{x_7} + F_8 u_{x_8} + F_9 u_{x_9}$$
$$u_y = F_1 u_{y_1} + F_2 u_{y_2} + F_3 u_{y_3} + F_4 u_{y_4} + F_5 u_{y_5} + F_6 u_{y_6} + F_7 u_{y_7} + F_8 u_{y_8} + F_9 u_{y_9}$$
$$u_z = F_1 u_{z_1} + F_2 u_{z_2} + F_3 u_{z_3} + F_4 u_{z_4} + F_5 u_{z_5} + F_6 u_{z_6} + F_7 u_{z_7} + F_8 u_{z_8} + F_9 u_{z_9}$$

$$(2.11)$$

Chapter 3

Finite Element Method

The Carrera Unified Formulation was introduced in previous chapter to model the displacement kinematics associated with a 1D beam problem. In this chapter, the weak form of the same problem will be presented as a weighted integral equation and governing equations are formed employing principle of virtual displacement. The Finite Element Method (FEM) is then used to solve these equations.

In the Finite Element formulation, the CUF generalized displacements $\mathbf{u}_\tau(y)$ from Eq.2.9 can be expressed as a weighted linear combination of arbitrary interpolation functions namely the shape functions represented as N_i; i.e.

$$\mathbf{u}_\tau(y) = N_i(y)\mathbf{q}_{\tau i}, \qquad i = 1, 2, ..., p + 1 \tag{3.1}$$

where i is the number of nodes of a beam element of the order p. The Eq.2.9 for displacements can now be written in terms of cross section functions $F_\tau(x, z)$ and length-wise interpolation functions N_i as:

$$\mathbf{u}(x, y, z) = F_\tau(x, z)N_i(y)\mathbf{q}_{\tau i}, \qquad i = 1, 2, ...p + 1; \quad \tau = 1, 2, ..., M \tag{3.2}$$

where $\mathbf{q}_{\tau i}$ is the vector consisting of generalized nodal unknowns:

$$\mathbf{q}_{\tau i} = \left\{ \begin{array}{ccc} q_{x_{\tau i}} & q_{y_{\tau i}} & q_{z_{\tau i}} \end{array} \right\}^T \tag{3.3}$$

The interpolation functions,F_τ, chosen to discretize the cross-section and the shape function N_i to discretize the beam are independent of each other.

In this thesis, 1D Lagrange Elements have been used as shape functions to approximate displacement variation along the length. These functions can be 2-noded

linear (p=1), 3-noded quadratic (p=2) and 4-noded cubic (p=3) and are given in many books on FEM such as [3]. For the sake of completeness, they are being reported here.

Two-noded B2 Beam Element:

$$N_1 = \tfrac{1}{2}(1-r), \quad N_2 = \tfrac{1}{2}(1+r), \qquad \begin{cases} r_1 = +1 \\ r_2 = -1 \end{cases} \quad (3.4)$$

Three-noded B3 Beam Element:

$$N_1 = \tfrac{1}{2}r(1-r), \quad N_2 = \tfrac{1}{2}r(1+r), \quad N_3 = -(1+r)(1-r), \quad \begin{cases} r_1 = +1 \\ r_2 = -1 \\ r_3 = 0 \end{cases} \quad (3.5)$$

Four-noded B4 Beam Element:

$$\begin{aligned} N_1 &= -\tfrac{9}{16}(r+\tfrac{1}{3})(r-\tfrac{1}{3})(r-1), \quad N_2 = +\tfrac{9}{16}(r+\tfrac{1}{3})(r-\tfrac{1}{3})(r+1), \\ N_3 &= +\tfrac{27}{16}(r+1)(r-\tfrac{1}{3})(r-1), \quad N_4 = -\tfrac{27}{16}(r+1)(r+\tfrac{1}{3})(r-1), \end{aligned} \quad \begin{cases} r_1 = -1 \\ r_2 = +1 \\ r_3 = -\tfrac{1}{3} \\ r_4 = +\tfrac{1}{3} \end{cases}$$
$$(3.6)$$

All the aforementioned shape functions are written in terms of natural coordinate r which ranges between -1 and +1 and r_i is the coordinate of the ith node along the natural coordinate r.

3.1   Static Structural Analysis

The principal of virtual work can be employed to obtain FEM equations for structural analyses. In case of static analysis, the virtual work done by the internal strain energy L_{int} is equal to the work done by external loads L_{ext} as follows:

$$\delta L_{\text{int}} = \delta L_{\text{ext}} \quad (3.7)$$

The virtual variation of strain energy is given as follows:

$$\delta L_{\text{int}} = \delta \mathbf{q}^{\text{T}} \mathbf{K} \mathbf{q} \quad (3.8)$$

where $\delta\mathbf{q}$ is the vector containing generalized nodal unknowns and $\mathbf{K}$ is the global stiffness matrix in the assembled form. The derivation of the matrix $\mathbf{K}$ is briefly discussed later in this chapter. The virtual variation of the external work done on the structure is given as follows:

$$\delta L_{\text{ext}} = \delta\mathbf{u}^T\mathbf{P} \tag{3.9}$$

where $\mathbf{P}$ is the vector of global generalized forces acting on the structure and is discussed in Sec.3.7. Substituting Eqs.3.8 and 3.9 in Eq.3.7 we obtain the algebraic equation for static analysis as follows:

$$\mathbf{K}\mathbf{q} = \mathbf{P} \tag{3.10}$$

3.2 Free Vibration Analysis

The free vibration problem is analysed by considering equilibrium between elastic and inertial forces. Employing principle of virtual displacement for this problem, the work done by internal strain energy and the inertia are related through the following equation:

$$\delta L_{\text{int}} = -\delta L_{\text{ine}} \tag{3.11}$$

The FEM approximation for the virtual variation of work of inertial forces is written as follows:

$$\delta L_{\text{ine}} = \delta\mathbf{q}^{\mathrm{T}}\mathbf{M}\ddot{\mathbf{q}} \tag{3.12}$$

where $\mathbf{M}$ is the global assembled mass matrix and $\ddot{\mathbf{q}}$ is the global vector of nodal generalized accelerations. Substituting Eqs.3.12 and 3.8 in 3.11, we get the equation of motion for the free vibration problem as follows:

$$\mathbf{K}\mathbf{q} + \mathbf{M}\ddot{\mathbf{q}} = 0 \tag{3.13}$$

Assuming a the solution $\mathbf{q}$ to be harmonic in time with amplitude $\mathbf{Q}$ and the angular frequency ω, the Eq.3.13 reduces to an eigenvalue problem as follows:

$$(\mathbf{K} - \omega^2\mathbf{M})\mathbf{Q}e^{i\omega t} = 0; \tag{3.14}$$

3.3 Dynamic Response Analysis

As a more general case, the works of internal strain energy, inertia and external forces are considered and their virtual variations are related as follows:

$$\delta L_{\text{int}} = \delta L_{\text{ext}} - \delta L_{\text{ine}} \tag{3.15}$$

for which the FEM form is as follows:

$$\mathbf{Kq} + \mathbf{M\ddot{q}} = \mathbf{P} \tag{3.16}$$

This equation is solved for variation of $\mathbf{q}$ in time domain using a suitable numerical technique.

3.4 Stiffness Matrix

The work done by the internal strain energy can be written as:

$$\delta L_{\text{int}} = \int_V \delta\boldsymbol{\epsilon}^T \boldsymbol{\sigma} \mathrm{d}V \tag{3.17}$$

where L_{int} stands for the *internal* strain energy and δ stands for the virtual variation. The Eq. 3.17 can be re-written using Eqs.2.3, 2.5 and 3.2 as follows:

$$\delta L_{\text{int}} = \delta\mathbf{q}_{\tau i}^T \mathbf{K}^{ij\tau s} \mathbf{q}_{sj} \tag{3.18}$$

where $\mathbf{K}^{ij\tau s}$ represents the stiffness matrix in compact form termed as *Fundamental Nucleus* (FN). The FN of the stiffness matrix comprises of nine components mentioned as follows:

$$
\begin{aligned}
K_{11}^{ij\tau s} &= (\lambda+2G)\int_\Omega F_{\tau,x}F_{s,x}\mathrm{d}\Omega\int_l N_iN_j\mathrm{d}y + G\int_\Omega F_{\tau,z}F_{s,z}\mathrm{d}\Omega\int_l N_iN_j\mathrm{d}y + \\
&\quad G\int_\Omega F_\tau F_s\mathrm{d}\Omega\int_l N_{i,y}N_{j,y}\mathrm{d}y
\end{aligned}
$$

$$
K_{12}^{ij\tau s} = \lambda\int_\Omega F_{\tau,x}F_s\mathrm{d}\Omega\int_l N_iN_{j,y}\mathrm{d}y + G\int_\Omega F_\tau F_{s,x}\mathrm{d}\Omega\int_l N_{i,y}N_j\mathrm{d}y
$$

$$
K_{13}^{ij\tau s} = \lambda\int_\Omega F_{\tau,x}F_{s,z}\mathrm{d}\Omega\int_l N_iN_j\mathrm{d}y + G\int_\Omega F_{\tau,z}F_{s,x}\mathrm{d}\Omega\int_l N_iN_j\mathrm{d}y
$$

$$
K_{21}^{ij\tau s} = \lambda\int_\Omega F_\tau F_{s,x}\mathrm{d}\Omega\int_l N_{i,y}N_j\mathrm{d}y + G\int_\Omega F_{\tau,x}F_s\mathrm{d}\Omega\int_l N_iN_{j,y}\mathrm{d}y
$$

$$
\begin{aligned}
K_{22}^{ij\tau s} &= G\int_\Omega F_{\tau,z}F_{s,z}\mathrm{d}\Omega\int_l N_iN_j\mathrm{d}y + G\int_\Omega F_{\tau,x}F_{s,x}\mathrm{d}\Omega\int_l N_iN_j\mathrm{d}y + \\
&\quad (\lambda+2G)\int_\Omega F_\tau F_s\mathrm{d}\Omega\int_l N_{i,y}N_{j,y}\mathrm{d}y
\end{aligned} \qquad (3.19)
$$

$$
K_{23}^{ij\tau s} = \lambda\int_\Omega F_\tau F_{s,z}\mathrm{d}\Omega\int_l N_{i,y}N_j\mathrm{d}y + G\int_\Omega F_{\tau,z}F_s\mathrm{d}\Omega\int_l N_iN_{j,y}\mathrm{d}y
$$

$$
K_{31}^{ij\tau s} = \lambda\int_\Omega F_{\tau,z}F_{s,x}\mathrm{d}\Omega\int_l N_iN_j\mathrm{d}y + G\int_\Omega F_{\tau,x}F_{s,z}\mathrm{d}\Omega\int_l N_iN_j\mathrm{d}y
$$

$$
K_{32}^{ij\tau s} = \lambda\int_\Omega F_{\tau,z}F_s\mathrm{d}\Omega\int_l N_iN_{j,y}\mathrm{d}y + G\int_\Omega F_\tau F_{s,z}\mathrm{d}\Omega\int_l N_{i,y}N_j\mathrm{d}y
$$

$$
\begin{aligned}
K_{33}^{ij\tau s} &= (\lambda+2G)\int_\Omega F_{\tau,z}F_{s,z}\mathrm{d}\Omega\int_l N_iN_j\mathrm{d}y + G\int_\Omega F_{\tau,x}F_{s,x}\mathrm{d}\Omega\int_l N_iN_j\mathrm{d}y + \\
&\quad G\int_\Omega F_\tau F_s\mathrm{d}\Omega\int_l N_{i,y}N_{j,y}\mathrm{d}y
\end{aligned}
$$

3.5 Mass Matrix

The mass matrix can be obtained by considering the virtual variation of the work of the inertial loadings:

$$
\delta L_{\mathrm{ine}} = \int_V \rho\delta\mathbf{u}^T\ddot{\mathbf{u}}\mathrm{d}V \qquad (3.20)
$$

where ρ is the material density and $\ddot{\mathbf{u}}$ is the acceleration vector. Rewriting Eq.3.20 using Eq. 3.2 we get

$$
\delta L_{\mathrm{ine}} = \delta\mathbf{q}_{\tau i}^{\mathrm{T}}\int_l N_iN_j\,dy\int_\Omega \rho F_\tau F_s\,d\Omega\,\ddot{\mathbf{q}}_{sj} = \delta\mathbf{q}_{\tau i}^{\mathrm{T}}\mathbf{M}^{ij\tau s}\ddot{\mathbf{q}}_{sj} \qquad (3.21)
$$

where $\mathbf{M}^{ij\tau s}$ is the fundamental nucleus of the mass matrix and its components are written as follows:

$$M_{xx}^{\tau sij} = M_{yy}^{\tau sij} = M_{zz}^{\tau sij} = \rho \int_l N_i N_j dy \int_\Omega F_\tau F_s d\Omega,$$

$$M_{xy}^{\tau sij} = M_{xz}^{\tau sij} = M_{yx}^{\tau sij} = M_{yz}^{\tau sij} = M_{zx}^{\tau sij} = M_{zy}^{\tau sij} = 0$$

(3.22)

The shape functions integrals are calculated through the use of Gauss integration method [85]. The integration procedure involves reduced integration method as it overcomes the problem of shear locking (see [3], [93]).

The Fundamental Nuclei (FNs) are independent of the order and choice of cross section functions F_τ. Thus, they manifest as nine lines of code in the FEM program affording any order of theory can be easily implemented. The assembly procedure of FNs into the stiffness and mass matrices is achieved by employing four indices τ, s, i and j as four loop cycles in the code. Figure 3.1 shows the position of a FN within the stiffness matrix of an element and the global stiffness matrix. Having obtained the global matrix, the boundary conditions are applied onto the matrices to render them non-singular for onwards solution of the problem.
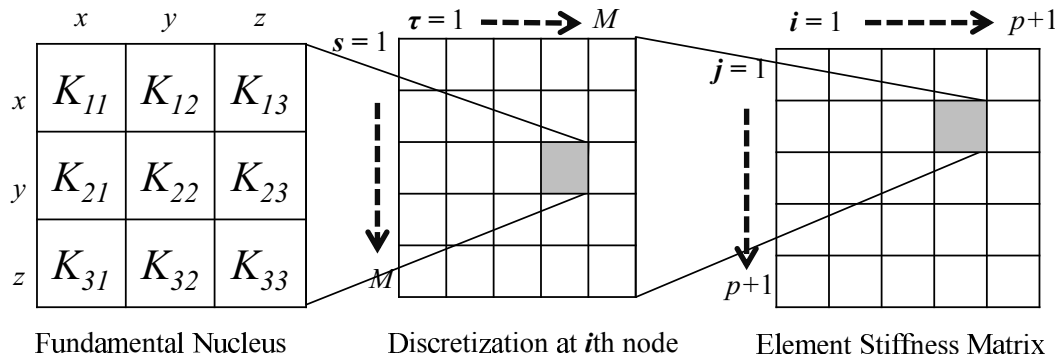
Figure 3.1 A 3×3 Fundamental Nucleus and its position in the element stiffness matrix
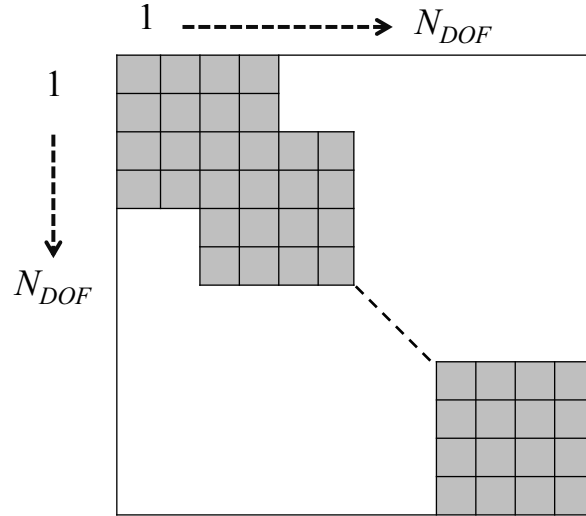
Figure 3.2 Element stiffness matrices assembled into Global Stiffness Matrix

3.6   Hydrostatic Stiffness Matrix

In present work (Part II of this thesis), the buoyancy has been modelled in the form of hydrostatic stiffness acting over the submerged area. Employing PVD, the virtual work done by strain energy of the hydrostatic stiffness can be written as follows:

$$\delta L_{\text{int}}|_{HS} = \delta \mathbf{u}^T \mathbf{K}_{HS} \mathbf{u} \tag{3.23}$$

where the subscript HS stands for Hydrostatic Stiffness and $\mathbf{u}$ is the generalized displacement. This hydrostatic stiffness is the product of stiffness per unit area times the area over which it acts. From Eq.3.2, we may write displacement in terms of shape functions and nodal displacements from so that:

$$\delta L_{\text{int}}|_{HS} = \delta \mathbf{q}_{\tau i}^{\text{T}} \int_l N_i N_j dy \ \ k_o \ \ \int_\Omega F_\tau F_s d\Omega \mathbf{q}_{sj} = \delta \mathbf{q}_{\tau i} \mathbf{K}_{HS}^{ij\tau s} \mathbf{q}_{sj} \tag{3.24}$$

where $\mathbf{K}_{HS}^{ij\tau s}$ is the 3×3 Fundamental Nucleus (FN) of Hydrostatic Stiffness. In the above equation, buoyancy is written in terms of linear 1D shape functions N_i which act over area $\int_\Omega F_\tau F_s d\Omega$. Since only the nodal value is the sole contribution of buoyancy spring to the global structural stiffness, we can write:

$$\int_l N_i N_j dy = 1 \tag{3.25}$$

Also, since buoyancy acts only vertically, depending on the axis aligned with gravity, the corresponding FN term is active and remaining 8 terms are all zero. For example, for the case with y-axis aligned with gravity we have:

$$\mathbf{K}_{HS}^{ij\tau s} = \begin{bmatrix} KHS_{xx}^{ij\tau s} & KHS_{xy}^{ij\tau s} & KHS_{xz}^{ij\tau s} \\ KHS_{yx}^{ij\tau s} & KHS_{yy}^{ij\tau s} & KHS_{yz}^{ij\tau s} \\ KHS_{zx}^{ij\tau s} & KHS_{zy}^{ij\tau s} & KHS_{zz}^{ij\tau s} \end{bmatrix} = \begin{bmatrix} 0 & 0 & 0 \\ 0 & KHS_{yy}^{ij\tau s} & 0 \\ 0 & 0 & 0 \end{bmatrix} \tag{3.26}$$

where

$$KHS_{yy}^{ij\tau s} = k_o \int_\Omega F_\tau F_s d\Omega \tag{3.27}$$

and

$$k_o = \text{Foundation Modulus of water } = \rho g$$
$$g = \text{Gravity acceleration constant} = 9.81 \text{ m}/s^2 \tag{3.28}$$

3.7 Loading Vector

For the case of a concentrated load $\mathbf{P}$ acting on a point P with coordinates x_p, y_p and z_p, a loading vector variationally coherent to the hierarchial model is obtained as follows:

$$\mathbf{P} = \left\{ \begin{array}{ccc} P_x & P_y & P_z \end{array} \right\}^T \tag{3.29}$$

For the other cases such as line or surface loads, the virtual variation in the work due to force $\mathbf{P}$ can be written as:

$$\delta L_{\text{ext}} = \delta \mathbf{u}^T \mathbf{P} \tag{3.30}$$

Introducing the shape functions and nodal displacements from Eq.3.2, we get

$$\delta L_{\text{ext}} = \delta \mathbf{q}_{\tau i} F_\tau N_i \mathbf{P} \tag{3.31}$$

where F_τ and N_i are functions of (x, z) and y coordinates respectively. The Eq.3.31 allows the proper assembly of FNs of load vector. This way each global displacement DOF can be assigned a load component.

3.7.1 Inertia Load

The virtual variation of external work done by acceleration due to gravity, $\ddot{\mathbf{u}} = \left\{ \begin{array}{ccc} \ddot{u}_x & \ddot{u}_y & \ddot{u}_z \end{array} \right\}^T = \left\{ \begin{array}{ccc} 0 & 0 & g \end{array} \right\}^T$, can be written from Eq. 3.20 as follows:

$$\delta L_{\text{ext}} = \delta \mathbf{q}_{\tau i}^{\mathrm{T}} \int_l N_i N_j dy \int_\Omega \rho F_\tau F_s d\Omega \ddot{\mathbf{q}}_{sj} = \delta \mathbf{q}_{\tau i}^{\mathrm{T}} \mathbf{M}^{ij\tau s} \ddot{\mathbf{q}}_{sj} = \delta \mathbf{q}_{\tau i}^{\mathrm{T}} \mathbf{P}^{js} \tag{3.32}$$

where $\mathbf{M}^{ij\tau s}$ is the mass matrix derived above and g is constant of acceleration due to gravity, 9.81 m/s^2.

Part I

Numerical Results
Hull in Vacuo

Chapter 4

Single Beam Models for Marine Vessels

This chapter is first of the series of chapters on results of application of CUF with CW models. As a start only simple marine structural configurations such as barges which resemble boxes and simplified boat-like geometries have been analysed for static and dynamic analysis. The analyses were performed on dry hull (without water) configurations. The efficacy of CW approach for the analysis of typical marine structures is demonstrated for dry configurations.

4.1   CW Single Beam Models

The Component-Wise (CW) models were introduced in second chapter which have pure displacement DOFs as the only unknowns. Geometrical complexities such as cross section discontinuities and localised warping and stresses can be efficiently captured using CW models of CUF. Only the *dry* models are analysed in this and next chapter since no effect of water is taken into consideration. The objective of this chapter is to introduce CW models for modeling typical marine structures such as barges and boat-like geometries. All the cases discussed in this chapter comprise of a *single* beam with multiple cross sections. Each cross section is associated to a beam element and thus the change of cross section along the beam length is materialised. The strength of CW approach and the refined displacement kinematics for these simple cases is presented here as an initial approach towards analysis of more complex geometries such as container ships later to appear in the thesis.

It is important to highlight here the fact that typical FE models of modern complex marine vessels may employ a mix of different elements types e.g. 1D, 2D or 3D

in a single model. For this purpose fictitious links are introduced to account for inconsistencies in DOFs at an interface location shared between two different element types. The present beam model effectively overcomes this issue by affording a rich displacement field over the cross section in the form of physical nodes (Lagrange element nodes). At the element-to-element interface (beam node), the sections share many common nodes thereby sharing DOFs and finally affording us with a realistic displacement field. Hence, no fictitious elements are needed at these interfaces.

4.1.1 Box-like structures-Barges

Barges are flat-bottomed floating vessels which may or may not be self propelled. Their usual purpose is to transport cargo over relatively shorter distances compared to large container ships. In configuration, they mostly resemble box-like shapes therefore they were chosen as initial cases for the application of CW models for marine vessels. The dynamic and static analyses for the box-like barges discussed hereinafter have been published in [15].

Referring to the Fig.4.1, the boxes have the longest dimension along y-axis which is also the longitudinal axis for the beam. Various cross sections are parallel to the xz-plane which is the transverse plane. Configuration Fig.4.1a is the simplest geometry involving only the two side walls and a floor. In the configuration shown in Fig.4.1b a longitudinal bulkhead is introduced in the middle and in Fig.4.1c a transverse bulkhead is added to the preceding two geometries.

(a) Box with 2 walls

(b) Box with 2 walls and 1 stiffener

(c) Box with 4 walls and 2 crossing stiffeners
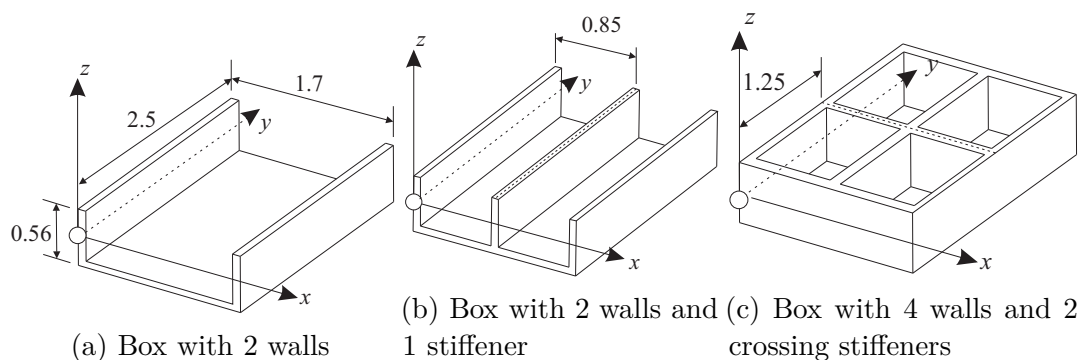
Figure 4.1 Box-like structure geometries (dimensions in meters)

In general, the configuration shown in Fig.4.1c may be modelled using three FE approaches as shown in Fig.4.2. Figure 4.2a shows the model meshed with 2D shell elements from a commercial software and Fig.4.2b shows the same model meshed with 3D solid elements. The model is finally meshed using CW approach in Fig.4.2c. The

shell mesh has ANSYS shell elements (Shell-281) meshed on the surface that lies mid-way through the wall thicknesses. Each node of shell element has 6 DOFs (i.e. three translations and three rotations). The shell model from hereinafter will be referred to as ANS2D. The ANSYS solid mesh comprises of 3D brick element (Solid-186) with each node having 3 DOFs (translations only). The solid model will be hereinafter referred to as ANS3D. In CW mesh, the beam nodes are along y-axis while the cross sections are meshed with nine nodded L9 Lagrange elements. The beam mesh is discretised in 13 elements along y-axis. The model comprises two cross sections types: 1 and 2 as shown encircled. Each node of the L9 element has a physical location in the 3D model and has three translation DOFs. As an example, the two cross sections meshed with Lagrange elements are shown in Fig.4.3.

(a) Shell element mesh   (b) Solid element mesh

(c) CUF LE Beam elements mesh with two cross section types
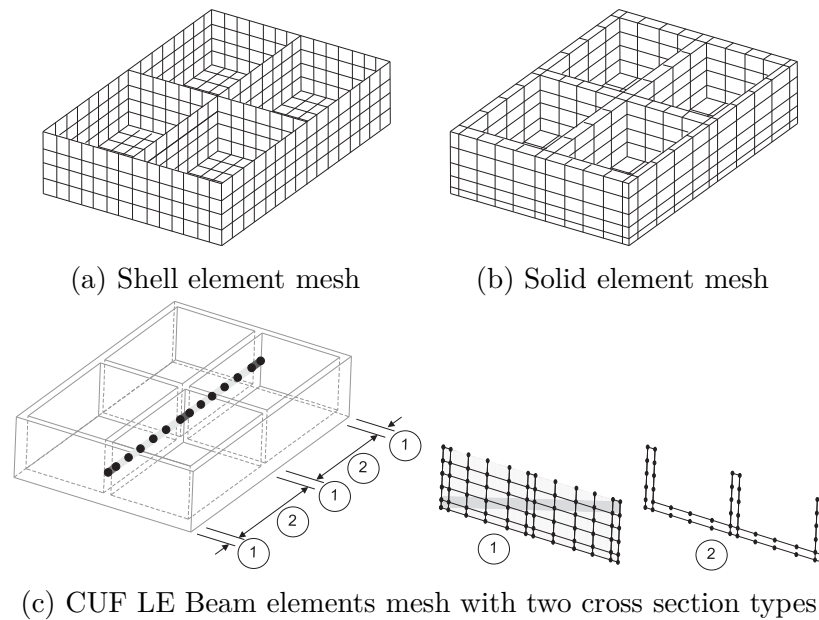
Figure 4.2 Various FE approaches to model the box-like structure of Fig.4.1c

(a) L9 Mesh for Cross section-1   (b) L9 Mesh for Cross section-2
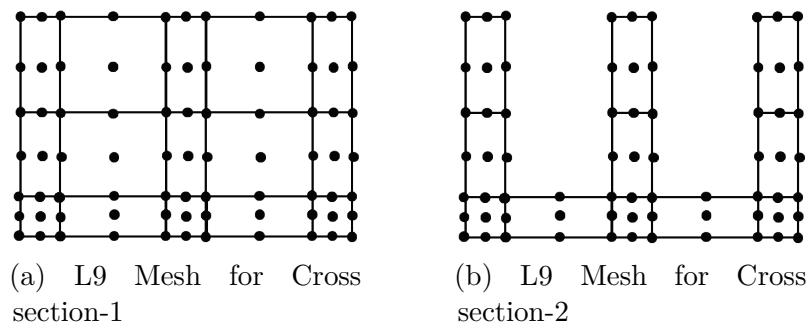
Figure 4.3 Two cross section mesh types used in Fig.4.2c

Modal analysis

This section describes the free vibration analysis of a box-like structure for the three configurations as shown in Fig.4.1. The structure has free-free boundary conditions and the material made of an aluminum alloy with the following material constants: $E = 75$ GPa, $\nu = 0.33$, and material density $\rho = 2700$ Kg/m3. The wall and floor thicknesses everywhere is 10 mm. Results of the analyses, natural frequencies, are presented in Tables 4.1 to 4.3 and the correspondingly their first and fourth mode shapes are shown in Fig.4.4.

Table 4.1 Natural frequencies (Hz) with free-free boundary conditions the case of Fig.4.1a

(DOFs)	5L9 Model (1023)	8L9 Model (4743)	12L9 Model (6975)	ANS2D (51678)	ANS3D (153948)
Mode 1	6.52	5.26	5.23	5.16	5.22
Mode 2	9.79	8.41	8.25	8.04	8.11
Mode 3	19.30	14.21	14.00	13.73	13.89
Mode 4	28.30	19.57	18.39	17.41	17.65
Mode 5	48.10	22.73	21.91	21.11	21.41
Mode 6	49.30	23.01	22.01	21.48	21.72
Mode 7	50.60	32.87	29.30	26.05	26.44
Mode 8	53.90	38.79	31.61	28.44	28.87
Mode 9	69.50	46.15	31.93	30.97	31.43
Mode 10	71.00	48.09	37.76	35.07	35.62

Table 4.2 Natural frequencies (Hz) with free-free boundary conditions the case of Fig.4.1b

(DOFs)	16L9 Model (6975)	ANS2D (61710)	ANS3D (73824)
Mode 1	5.65	5.54	5.61
Mode 2	7.75	7.50	7.59
Mode 3	12.61	12.23	12.39
Mode 4	15.03	14.49	14.70
Mode 5	19.73	19.16	19.44
Mode 6	25.84	22.80	23.21
Mode 7	27.77	24.92	25.36
Mode 8	29.21	26.43	27.01
Mode 9	31.19	28.68	29.26
Mode 10	31.30	30.46	30.91
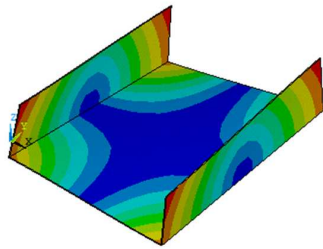
(a) Config. Fig.4.1a Mode 1: ANSYS
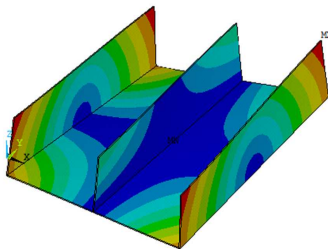
(b) Config. Fig.4.1b Mode 1: ANSYS
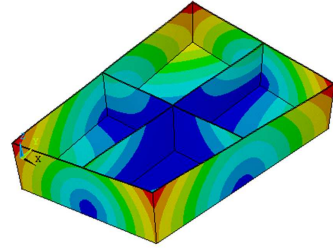
(c) Config. Fig.4.1c Mode 1: ANSYS
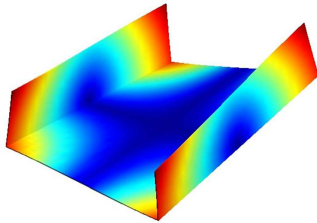
(d) Config. Fig.4.1a Mode 1: CW Model
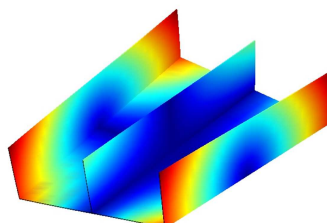
(e) Config. Fig.4.1b Mode 1: CW Model
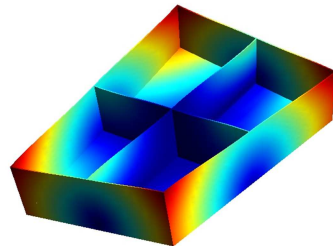
(f) Config. Fig.4.1c Mode 1: CW Model
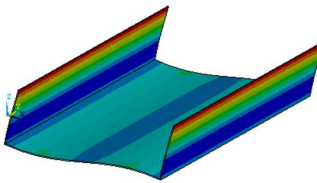
(g) Config. Fig.4.1a Mode 4: ANSYS
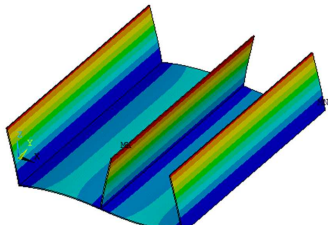
(h) Config. Fig.4.1b Mode 4: ANSYS
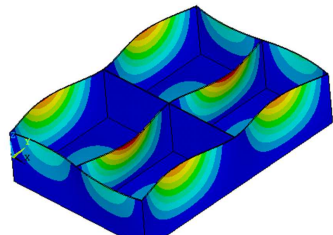
(i) Config. Fig.4.1c Mode 4: ANSYS
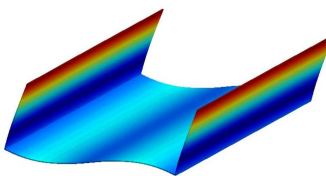
(j) Config. Fig.4.1a Mode 4: CW Mode4
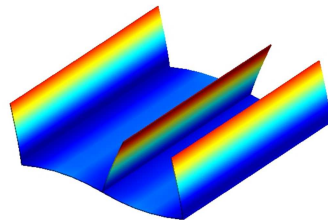
(k) Config. Fig.4.1b Mode 4: CW Model
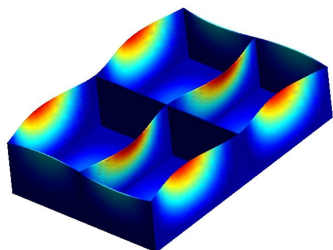
(l) Config. Fig.4.1c Mode 4: CW Model

Figure 4.4 First and forth mode shapes for the box-like configurations of Figs.4.1a, 4.1b and 4.1c

Table 4.3 Natural frequencies (Hz) with free-free boundary conditions the case of Fig.4.1c

(DOFs)	15L9 Model (8352)	20L9 Model (10872)	28L9 Model (14364)	ANS2D (81114)	ANS3D (99366)	ANS3D (238200)
Mode 1	8.60	8.48	7.47	7.10	7.19	7.19
Mode 2	40.29	39.88	39.66	37.95	38.69	38.52
Mode 3	44.51	44.19	41.89	39.01	39.78	39.61
Mode 4	55.90	55.011	44.15	42.70	43.44	43.28
Mode 5	56.10	55.21	46.02	43.53	44.28	44.12
Mode 6	58.86	57.95	49.29	45.71	46.66	46.47
Mode 7	61.90	61.04	55.20	52.11	53.08	52.88
Mode 8	76.03	74.88	74.43	62.84	64.05	63.83
Mode 9	79.81	78.77	78.09	64.21	65.42	65.23
Mode 10	88.84	87.51	86.15	68.32	69.58	69.37

Static analysis

The CW model shown in Fig.4.5 was analysed for its static analysis with a variety of loading and boundary conditions. The first two loading cases are shown in Fig. 4.5a and 4.5b, where a 10 kN vertically downward point load is applied at intersection of longitudinal and transverse bulkheads. The other two loading cases as shown in Fig.4.5c and 4.5d are where a Uniformly Distributed Load (UDL) is applied on the top of longitudinal bulkhead. The four cases shown in the Fig.4.1c have the two types of boundary condition sets applied to the four bottom edges. An edge with a Simply-supported boundary condition is denoted as "S" and a Free edge with "F" and the two types of boundary conditions are denoted as SSSS and SFSF.

The deflections and stresses obtained from the static analyses are are presented in Tables 4.4 to 4.7, and the deformed shapes, as obtained from ANS3D and the present CW beam model, are shown in Fig.4.7 to 4.10 for the respective cases. Fig.4.6 shows a plan view of the box highlighting eight selected locations (A to H) on the surface lying midway through the floor thickness at $z = -0.275$ m. Taking into account the symmetry in the structure, only the results at points A and E are being reported here.

It can be inferred from the results of the static analysis that the CW requires much less DOFs compared to ANS3D models for fairly close results. The efficacy of CW is manifest in the fact that the loads and boundary conditions are applied at realistic geometrical locations. Apart from vertical bending of the beam in yz-plane, the out-of-plane and in-plane displacement kinematics are quite obvious and realistic for the walls and bulkheads. It is observed that introducing more supports reduces the

(a) Point Load with SFSF Boundary Condition

(b) Point Load with SSSS Boundary Condition

(c) Uniformly Distributed Load with SFSF Boundary Condition

(d) Uniformly Distributed Load with SSSS Boundary Condition
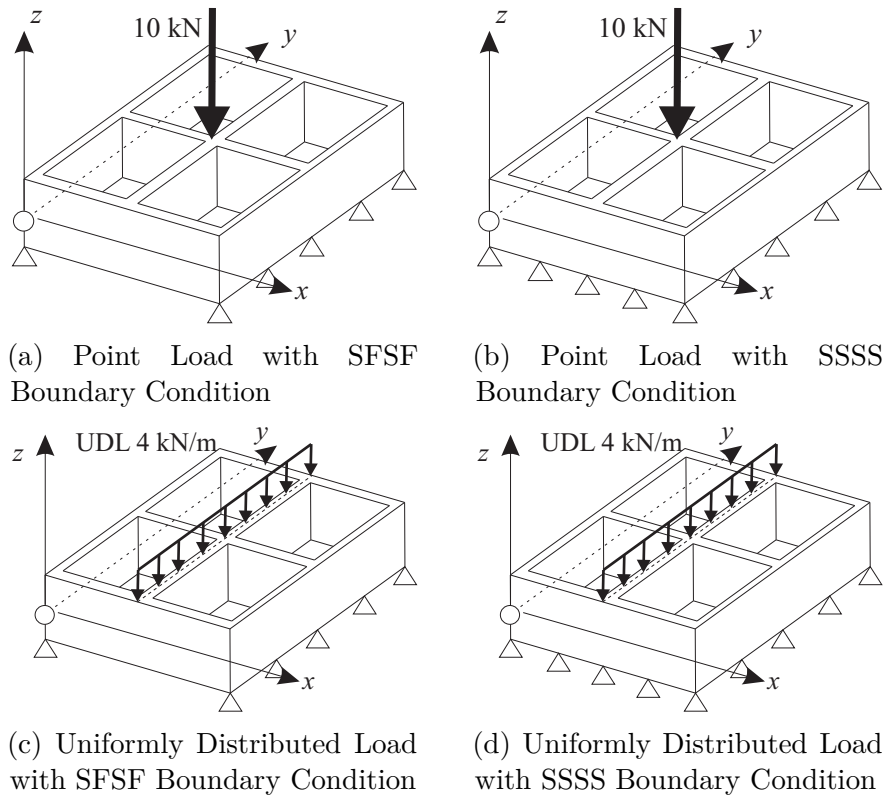
Figure 4.5 Four cases of loading and boundary conditions
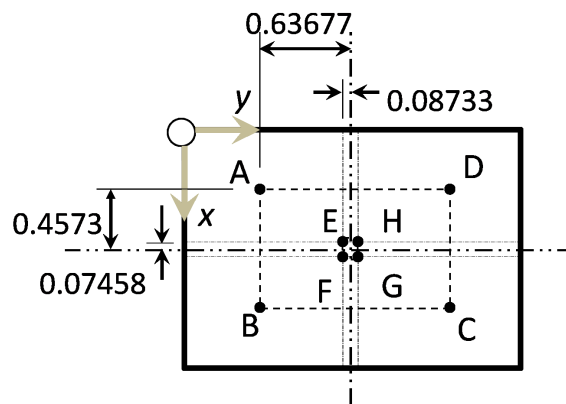
Figure 4.6 Plan view of the verification points for results

Table 4.4 Results under the loading shown in Fig.4.5a; CW and ANS3D refer to 77/29L9 and ANSYS Solid Models respectively

Point	Model (DOFs)	Displacements ($\times 10^{-6}$ m)		
		u	v	w
A	CW (27288)	0.289	-0.843	-18.576
	ANS3D (515103)	0.294	-0.857	-18.776
E	CW (27288)	-0.336	-0.088	-42.476
	ANS3D (515103)	-0.334	-0.090	-42.997

Point	Model (DOFs)	Stresses ($\times 10^5$ Pa)					
		$\boldsymbol{\sigma}_{xx}$	$\boldsymbol{\sigma}_{yy}$	$\boldsymbol{\sigma}_{zz}$	$\boldsymbol{\sigma}_{xy}$	$\boldsymbol{\sigma}_{xz}$	$\boldsymbol{\sigma}_{yz}$
A	CW (27288)	0.130	0.726	0.004	-0.543	-0.007	-0.009
	ANS3D (515103)	0.122	0.744	0.000	-0.549	-0.003	-0.002
E	CW (27288)	4.058	2.892	-0.028	-1.049	-0.637	0.052
	ANS3D (515103)	4.278	2.919	-0.008	-1.038	0.017	-0.018
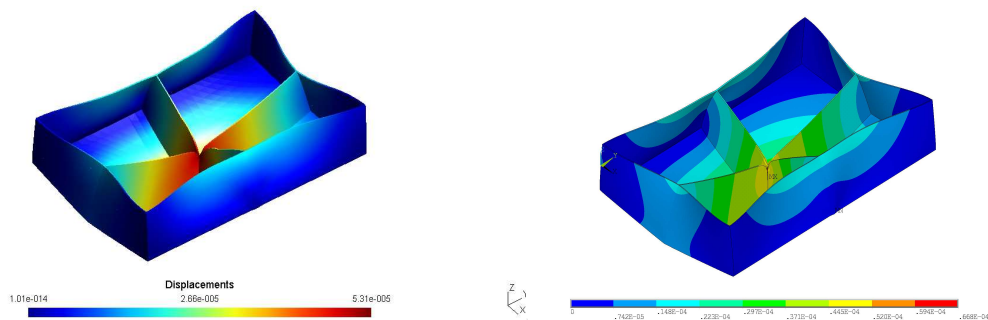
(a) Static Deflection from CW Model   (b) Static Deflection from ANSYS

Figure 4.7 Deflected box under the loading shown in Fig. 4.5a

Table 4.5 Results under the loading shown in Fig. 4.5b; CW and ANS3D refer to 77/29L9 and ANSYS Solid Models respectively.

Point	Model (DOFs)	Displacements ($\times 10^{-6}$ m)		
		u	v	w
A	CW (27288)	0.063	-0.2382	-13.017
	ANS3D (515103)	0.067	-0.248	-13.120
E	CW (27288)	-0.302	-0.048	-38.350
	ANS3D (515103)	-0.300	-0.049	-38.849

Point	Model (DOFs)	Stresses ($\times 10^5$ Pa)					
		σ_{xx}	σ_{yy}	σ_{zz}	σ_{xy}	σ_{xz}	σ_{yz}
A	CW (27288)	-0.078	-0.067	0.002	-0.089	-0.011	-0.016
	ANS3D (515103)	-0.073	-0.051	0.000	-0.103	-0.004	-0.002
E	CW (27288)	3.618	2.290	-0.024	-1.049	-0.503	0.046
	ANS3D (515103)	3.843	2.329	-0.007	-1.021	0.005	-0.013

(a) Static Deflection from CW Model

(b) Static Deflection from ANSYS
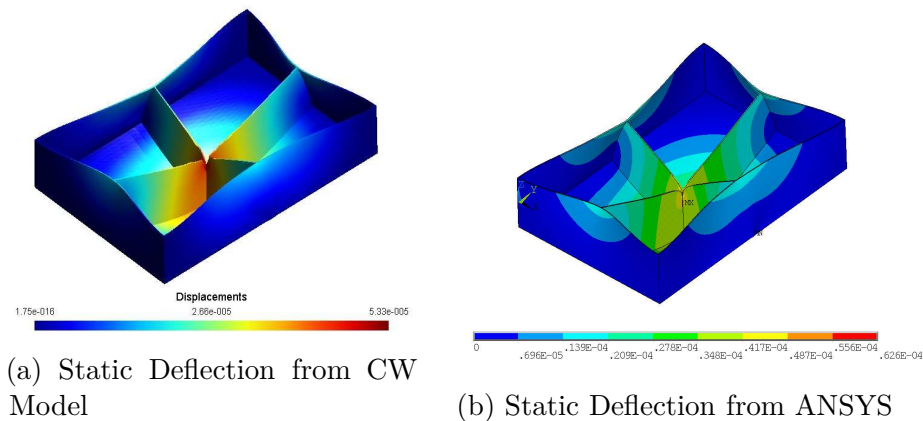
Figure 4.8 Deflected box under the loading shown in Fig.4.5b

Table 4.6 Results under the loading shown in Fig. 4.5c; CW and ANS3D refer to 77/29 L9 and ANSYS Solid Models respectively

Point	Model (DOFs)	Displacements ($\times 10^{-6}$ m)		
		u	v	w
A	CW (27288)	0.318	-0.587	-18.642
	ANS3D (515103)	0.335	-0.593	-19.047
E	CW (27288)	-0.356	0.217	-31.703
	ANS3D (515103)	-0.362	0.234	-31.524

Point	Model (DOFs)	Stresses ($\times 10^5$ Pa)					
		$\boldsymbol{\sigma}_{\mathrm{xx}}$	$\boldsymbol{\sigma}_{\mathrm{yy}}$	$\boldsymbol{\sigma}_{\mathrm{zz}}$	$\boldsymbol{\sigma}_{\mathrm{xy}}$	$\boldsymbol{\sigma}_{\mathrm{xz}}$	$\boldsymbol{\sigma}_{\mathrm{yz}}$
A	CW (27288)	0.268	0.628	0.000	-0.421	-0.005	-0.005
	ANS3D (515103)	0.281	0.654	0.000	-0.425	-0.004	-0.001
E	CW (27288)	3.081	0.097	-0.034	-0.214	0.051	-1.078
	ANS3D (515103)	3.154	-0.152	-0.008	-0.268	-0.029	0.084
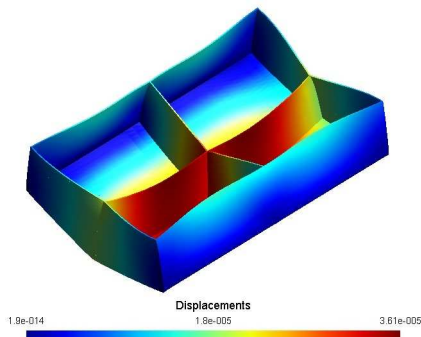
(a) Static Deflection from CW Model
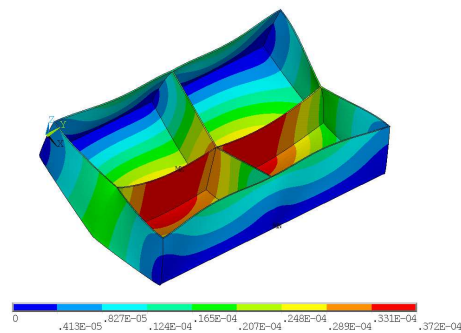
(b) Static Deflection from ANSYS

Figure 4.9 Deflected box under the loading shown in 4.5c

Table 4.7 Results under the loading shown in Fig. 4.5d; CW and ANS3D refer to 77/29 L9 and ANSYS Soild Models respectively

Point	Model (DOFs)	Displacements ($\times 10^{-6}$ m)		
		u	v	w
A	CW (27288)	0.094	-0.055	-11.460
	ANS3D (515103)	0.099	-0.037	-11.733
E	CW (27288)	-0.284	0.201	-25.199
	ANS3D (515103)	-0.288	0.221	-24.817

Point	Model (DOFs)	Stresses ($\times 10^5$ Pa)					
		σ_{xx}	σ_{yy}	σ_{zz}	σ_{xy}	σ_{xz}	σ_{yz}
A	CW (27288)	0.065	-0.082	-0.002	0.013	-0.010	-0.016
	ANS3D (515103)	0.082	-0.086	0.000	0.022	0.000	-0.004
E	CW (27288)	2.405	-0.184	-0.028	-0.230	0.042	-0.862
	ANS3D (515103)	2.457	-0.440	-0.007	-0.256	-0.022	0.065
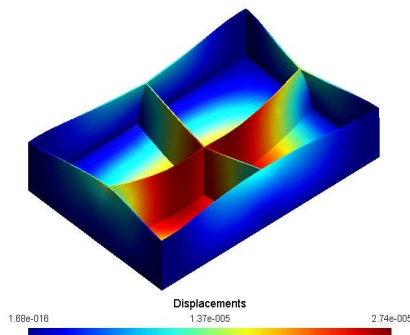
(a) Static Deflection from CW Model
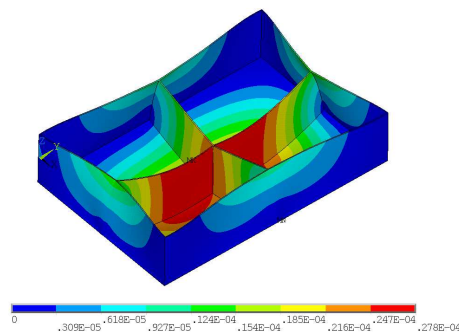
(b) Static Deflection from ANSYS

Figure 4.10 Deflected box under the loading shown in Fig.4.5d

vertical deflection which is again a realistic behaviour. The sharp vertical deflection is lessened when a UDL replaces the Point load.

4.1.2   Boat-like structures

Boat-like configurations were chosen to demonstrate the usefulness of CW model through free vibration analysis. The four configurations are shown in Fig. 4.11. The structure has free-free boundary conditions and the material is the same aluminum alloy as was used in box problems. Figure 4.11a is the simple hull with flat faces, then it is stiffened through a stiffener in the middle as shown in Fig. 4.11b and then further stiffened by introducing three transverse and two edge stiffeners as shown in Fig.4.11c. Finally, Fig.4.11d shows the configuration has four edge stiffeners and two end walls and has simply supported boundary conditions applied to edge fillets of R0.2. The height of each stiffener is 100 mm and wall thickness is 10 mm at all places.

(a) Flat hull with no stiffeners   (b) Flat hull with 1 stiffener

(c) Hull with 2 crossing and 2 edge (d) Hull with various stiffeners and 2
stiffeners   end walls
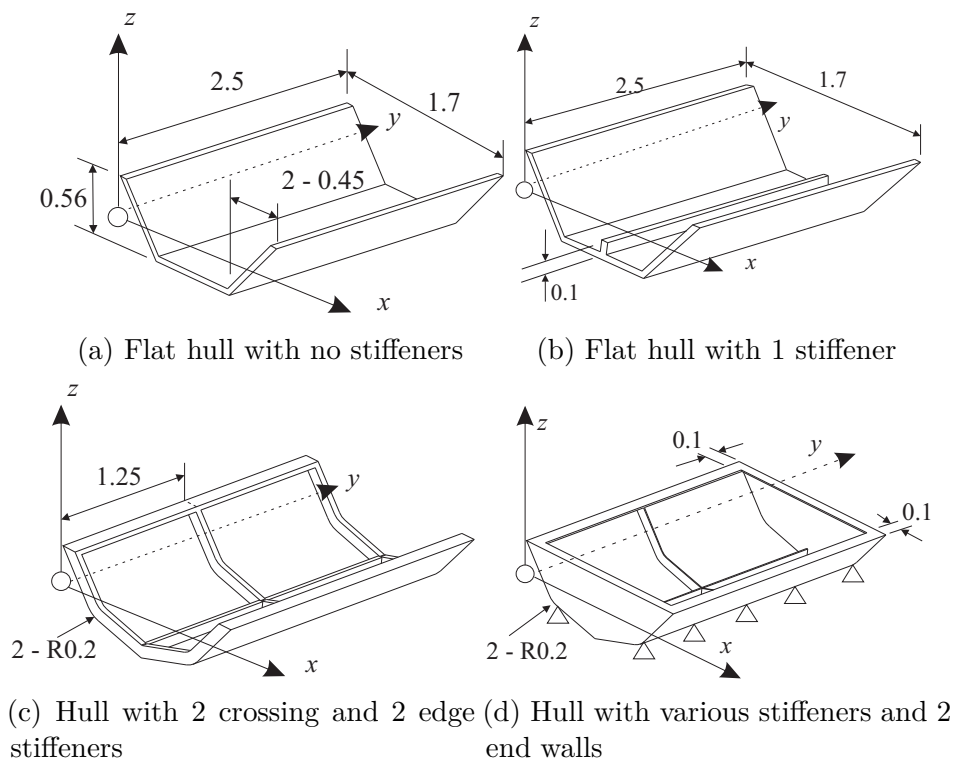
Figure 4.11 Boat-like structure geometries (dimensions in meters)

The natural frequencies obtained from the modal analysis of the boat-like configurations of Fig.4.11a to 4.11c are given in Tables 4.8 to 4.10 and mode shapes for the configurations shown in Fig.4.11c and Fig.4.11d are presented in Figs. 4.12 and 4.13.

Table 4.8 Comparison of natural frequencies of the boat-like structure of Fig. 4.11a

(DOFs)	CW 13L9 (7533)	CW 19L9 (10881)	ANS2D (117126)	ANS2D (29766)	ANS3D (53910)	ANS3D (121695)
Mode 1	6.47	6.46	6.37	6.37	6.45	6.45
Mode 2	9.98	9.88	9.65	9.65	9.84	9.83
Mode 3	14.48	14.40	14.13	14.13	14.35	14.34
Mode 4	24.23	24.11	23.71	23.71	23.99	23.98
Mode 5	26.42	26.10	25.46	25.46	25.83	25.81
Mode 6	27.52	27.09	26.19	26.19	26.73	26.70
Mode 7	30.81	30.43	29.56	29.56	30.10	30.07
Mode 8	40.16	39.97	39.42	39.41	39.76	39.75
Mode 9	42.26	41.83	41.05	41.05	41.44	41.42
Mode 10	61.55	60.63	58.51	58.51	59.39	59.37

Table 4.9 Comparison of natural frequencies of the boat-like structure of Fig. 4.11b

(DOFs)	CW 20L9 (11439)	ANS2D (32280)	ANS3D (63324)
1	6.66	6.54	6.62
2	9.81	9.54	9.73
3	14.29	13.98	14.19
4	25.76	25.24	25.43
5	26.10	25.42	25.75
6	26.79	25.91	26.34
7	30.29	29.38	29.84
8	41.54	40.69	41.00
9	41.88	41.06	41.39
10	58.96	55.96	57.15

Table 4.10 Comparison of natural frequencies of the boat-like structure of Fig. 4.11c

(DOFs)	CW 30L9 (11184)	CW 54L9 (18672)	ANS2D (94302)	ANS2D (150270)	ANS3D (90702)	ANS3D (149637)
Mode 1	8.59	6.78	6.44	6.44	6.70	6.70
Mode 2	43.78	41.71	42.34	42.34	41.2	41.20
Mode 3	57.49	54.51	55.06	55.06	53.80	53.78
Mode 4	100.53	98.21	97.35	97.35	96.36	96.36
Mode 5	111.83	105.21	100.70	100.70	101.99	101.97
Mode 6	113.98	109.15	109.93	109.93	107.33	107.38
Mode 7	130.00	126.85	123.49	123.49	123.71	123.75
Mode 8	152.82	140.60	128.80	128.80	133.52	133.47
Mode 9	154.19	149.92	141.49	141.49	145.52	145.56
Mode 10	165.65	154.40	145.04	145.04	146.83	146.81

The results of modal analysis for the boat-like configurations are quite close to those obtained from ANSYS models. Similar to the box-like configurations, the torsional modes are the initial modes which realistically corresponds to the fact that boats without decks have very low torsional rigidity. It is evident that the natural frequencies from CW model fall quite close to those from commercial software yet requiring much less DOFs.
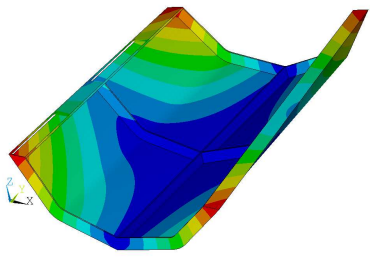
(a) Mode 1: ANS3D Model
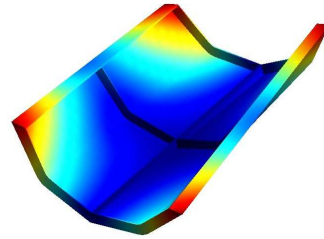
(b) Mode 1: CW Model
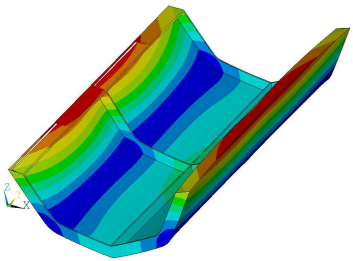
(c) Mode 2: ANS3D Model
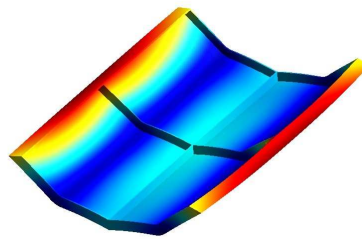
(d) Mode 2: CW Model
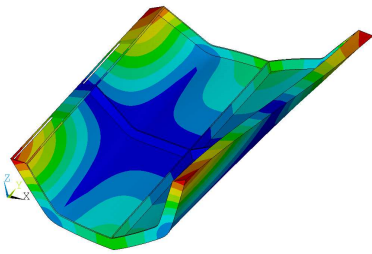
(e) Mode 3: ANS3D Model
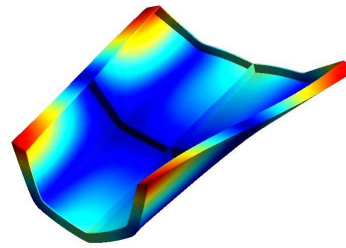
(f) Mode 3: CW Model
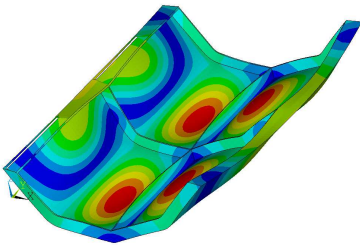
(g) Mode 4: ANS3D Model
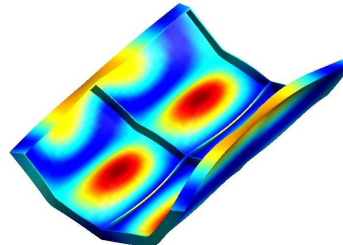
(h) Mode 4: CW Model

Figure 4.12 First four mode shapes for the boat-like configurations of Figs.4.11c and 4.11d

(a) Mode 1: 81.748 Hz   (b) Mode 2: 91.137 Hz

(c) Mode 3: 139.666 Hz   (d) Mode 4: 148.293 Hz

(e) Mode 5: 167.326 Hz   (f) Mode 6: 167.972 Hz

(g) Mode 7: 194.656 Hz   (h) Mode 8: 203.411 Hz
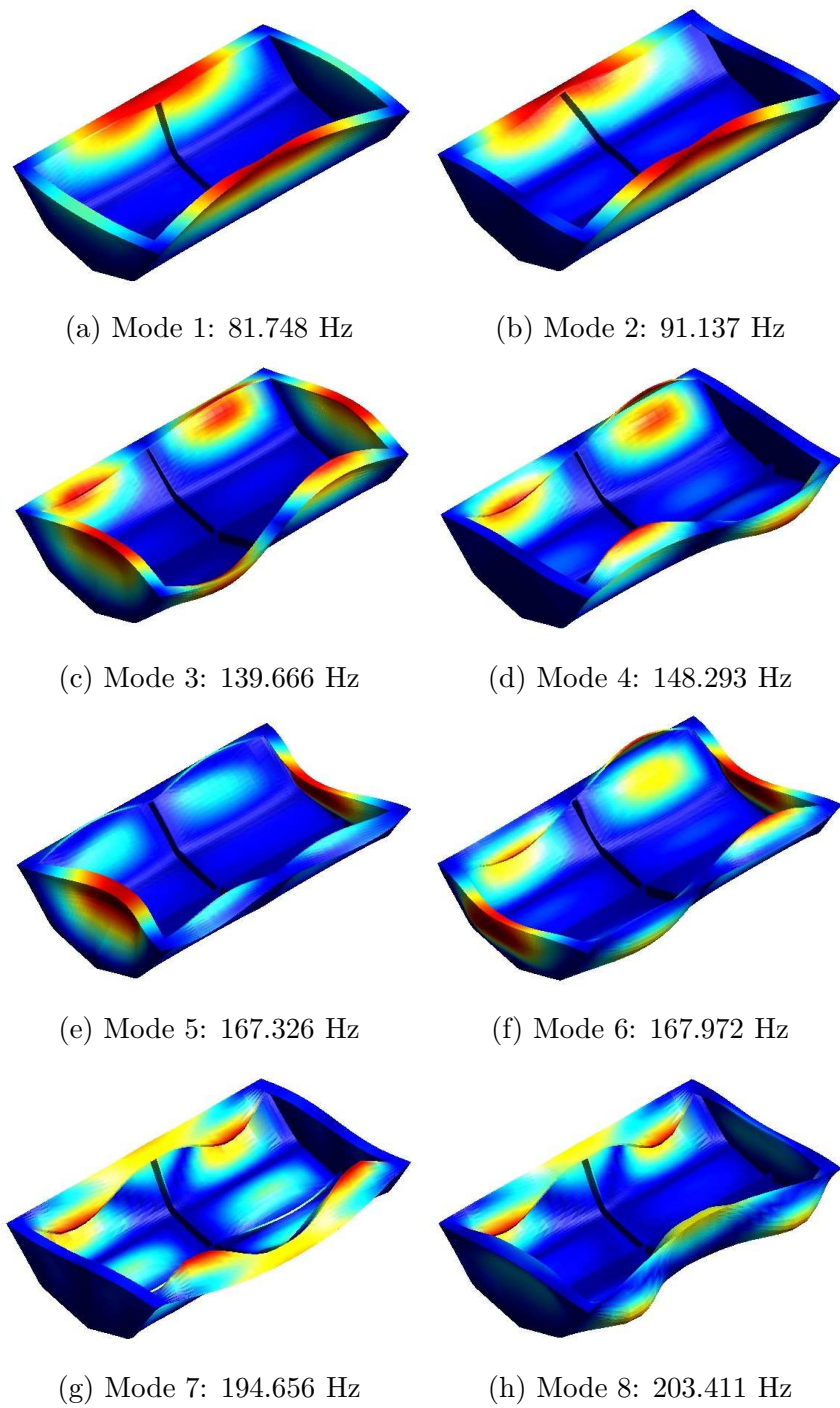
Figure 4.13 First eight mode shapes for the boat-like configurations of Figs.4.11d using CW model

Chapter 5

Single Beam Models for Container Ship

Modern container ships are complex structures. They resemble beam in their global appearance but classical beam theories are too simple to capture the bending-torsion coupling behaviour they usually exhibit under torsional loads. The CW models presented earlier, are used in this chapter to capture the detailed kinematics such as out-of-plane and in-plane warping and stresses associated with them.

5.1 Simplified Container Ship Model

Modern container ships can be idealised as large sized beams with a very complex cross section geometry. Despite the addition of stiffeners to the free edges and doubling the side walls and bottom, the overall form of the cross section remains close to a U-channel. This means that the shear center has to lie below the keel and the beam will display significant bending-torsion coupling in addition to the out-of-plane warping when subjected to torsional loads.

A container ship is subjected to torsional loads when it encounters waves at an angle to the longitudinal axis. In such situation, the wave pattern is not symmetrical about the vertical plane of symmetry. Typical container ships have the main hull in the form of a channel while the bow and the stern are built-up by engine room or other infrastructure for the crew. The container ship has large hatch openings and a larger portion of the length remains in the form of open channel section. Under a torsional load, the built-up ends of the beam restrain the transverse section from warping out-of-plane and as a result, significant warping stresses are developed at the corners interfaces where opened-sections meet closed-sections.

Researchers have developed ad-hoc formulations to deal with the bending-torsion coupling of channel idealization of container with large hatch openings. In this regards, works of Senjanovic et al. [40, 80, 99, 43, 42, 79] are quite pertinent. This and many other models still employ some assumptions and many higher modes cannot be detected through these models. The advantage of CW models over classical beam models is clearly explained in earlier chapters for box-like and boat-structures. This chapter will introduce the efficacy of their use to model global structural behaviour of container ships. Like previous chapters, the container ship will also be modelled as a single beam model whereby a single cross section is extruded to form a 3D shape of a container ship. All the analyses are performed without the effect of water or buoyancy forces.

Firstly, the container ship is modelled as a simple channel shape to observe and validate the warping behaviour under a torque load and later a cross section with realistic scantlings is employed for a prismatic representation of a container ship under distributed torsional loads. The results are subsequently compared to analytical and commercial software. The two analyses have been published in Ref.[69].

5.1.1 Case-1: Simple Channel Idealization for a Container Ship Hull

A typical container ship can be idealised as a prismatic beam (C-Chennel)[47, 81]. The cross section of such beam is symmetric about the vertical plane, passing through the beam axis but asymmetric about any horizontal plane. This results in a significant distance between the geometric centroid and shear center of the cross section in vertical plane. Because of this reason, following are observed:

a. Under horizontal transverse loads passing through the area centroid of cross section, the beam not only bends in the horizontal plane but also twists about the twist axis.

b. The cross sections warp out of their planes through out the beam length except at places where beam has a built-up end.

c. Under pure torsional loads, a channel beam will not undergo bending but all the cross sections rotate in the manner that their projections in vertical plane rotate as rigid body. Additionally, significant *out-of-plane* warping of the cross section is observed.

In the following, the case of a channel (Fig.5.1) subjected to an end torque is presented. The beam is constrained rigidly at one end in a manner that both the twist

and the warping are prevented. The other end is free and is the end where a torque is applied. The longitudinal beam axis is along y-axis. The case is a *Non-uniform Torsion* problem since the rate of twist along the length, $d\theta/dy$, is not a constant. Such loading configuration results in warping stresses (axial stresses) at places where beam is restrained. The end torque is T=2600000 Nm. The beam width is $b = 26$ m, height $h = 16.2$ m, all the walls have thickness $t = 0.05$ m and length $l = 120$ m and the material is alloy steel ($E = 210$ GPa, $\nu = 0.33$). A comparison between analytical and CW model is presented in order to demonstrate the capability of CW models to capture warping and associated stresses. Travelling along the length from fixed to free end, the out-of-plane warping becomes pronounced whereas the warping stresses vanish. Within a cross section, the warping or axial stress assumes the same distribution as that of warping displacement and warping function ω, which depends on cross section geometry as well as the rate of twist. The warping function, ω has the distribution as shown in Fig.5.2. Its distribution over the segments s_1, s_2 and s_3 of the cross sections is given by Eqs. 5.4(Ref [47]). The maximum rotation of the tip $\theta_{\max}$ and its rate at root $\theta''_{\max}$ are respectively given by Eq. 5.1 and Eq. 5.2 (Ref[6]). Employing these and various terms defined in the following the warping stress, σ_w, can be calculated from Eq. 5.3 (Ref[81]). It can be seen that the warping pattern is antisymmetric and so is the warping stress over the cross section of the channel beam.
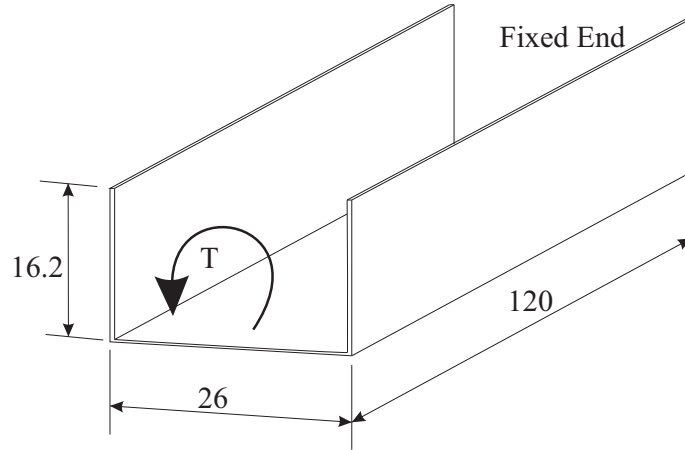
Figure 5.1 Loading and constraints on a channel beam

$$\theta_{\max} = \frac{T}{C_w E \beta^3}(\beta l - \tanh \beta l) \tag{5.1}$$

$$\theta''_{\max} = \frac{T}{C_w E \beta} \tanh \beta l \tag{5.2}$$
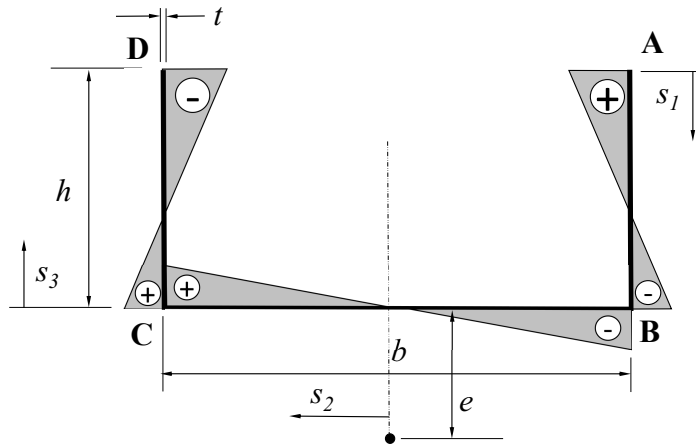
Figure 5.2 Sectorial diagram of warping function over cross section

$$\sigma_w = \frac{\omega M}{C_w} \tag{5.3}$$

and

$$
\begin{aligned}
\omega_1(s_1) &= \frac{b}{2}(s_1 + e - h) \\
\omega_2(s_2) &= -es_2 \\
\omega_3(s_3) &= \frac{b}{2}(s_3 - e)
\end{aligned}
\tag{5.4}
$$

where

ω	:	Warping function			
M	:	Bi-moment acting over the cross section	$=$	$EC_w\theta''$	
C_w	:	Warping constant	$=$	$\dfrac{b^2h^3t}{12}\dfrac{2b+3h}{b+6h}$	$=$ 9778.4 m^6
J_t	:	Torsional constant	$=$	$\dfrac{t^3}{3}(b+2h)$	$=$ 0.00243 m^4
β	$=$ $\left[\dfrac{GJ_t}{EC_w}\right]^{1/2}$		$=$	0.00031	
e	:	Vertical offset of shear center	$=$	$\dfrac{3h^2}{b+6h}$	
E	:	Young's modulus			
G	:	Shear modulus			

The component-wise model for the present problem employed 12 B3 elements along the beam length. The thin-walled cross section was meshed with 14 L9 Lagrange elements. All the cross section nodes of the first section were fully constrained. The torque was applied on two corner Lagrange nodes in the form of a couple at the free end of the beam.

The CW model results for the torsional analysis of channel beam are discussed as follows. The torsional displacement of CW model is shown in Fig.5.3. Magnitudes of torsional rotation and warping stresses obtained through analytical formulas and CW model are compared in Table 5.1. Figures 5.4a and 5.4b show comparison of the warping stress distribution in the vertical side wall and the floor for the CW and analytical models.
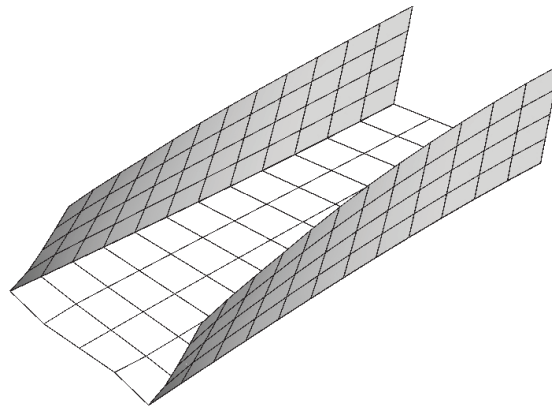
Figure 5.3 Torsional deflection of CW mesh for channel beam

Table 5.1 Maximum torsional deflection and warping stress in the channel

	Model (DOFs)	**Value**
$\theta_{\max}$ (deg)	Analytical (Eq.5.1)	0.04176
	CW (6525)	0.04289
σ_w (MPa) at Point **A** in Fig.5.2	Analytical (Eq.5.3)	4.06701
	CW (6525)	5.31933
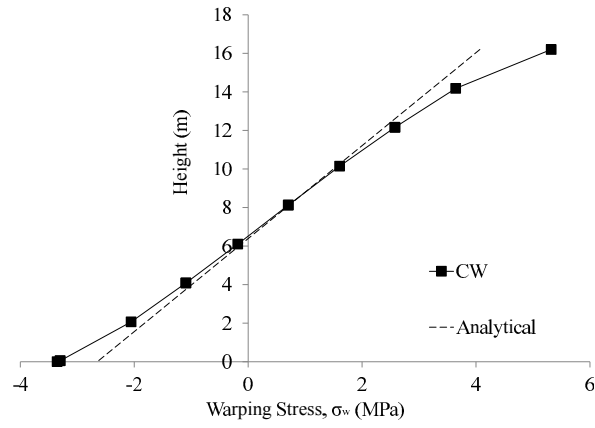
(a) Stress distribution in wall
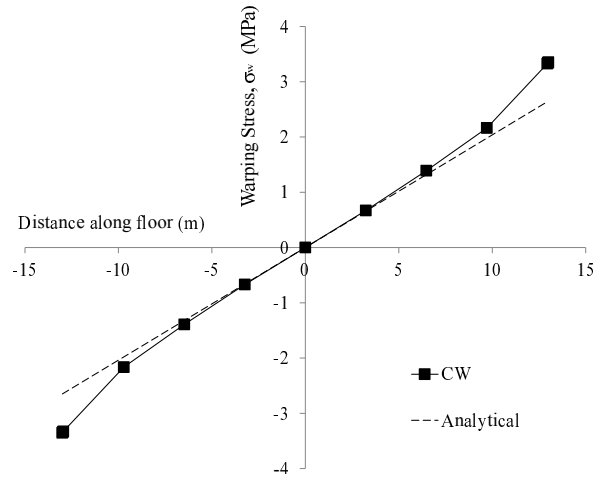
(b) Stress distribution in floor

Figure 5.4 CW and analytical warping stress plots

The results in Table 5.1 show that torsional displacements are satisfactorily captured by the CW model while the stress values for location A are reasonably close. The warping stresses shown in Fig.5.4 bear the same antisymmetric pattern as assumed by the warping function. The overall warping stress distribution from CW model is quite close to the analytical one except the values at the ends. Main reason for slight deviations is that the stresses employ derivatives of the displacements whereas the shape-functions of the elements are C^0 continuous and their derivatives are not continuous resulting is visible disunities in stress values at element interfaces or edges.

5.1.2   Case-2:   Container Ship Hull with Realistic Mid-ship Section

This section discusses the torsion of a container ship modelled as a prismatic single beam with a realistic mid-ship section. The loading and overall geometry is shown in Fig. 5.5 and the cross section geometry employed here is shown in Fig 5.6. The section is a multi-cell double-walled and its overall configuration resembles that of the channel analysed earlier. This way it is implied that the shear center lies below the keel and significant warping stresses will arise. The torsional load is distributed over the entire length of the ship and is in triangular form along the length to approximate the effect of a wave load.

Figure 5.5 Container ship torsional loading

Figure 5.6 Mid-ship section for a container ship (dimensions in mm)

The bow and stern of the ship have built-up construction and thus the out-of-plane warping is resisted. The torsional rotation is also resisted at the two ends. The ship

length is aligned with y-axis and the cross section is in x-z plane. The flexible portion has length 2a=L=120 m, being the length under torsion. The applied torque is 8100 ton-m. The ship width is 26 m and height is 16.2 m. The material is alloy steel. Figure 5.7 shows the CW mesh for the current analysis along with the loading. The arrows in the figure indicate the loading direction. A rigid wall is introduced at mid-length position which prevents the differential bending and ensures the torsional behaviour. The CW model employed 11 Lagrange (B3) elements along the length and the cross section was meshed using 76 L9 elements. The analysis was also performed using ANSYS solid element SOLID-185 in order to compare the computational efficacy.
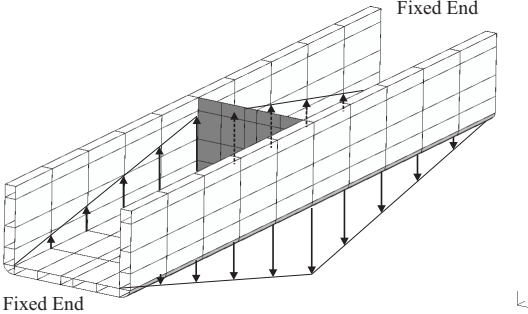
Figure 5.7 CW model with loading and constraints

The deflections from the CW and ANS3D models are shown in Fig 5.8 whereas the warping stresses over an inner edge located in constrained section are plotted in Fig 5.9. The CW model required 31473 DOFs while those required by ANS3D were 762264. The results clearly show the two stress distributions closely match and that the pattern is indicative of anti-symmetric distribution. Achieving close accuracy of the results of 3D solid elements through a few DOFs establishes the computational advantage of CW models. The CW results also imply that thin-walled section comprise of lagrange elements with large aspect ratios yet affording accurate solid-like results. This, in case of solid elements, requires a heavy mesh to avoid element shape warnings and thus warrants computationally a heavy mesh.

(a) CW deformed mesh, Max. displace-
ment=1.033 mm (DOF=31473)

(b) ANS3D deformed mesh, Max. dis-
placement=0.99 mm (DOF=762264)
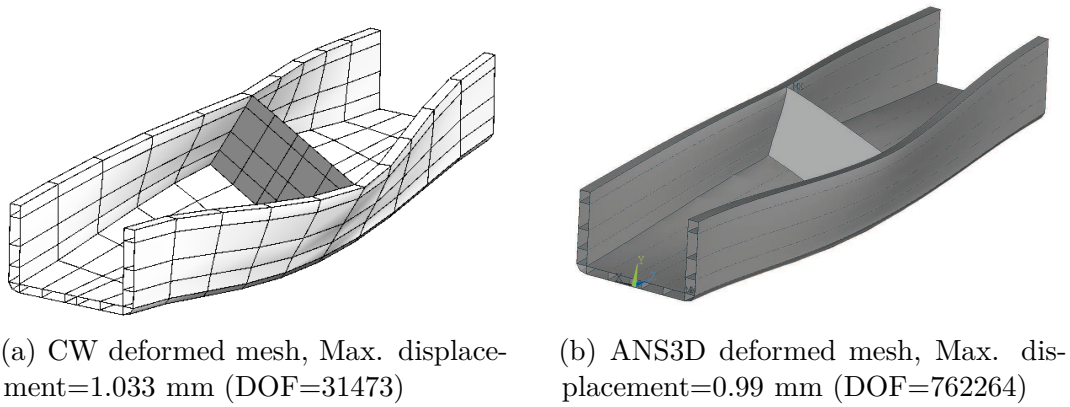
Figure 5.8 Torsional deflection of CW and ANS3D models
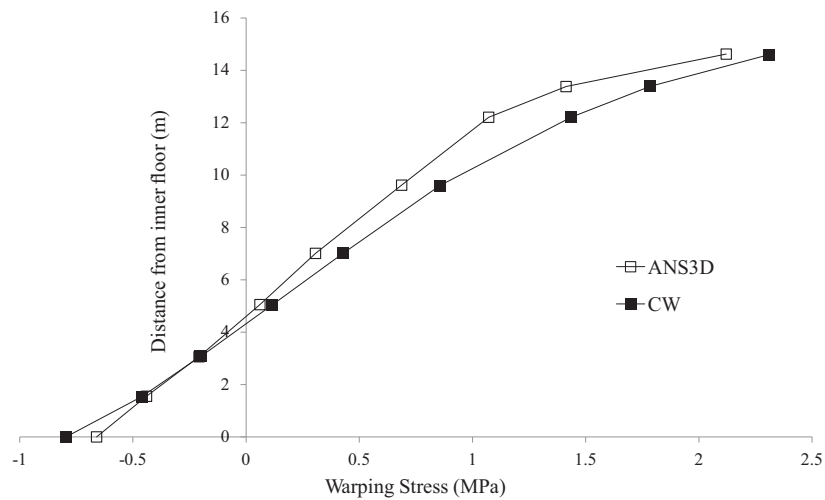
Figure 5.9 Comparison of warping stress distribution over the inner vertical wall in
constrained plane

Chapter 6

Multiple Beams for a 3D Hull

The strength of the Component-wise (CW) models for thin walled idealization of ship hulls using single and prismatic beam models is well established through the results of previous chapters. The CW models will now be discussed for much realistic sections that entail inclined boat faces which are typical feature of any boat hull. The complex shaped boats analysed in this chapter comprise of various 1D beams connected to each other at angle so the problem dimensionality is 3D. Finally, the results of CW models are then compared to those from 3D element of a commercial software.

6.1 Rotated Beam Configuration

In earlier cases discussed, the configurations comprised of structural features, e.g. walls, floors or bulkheads, that were all mutually orthogonal. For this reason, only a single beam model was required that could accommodate cross section changes. Change of cross section was incorporated by associating every cross section to a beam node. In this chapter, the idea is extended to relatively complex models employing:

a Features such as hull walls, floors or bulkheads are not necessarily mutually perpendicular

b Thin-walls can be conveniently modelled as beams with beam length being the wall thickness while the large face of the wall modelled as beam's cross section. Thanks to Carrera Unified Formulation (CUF), the extra ordinary aspect ratios do not affect results since the beam interpolation functions are independent of cross section expansion functions . . .

In such models individual beams are *rotated* to assume the slanted position relative to the other beam in a global reference system. Carrera and Enrico [23] introduced

the idea of beam rotation for CUF whereby the stiffness and displacements matrices of rotated beams were calculated in global reference system instead of local one. Thus, the final structure was an assembly of various beams connected with each other at Lagrange nodes.

Consider, for example, a hull wall and a floor inclined to the axes of global reference system as shown in Fig.6.1. The two structural components have an arbitrary oreintation with respect to the global reference system and their wall thickness is much smaller than the other dimensions of the face. CW approach allows the face to be considered as the cross section Ω and the wall thickness as beam length l. Classical beam models will give highly erroneous results for such *beam* configuration. The 3D FEM, on the other hand, requires a very fine mesh to avoid shape warnings arising because of highly distorted solid elements. The 2D shell elements do not give accurate results, especially at the interface edges of structural components.
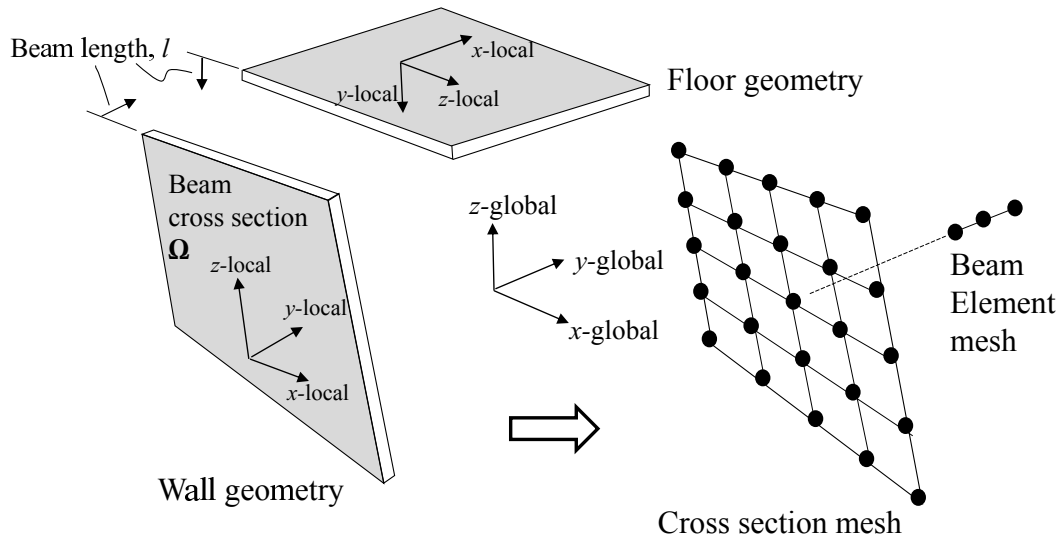
Figure 6.1 A wall and floor represented as rotated beams

6.2   3D Boat Configurations

Employing rotated beams as structural components, CW models were developed and analysed for the three boat configurations shown in Fig.6.2. The configuration-1 as shown in Fig.6.2a has four faces inclined to vertical plane while other faces are parallel or perpendicular to vertical plane. The hull in configuration-2 (Fig.6.2b) includes faces inclined to both vertical and horizontal planes. This configuration is further made complex by introducing a cabin in configuration-3 (Fig.6.2c). In the discussion

to follow, a modal analysis for the three configuration is presented which is followed by a static analysis performed on configuration-1.

(a) Configuration-1: Boat with One-sided tapered Wall

(b) Configuration-2:Boat with Two-sided tapered Wall

(c) Configuration-3: Cabin added to the boat with two-sided taper
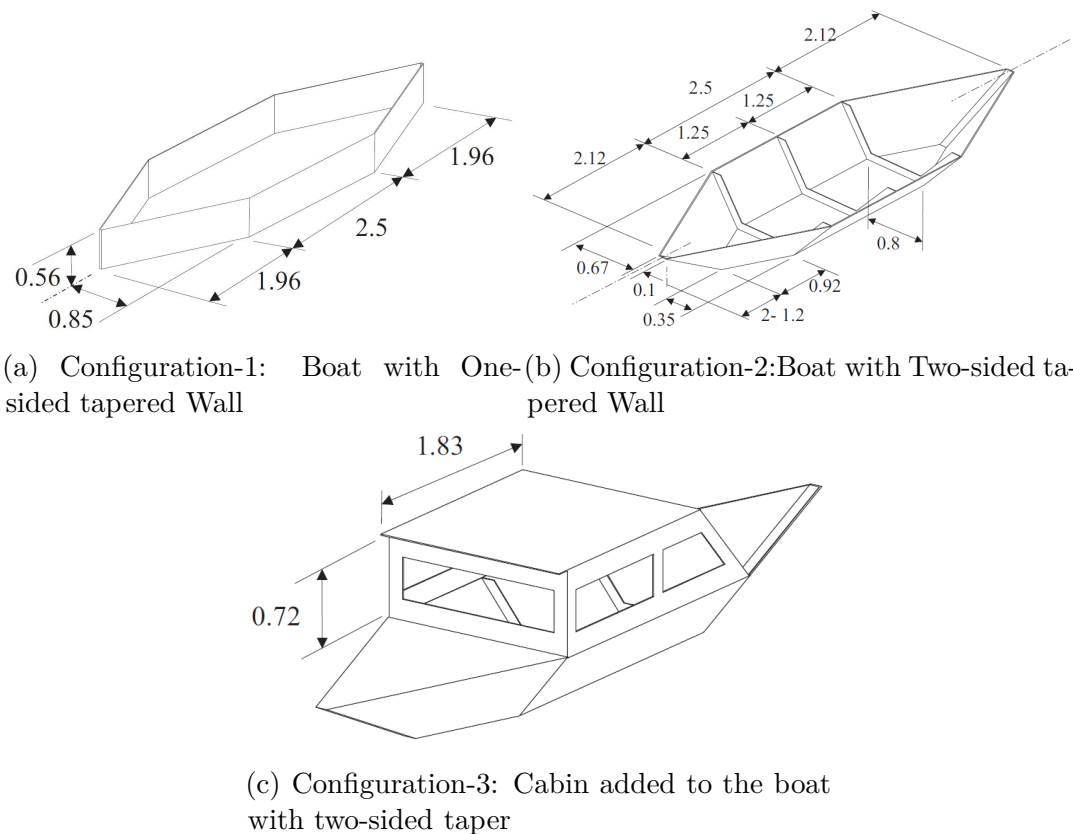
Figure 6.2 Boat geometries with tapered walls incorporated in front and rear (all dimensions in meters, all wall thicknesses are 10 mm and ribs are 100 mm wide

6.2.1 Modal Analysis

Modal analyses of the three configurations shown in Fig.6.2 were performed and the mode shapes and natural frequencies obtained from CW model were compared to those from ANSYS. It is clear that given the complexity of geometry of these models, they cannot be modelled using classical beam theories and 2D/3D FEM require heavy mesh rendering the computations heavy.

From the results of the CW and ANS3D models, a comparison of the natural frequencies for the three configurations is given Tables 6.1 and 6.2 and various modes are compared in Figs.6.3 to 6.5.

The results of the modal analyses clearly establish the efficacy of CW models over commercial software by requiring much less DOFs (6777 for configuration-1, 12825 for

Table 6.1 Comparison of natural frequencies for the three boat configurations of Fig.6.2

(DOF)	CW (6777)	ANS3D (193425)	CW (12825)	ANS3D (217539)
	Configuration-1 Fig.6.2a		Configuration-2 Fig.6.2b	
Mode 1	7.522	7.433	15.831	14.937
Mode 2	10.498	10.835	20.126	18.434
Mode 3	13.462	13.485	25.478	25.130
Mode 4	14.527	14.608	28.022	28.201
Mode 5	22.020	23.420	28.276	28.866
Mode 6	24.286	24.390	32.072	33.230
Mode 7	27.857	25.331	32.899	34.315
Mode 8	29.087	26.696	37.542	38.260
Mode 9	29.436	32.591	41.307	39.019
Mode 10	30.105	33.967	43.371	44.954

Table 6.2 Selected natural frequencies for the boat Configuration-3 of Fig.6.2c

(DOF)	CW (19125)	ANS3D (434130)
Mode 3	22.840	19.402
Mode 4	26.490	25.019
Mode 8	50.080	48.717
Mode 11	57.460	53.662

(a) Config-1, Mode-1: CW Model

(b) Config-1, Mode-1: ANS3D Model

(c) Config-1, Mode-2: CW Model

(d) Config-1, Mode-2: ANS3D Model
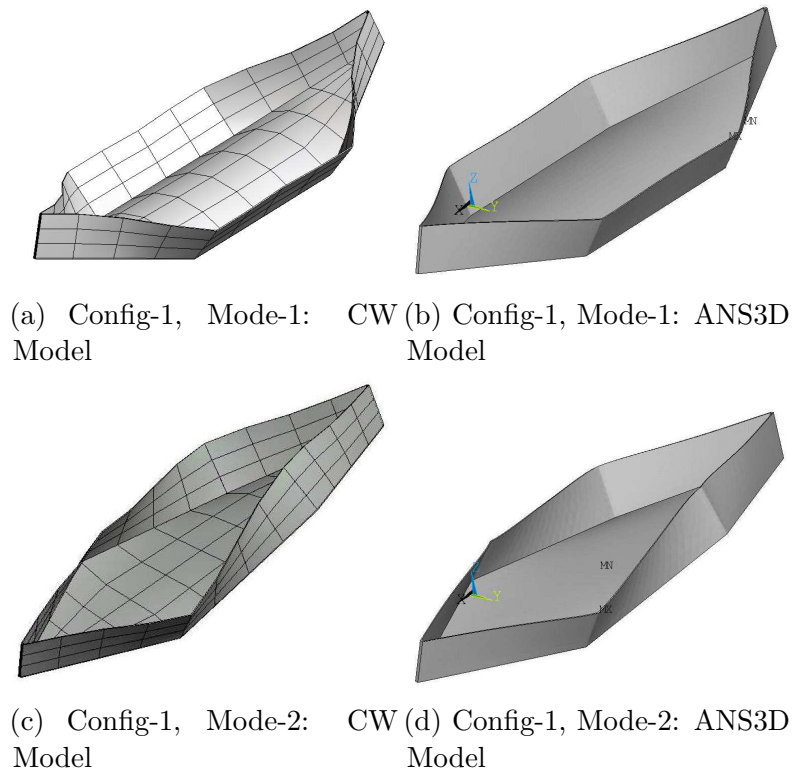
Figure 6.3 Comparison of the first two mode shapes of configuration-1

(a) Config-2, Mode-1: CW Model

(b) Config-2, Mode-1: ANS3D Model

(c) Config-2, Mode-2: CW Model

(d) Config-2, Mode-2: ANS3D Model
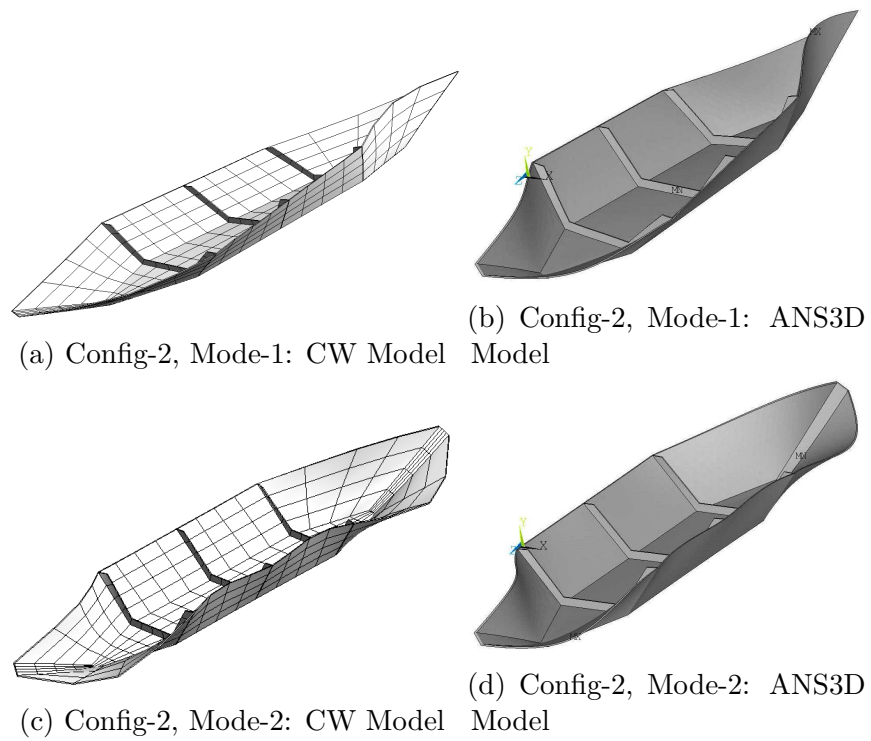
Figure 6.4 Comparison of the first two mode shapes of configuration-2

(a) Config-3, Mode-1: CW Model

(b) Config-3, Mode-1: ANS3D Model

(c) Config-3, Mode-2: CW Model

(d) Config-3, Mode-2: ANS3D Model
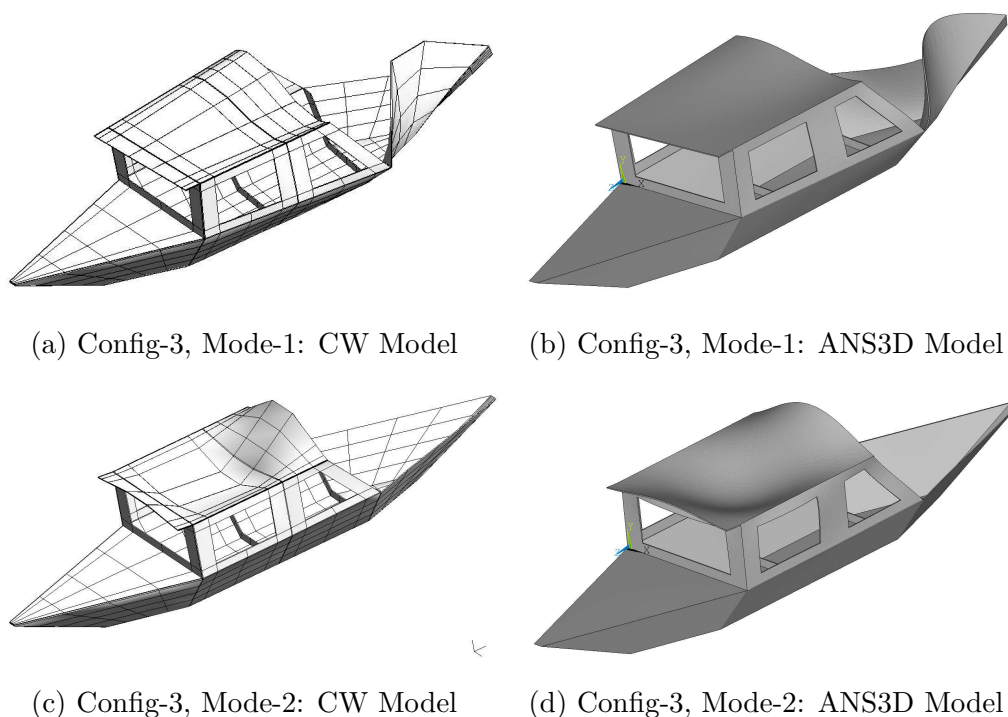
Figure 6.5 Comparison of the third and forth mode shapes of configuration-3

configuration-2 and 19125 for configuration-3) compared to ANS3D which required respectively 193425, 217539 and 434130 DOFs to achieve close values of natural frequencies. Except for some modes , the values in general are quite close even for higher modes. The observed discrepancies can be overcome by refining mesh along particular directions to which the respective mode is sensitive. In general, the mode shapes from CW and ANS3D models are very much same. These results demonstrate that complex 3D geometrical configurations, such as boat hulls with slanted faces, are easily modelled using CW models with relatively much less computational cost.

6.2.2 Static Analysis

The boat Configuration-1 was chosen for a static analysis to demonstrate further the computational capability of CW models. The loading and boundary conditions are shown in Fig.6.6. A point load of 1kN was applied at point located in the middle of the floor and on its upper face. The boundary conditions were simply-supported applied to the two bottom edges on either sides of the boat. Two points A and B were chosen as shown in Fig.6.6 for the values of deflections and stresses. The deflections

at the two locations and stresses at point A are given in Table6.3. A deformed mesh is plotted in Fig.6.7.
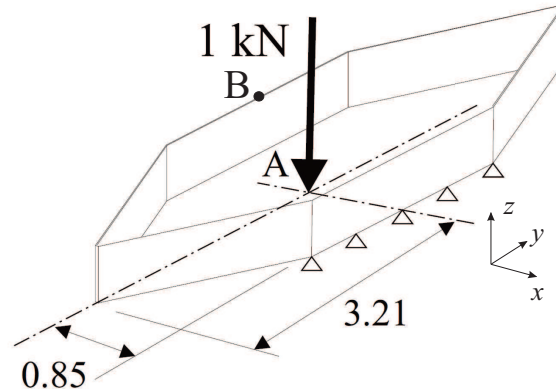
Figure 6.6 Point load and boundary conditions for static analysis for configuration-1 (all dimensions in meters and all wall thicknesses are 10 mm)

Table 6.3 Results under the loading shown in Fig. 6.6

Point	Model (DOFs)	Displacements (mm)		
		u	v	w
A	CW (6777)	0.000	0.000	-3.781
	ANS3D (193425)	0.000	0.000	-3.673
B	CW (6777)	1.754	0.000	-0.002
	ANS3D (193425)	1.732	0.000	-0.002

Point	Model (DOFs)	Stresses (MPa)		
		σ_{xx}	σ_{yy}	σ_{zz}
A	CW (6777)	7.72	9.57	0.619
	ANS3D (193425)	7.65	6.93	0.737

The results of the static analysis clearly demonstrate that the CW model captures the displacements accurately and the magnitude of the displacements is very close to those of 3D solid elements of ANSYS. This accuracy is achieved requiring much lower DOFs and the high aspect ratio of the CW elements has not affected the accuracy of the results. The results of the stresses are however not satisfactory for all stress components. Indeed, further mesh refinement along the thickness direction can improve

(a) Static Deflection from CW beam (b) Static Deflection from AN-
model   SYS
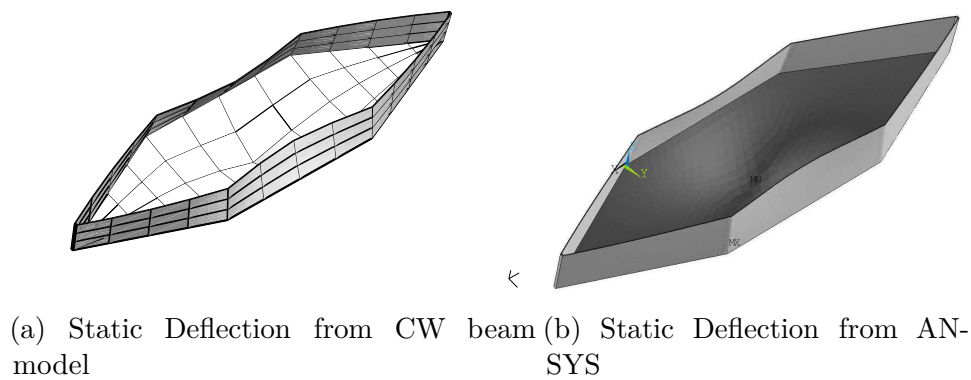
Figure 6.7 Deflected plots for boat under the loading shown in Fig. 6.6

the results. Many stress components obtained from the CW models have very close
magnitudes to the values from a commercial software in over-all stress distribution.
However, since the stress is calculated from the derivatives of the displacements, they
are discontinuous at the element interfaces.

6.2.3   Conclusion

The global structural response of the ships and barges *in vacuo* (without water) was
satisfactorily captured using CW models based on CUF. The free vibration and static
analyses of these models were performed. The open-hatch configuration of such vessels,
e.g. container ships, exhibit warping displacements and stresses and present CW
models captured them within close approximation to the analytical and commercial
software results. The analyses were performed following the practices in published
literature for global bending and torsional behaviour. The results of modal and static
analysis were compared to analytical and commercial software. For very simple cases
where the analytical solution was available, the CW models produced accurate results.
The results additionally comprised of in-plane and out-of-plane displacements which
could not be captured using analytical models. The CW models also proved their
efficacy over commercial 3D solid finite element models as the former required much
less DOFs compared to the ANSYS yet affording quite accurate results. The thin-
walled configurations had high aspect ratio (cross section dimensions to beam length
length) which, in case of 3D solid elements, generates distorted solid elements unless
a very fine mesh is employed. CW models, on the other hand required fewer elements
that produced accurate results even with elements of higher aspect ratios.

Part II

Numerical Results
Hull under Hydrostatic and
Hydrodynamic Loads

Chapter 7

Buoyancy as Elastic Foundation

The CW models based CUF were employed to simulate the structural analyses of dry hull configurations of marine vessels in previous chapters. Global bending, torsion and vibration modes were analysed involving typical boundary conditions of a structure in vacuo. This part of the thesis introduces buoyancy as boundary conditions applied to the realistic 3D geometries of marine vessels. Component-wise model are best suited beam models for this purpose as their physical surfaces can easily be attached to 1D buoyancy springs. Initially, the idea is validated for simple cases. Then various scenarios such as rigid-body and flexible body deflections, structural behaviour under still waters and wave loads have been studied and validated through well known examples.

7.1 FEM Beam as a Floating Vessel

A floating vessel may be considered as a beam floating in water. Taking advantage of CW model (introduced in Chapter 4) the floating vessel may be modelled as prismatic beam using two possible approaches:

  a Vessel modelled as a beam with beam length along the vessel's longitudinal axis or ship length regarded as *Hull Beam Model*

  b Vessel modelled as a beam with beam length along vessel height *Hull Planform Model*

7.1.1 Hull Beam Model

This approach is illustrated in Fig.7.0c. The ship length is along y-axis which is the beam axis and is perpendicular to gravity. The beam cross section is along $x - z$ plane

which is perpendicular to horizontal plane. The ship is prismatic along its length but cross sections can take arbitrary shape. Utilizing this approach, many vessel with arbitrary section shapes have been analysed in this thesis. For this case, $\mathbf{K}_{HS}^{ij\tau s}$ will have non-zero terms only for the submerged nodes lying on contours of each beam section (colored in blue in Fig.7.0c).

7.1.2 Hull Planform Model

This approach is illustrated in Fig.7.0d. The ship height is along y-axis which is the beam axis and is parallel to gravity. The beam cross section is along $x - z$ plane which is parallel to *keel*. The ship is prismatic along its height but cross sections can take arbitrary shape. Utilizing this approach, many vessel with arbitrary section shapes have been analysed in this thesis. For this case, $\mathbf{K}_{HS}^{ij\tau s}$ will have non-zero terms only for the nodes falling at the first beam section (i.e. $i, j = 1$).

The remaining of the thesis discusses various vessel shapes analysed by either of the two approaches. The choice of using one of the two modeling approaches is arbitrary. The hull beam model has the advantage that arbitrary hull sections can be analysed through this approach and the planform model allows to model planform of any arbitrary shape. Both model mesh geometries are prismatic in nature. That is, beam section cannot be varied within a single element. At present, the two approaches could not be combined and this can be useful a future work. Chapter 7 to 11 of this thesis utilize the hull beam model approach except at a few places where planform approach is used. Thereby, the beam cross sections are ship's transverse sections.

7.2 Elastic Beam on Winkler Foundation

Structures floating on water can be modeled by considering them resting on elastic foundations which in case of water is the buoyancy force. The ships have been repeatedly represented over the years as simple continuous beams resting on springs to demonstrate certain fundamental structural aspects such as ship vibration. As shown in Fig. 7.1 from Ref [58], the ship is represented as an Euler beam with springs and dampers attached to it simulating the effect of buoyancy. The ship is subjected to a forcing function $f(x, t)$ applied near the stern as a result of propeller vibrations.

The beams on elastic foundation have been studied in detail by Hetenyi [38] and it will be shown that the same approach works well when elastic foundations are
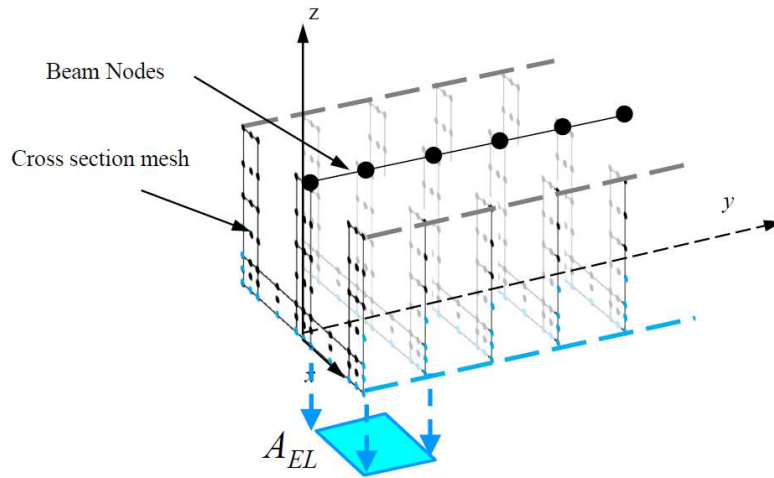
(c) Beam elements along ship length
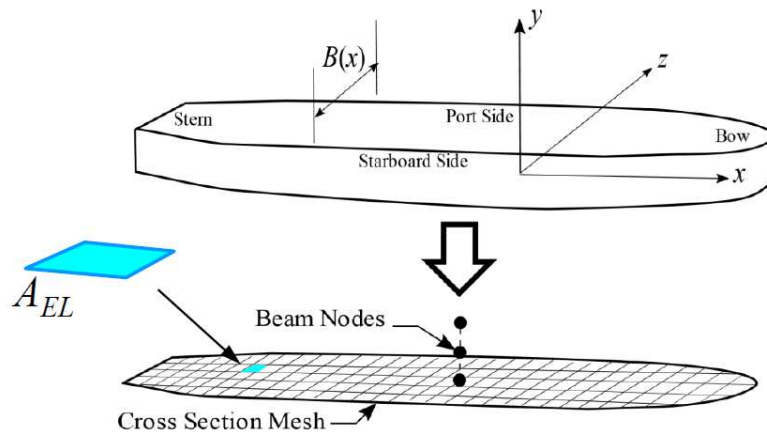
(d) Beam elements along ship height

Figure 7.0 Two ways to model ship with hydrostatic stiffness
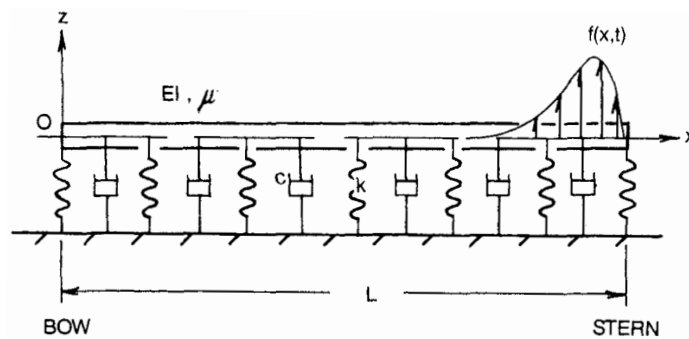
Figure 7.1 Ship hull beam model, Ref. [58]

applied to CW models. This chapter presents validation of CW models using elastic foundations as boundary condition for beams.

Referring to Fig. 7.2 consider a square cross section beam under such conditions with a point load **P** acting at mid-length and the ends of the beam being free. The beam cross section has sides b and length l. The vertical beam deflection z at a point located at distance y from point C generates reaction force per unit beam length in underlying material which is $kz = bk_{\text{o}}z$ [N/m²]. Thus, $k = bk_{\text{o}}$ is the reaction force to produce unit vertical deflection over span of unit beam length. The term k_{o} is the foundation modulus [N/m³]. The symbol λ denotes $\sqrt[4]{k/4EI}$ where EI is beam rigidity. The deflection z is given using Eq. 7.1 from Ref [38]:

$$
\begin{aligned}
z = \frac{P\lambda}{2k} \frac{1}{\text{Sinh}\lambda l + \sin\lambda l} & [\text{Cosh}\lambda y\cos\lambda(l-y) + \cos\lambda y\text{Cosh}\lambda(l-y)- \\
& \text{Sinh}\lambda y\sin\lambda(l-y) + \sin\lambda y\text{Sinh}\lambda(l-y) + 2\text{Cosh}\lambda y\cos\lambda y]
\end{aligned}
\tag{7.1}
$$
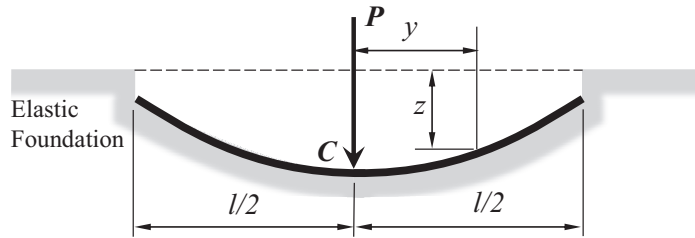
Figure 7.2 Schematic of analytical beam model resting over elastic foundations

7.3   Addition of Buoyancy Springs

The effect of buoyancy can be modelled by employing 1D linear springs attached to the beam mesh as boundary conditions. Thanks to the CW approach, the beam mesh has physical nodes on the outer surface much like a 3D solid mesh. Let N_{BS} be the number of nodes of the original beam mesh that are in contact with water where the subscript BS stands for "Buoyancy Springs". Then, there will be N_{BS} springs with their upper nodes connected to those beam nodes while their other ends are fixed to the ground (See Fig 7.3).

Let $\mathbf{K}_B$ denote the stiffness matrix of the beam mesh for which Fundamental Nuclei $\mathbf{K}^{ij\tau s}$ were derived using Eq. 3.8. It has dimensions $N_B \times N_B$ and correspondingly, the force and displacement vectors have dimensions $N_B \times 1$. Here N_B denotes the
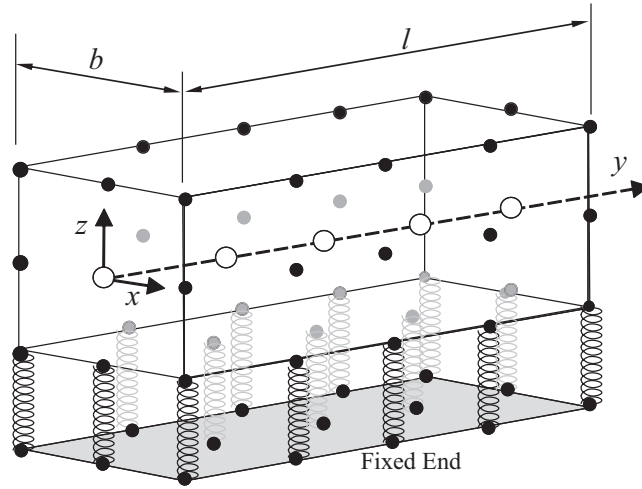
Figure 7.3 Finite element model of beam on elastic support

total DOFs for all the nodes of beam mesh. For M nodes in a cross section mesh and N_N beam nodes, $N_B = 3 \times m \times N_N$.

The stiffness matrix $\mathbf{K}_{BS}$ of a 1D spring element can be obtained by considering the element shown in Fig. 7.4.
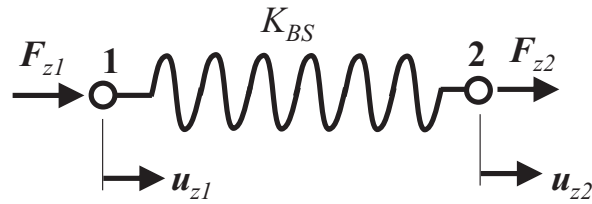
Figure 7.4 Loads and displacements of 1D spring element

Thus, the loads and displacements for the 1D spring are related through Eq. 7.2:

$$\begin{bmatrix} K_{BS} & -K_{BS} \\ -K_{BS} & K_{BS} \end{bmatrix} \begin{Bmatrix} \mathbf{u}_{z_1} \\ \mathbf{u}_{z_2} \end{Bmatrix} = \begin{Bmatrix} \mathbf{F}_{z_1} \\ \mathbf{F}_{z_2} \end{Bmatrix} \tag{7.2}$$

Procedure to determine spring constant is mentioned later in this section. The final stiffness matrix is obtained by assembling the original beam stiffness $\mathbf{K}_B$ and the spring stiffness matrices $\mathbf{K}_{BS}$. The DOFs are shared for the nodes where buoyancy springs are connected to the existing beam mesh. Thus the only additional DOFs added to the total system are associated to the grounded ends of the buoyancy springs which are $3 \times N_{BS}$ corresponding to the three components of displacement; x, y and z.
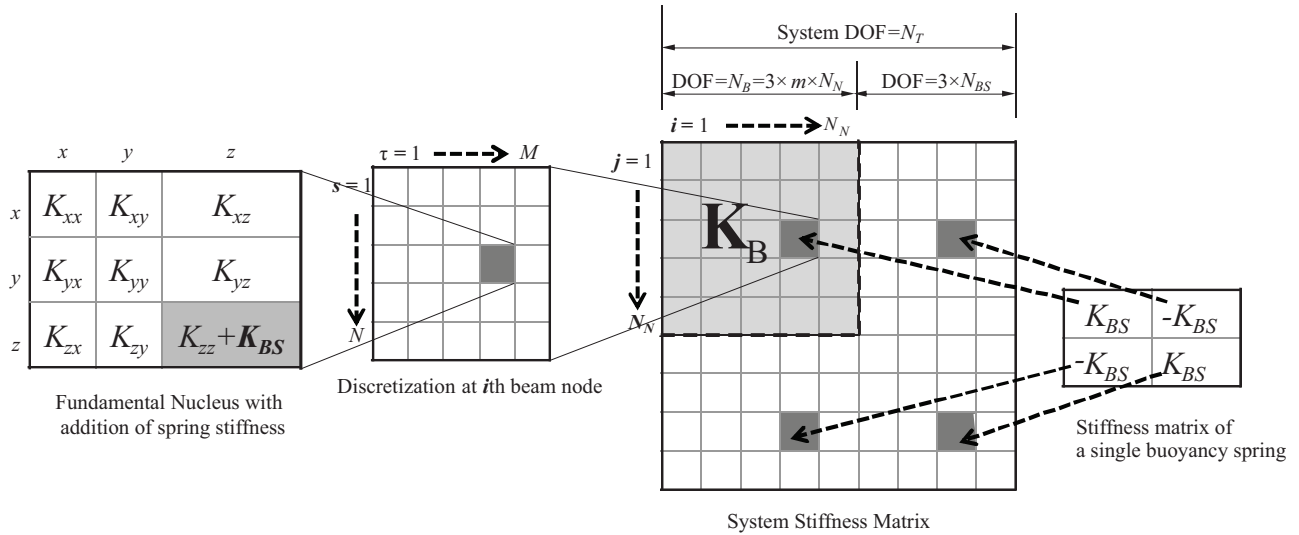
Figure 7.5 Procedure for assembling single spring stiffness into system stiffness

The stiffness $\mathbf{K}$ of complete system is now an assembly of original beam stiffness $\mathbf{K}_\mathrm{B}$ and the stiffness of N_{BS} buoyancy springs $\mathbf{K}_{BS}$. Fig. 7.5 elaborates the assembly procedure adopted to assemble an individual spring into the stiffness matrix of the system. The system stiffness matrix will have the size $N_T \times N_T$ where $N_T = N_B + (3 \times N_{BS})$. It can be observed that out of four terms of stiffness matrix of Eq. 7.2, only one term is added to the matrix $\mathbf{K}_\mathrm{B}$ for the shared nodal location. The other three correspond to the grounded DOFs of springs.

7.3.1   Determining Spring Constant

The total buoyancy force on the floating structure acts like a spring with cumulative stiffness of all springs as K_T allowing a displaced weight of $W = \rho_\mathrm{w} g A_\mathrm{T} l$ to displace through a distance h. This can be written as Eq. 7.3.
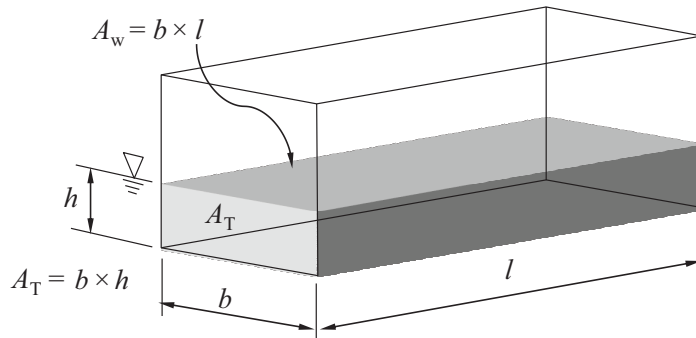
Figure 7.6 Floating beam with rectangular cross section

$$h = \frac{\rho_{\text{w}} g A_{\text{T}} l}{K_{\text{T}}} \tag{7.3}$$

where

ρ_w :   Density of sea water $[\text{kg/m}^3]$

g :   Gravity constant $[\text{N/m}^2]$

K_{T} : :   Total buoyancy stiffness $[\text{N/m}]$

A_{T} : :   Area of the immersed region in the transverse plane $[\text{m}^2]$

Figure 7.6 shows a rectangular section beam under floating equilibrium. For this case, $A_{\text{T}} = bh$, Eq. 7.3 becomes:

$$h \quad = \quad \frac{\rho_{\text{w}} g b h l}{K_{\text{T}}}$$

or $K_{\text{T}} = \rho_{\text{w}} g b l$. Since from Fig. 7.6, $bl = A_{\text{w}}$, we have $K_{\text{T}} = \rho_{\text{w}} g A_{\text{w}}$ and finally we get:

$$K_{\text{T}} = k_{\text{o}} A_{\text{w}} \tag{7.4}$$

where k_{o} is defined as foundation modulus of water.

As evident from Figs. 7.6, the buoyancy springs will act vertically only at the bottom face with area $A_{\text{w}} = bl$. This area is contained at the water-plane and is purely the projection of the bottom face of the beam for the rectangular section beam.

Each buoyancy spring is attached to a node from beam mesh above it. Thus, the area A_{w} can be considered as meshed with 9-noded Lagrange elements. The total buoyancy stiffness acting on a Lagrange element is considered divided and lumped into its nine nodes. Mathematically, the spring stiffness over the area of Lagrange element can be written as:

$$K_{\text{EL}} = k_{\text{o}} A_{\text{EL}} \tag{7.5}$$

where the subscript EL stands for Lagrange Element. The area A_{EL} may have arbitrary shape and can be obtained employing shape functions F_{τ} give by Eq.A.1. That is:

$$K_{\text{EL}} = k_o \int_{\Omega} F_{\tau} F_s d\Omega, \quad \tau, s = 1...9 \tag{7.6}$$

This nodal stiffness acts along gravity axis and becomes a component of Fundamental Nuclei $\mathbf{K}_{HS}^{ij\tau s}$ representing Hydrostatic Stiffness matrix (See Eq. 3.26).

Iterative Procedure to Determine the Draught, h

In the procedure above, the area A_{w} was determined (and consequently the buoyancy spring constant) if the draught h is known a priori. In this section, the procedure is explained whereby h is determined through an iterative procedure when h is unknown. The procedure is illustrated in a flow chart shown in Fig. 7.7 and an example as follows.
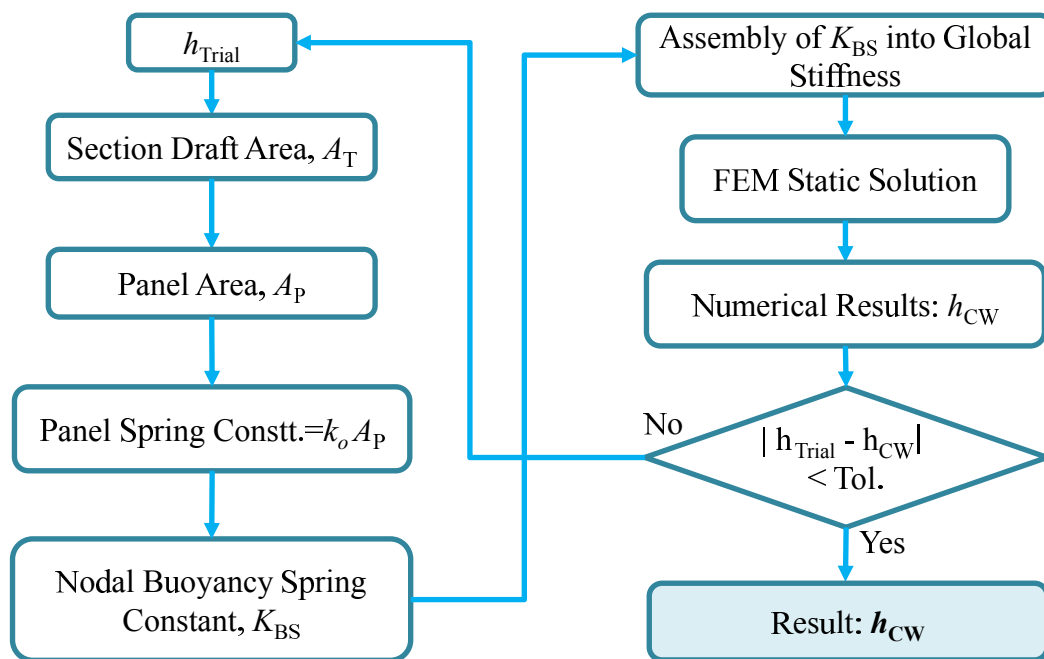
Figure 7.7 Iterative procedure to determine draught depth, h

A vessel is considered with front view shown in Fig.7.8. The vessel has length of 7 meters and the material is aluminum. The objective is to determine the draught depth h at equilibrium as the vessel descends under gravity. The procedure physically resembles the way a typical vessel is lowered below a water line until an equilibrium is reached.

The numerical procedure begins by iteratively assuming trial draught values denoted here as h_{trial}. Running the numerical solution, the CW model returns a draught value h_{CW} which may have a certain degree of deviation d from the assumed draught.
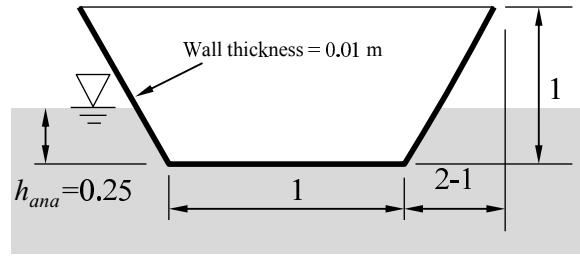
Figure 7.8 Front view of the vessel (all dimensions in m)

The deviation is thus defined as follows:

$$d = |h_{\text{CW}} - h_{\text{trial}}| \tag{7.7}$$

Amongst these deviations obtained against each iteration, the solution corresponding to the smallest deviation, falling within a prescribed tolerance, holds as the final draught value, h_{CW}. For present problem, the plot shown in the Fig. 7.9 shows this process where the following values are obtained:

$$
\begin{aligned}
d &= 0.001 \\
h_{\text{trial}} &= 0.25 \\
h_{\text{CW}} &= 0.249 \\
h_{\text{ana}} &= 0.25
\end{aligned}
$$
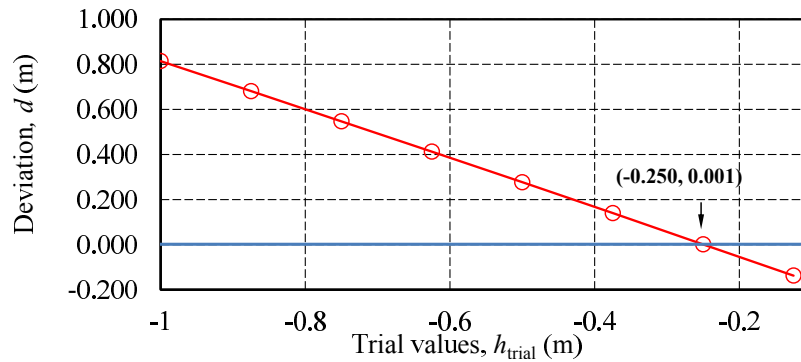
Figure 7.9 Plot of deviation values against iteration values

The converged value of draught h_{CW} can finally be compared to the analytical value h_{ana} obtained through the procedure previously explained.

7.4 Validation for Beam on Winkler Foundation

The analytical problem discussed in previous section has been numerically modeled using 1D Carrera Unified Formulation (CUF) [9] with *Component − wise* (CW) ap-

proach [13]. The advantage of CW model is that it affords displacements as degrees of freedoms which can be easily manipulated for further processing requirements. This facilitates ease of connecting other element types to the beam mesh. Figure 7.3 shows the mesh for CW beam model. The springs attached to the mesh provide the effect of elastic foundation. Beam length is along y axis while x and z axes are parallel to cross section. Beam has been meshed with the second order Lagrange polynomials (B3 elements [3]) with nodes shown as solid white circles along y axis and the cross section associated to each beam node comprises of a mesh of 9 noded Lagrange elements whose nodes are shown in solid black circles. The bottom surface of the beam is connected to springs that on the other ends are connected to the rigid ground. Thus, only the shared node between the beam and the spring can move.

7.5   Results and Convergence

The vertical deflection plots obtained through analytical (Hetenyi) and CW models are shown in Fig. 7.10. The figure clearly indicates the closeness between the two plots implying the suitability of CW for the present problem. Table 7.1 shows the convergence behaviour of vertical displacements for the beam with loading configuration shown in Fig. 7.2. The table shows results obtained using analytical model of Eq. 7.1 and three CW models with increasing beam elements. The results for CW model were obtained using 10, 15 and 30 B3 beam elements. The beam length is 20m and has square cross section with sides of 1 m. The beam material was aluminum with young's modulus $E = 72$ GPa and poisson's ratio $\nu =$0.3. The cross section was meshed with 1 Lagrange element. Following can be inferred from the results:

   Another convergence plot is shown in Fig.7.11 whereby vertical deflection of the mid point of the beam is plotted against varying beam elements as well as the cross section elements. Beam elements range from 5 to 30 in steps of 5 where as the cross section elements (Lagrange Elements, LE) vary as 1, 4 and 16 L9 elements per cross section. For the square section under study, all edges were regularly divided. The figure shows that all the CW plots converge towards analytical value of z=-0.49767 m. The convergence of cross section refinement is faster compared to the refinement along beam length.

   Based on the results of beam deflection and its validation, the following conclusions can be drawn:

   The effect of buoyancy on a partially submerged floating vessel is accurately simulated by employing 1D springs. Since the nodes are required to be physically attached
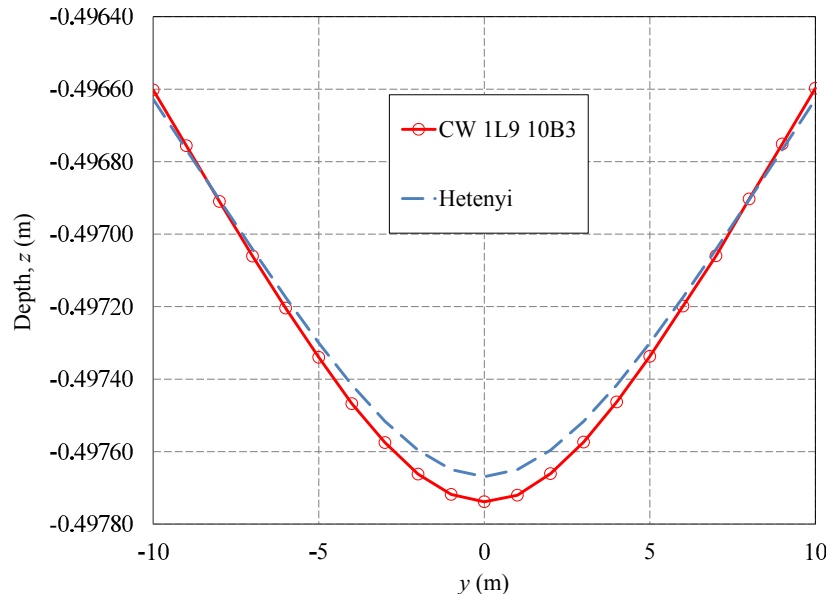
Figure 7.10 Vertical deflection of beam over elastic foundation

Table 7.1 Comparison of vertical deflections for beam loading shown in Fig. 7.2

y (m)	Hetenyi (mm)	10B3 (mm)	15B3 (mm)	30B3 (mm)
-10	-496.628	-496.603	-496.612	-496.625
-8	-496.905	-496.910	-496.909	-496.906
-6	-497.174	-497.204	-497.191	-497.184
-4	-497.416	-497.468	-497.448	-497.431
-2	-497.596	-497.662	-497.638	-497.618
0	-497.669	-497.738	-497.716	-497.694
2	-497.596	-497.661	-497.639	-497.620
4	-497.416	-497.463	-497.451	-497.431
6	-497.174	-497.198	-497.190	-497.184
8	-496.905	-496.903	-496.902	-496.908
10	-496.628	-496.597	-496.605	-496.622
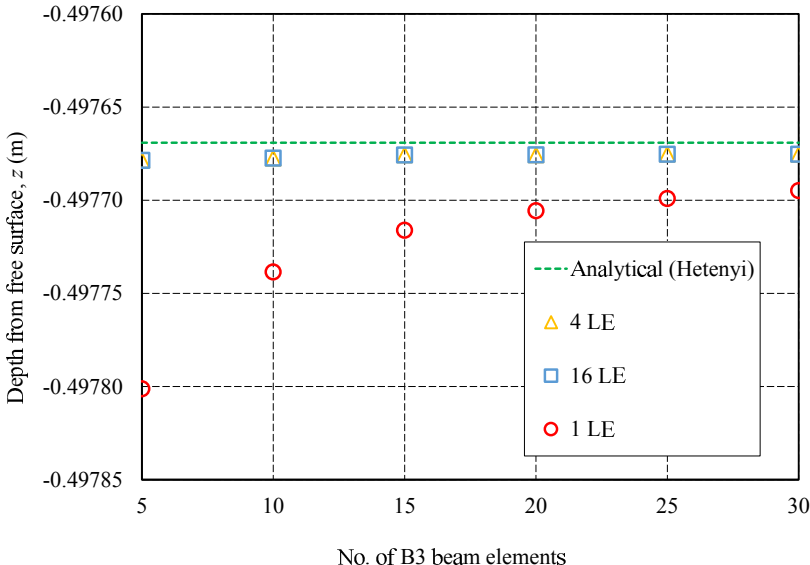
Figure 7.11 Convergence plots for vertical deflection of mid point

to the 3D nodal positions on the surface of the beam mesh, Component-wise (CW) models are best suited for this purpose.

The procedure adopted to determine the spring constant is validated as it affords results that are significantly close to the analytical solutions obtained for the beam resting on elastic foundation.

Chapter 8

Hulls with Slanted Immersed Faces

8.1   Corrected Water Plan Area

The idea of attaching Buoyancy Springs to the CW models was introduced in previous chapter. The beam involved flat surface at bottom so that the side walls did not receive the buoyancy forces. Towards achieving the main objective of modeling realistic ship hulls through CW models, this chapter introduces hull configurations that have immersed faces at an angle or are curved so that the buoyancy forces acting on them cannot be ignored.

(a) Floating beam with rectangular cross section

(b) Floating beam with trapezoidal cross section
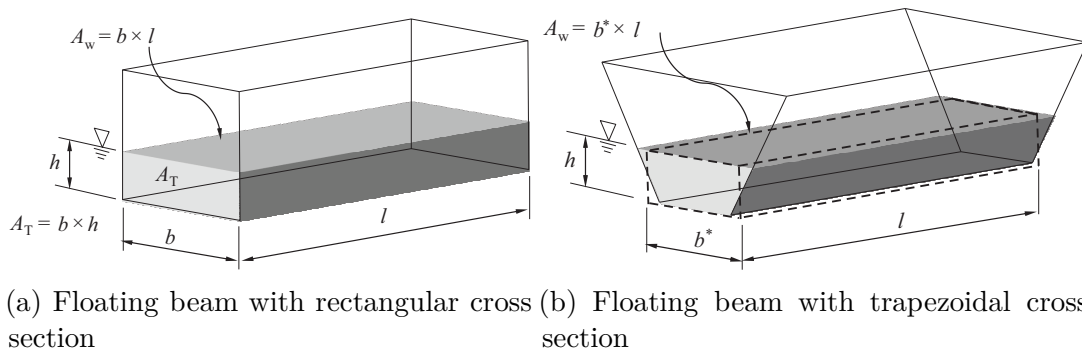
Figure 8.1 Beam geometries under floating equilibrium

As discussed earlier, the procedure to determine the spring constant K_{BS} involves determination of water plan area A_w (Eq.7.5). For simple rectangular section, (Fig.8.1a), A_w is $b \times l$ which is the exact projection of immersed areas on the free water surface. However, for the case of inclined immersed faces (Fig.8.1b), the area A_w is not simply

the projection of immersed regions. Instead, as shown, the area A_w is now $b^* \times l$. The dimension b^* is found from the transverse area A_T. The area A_T has a trapezoidal shape and can now be represented as a rectangle with depth h and width b^*. Thus, $b^* = A_T/h$. Generally, the immersed area A_T may assume any arbitrary shape depending on equilibrium conditions and vessel geometry. The aforementioned area A_w is now product of b^* and l and the total buoyancy stiffness can be found using Eq. 7.5.

8.1.1 Cases for Hulls with Slanted Faces

The capability of present model is genuinely highlighted through the structural analysis of realistic geometries of marine vessels. The procedure adopted begins by determining the transverse immersed area A_T and displacement depth h under equilibrium conditions. Analytically obtained water depth h thus can be compared to the one from CW model for various boat-like configurations. Cases of static deflection due to self weight for various boat-like configurations floating over water are shown in 8.2. All vessels have length $l = 7$ m. It is assumed that any wet face perpendicular to the water line is not acted upon by any buoyancy force. Thus, in the first three cases, the end walls have not been modelled for simplicity of the problem. However, presence of vertical walls do affect the stiffness of the vessel against structural deflection as is evident in the result from last case. Results for each case are presented in the following.

(a) Vessel-1

(b) Vessel-2
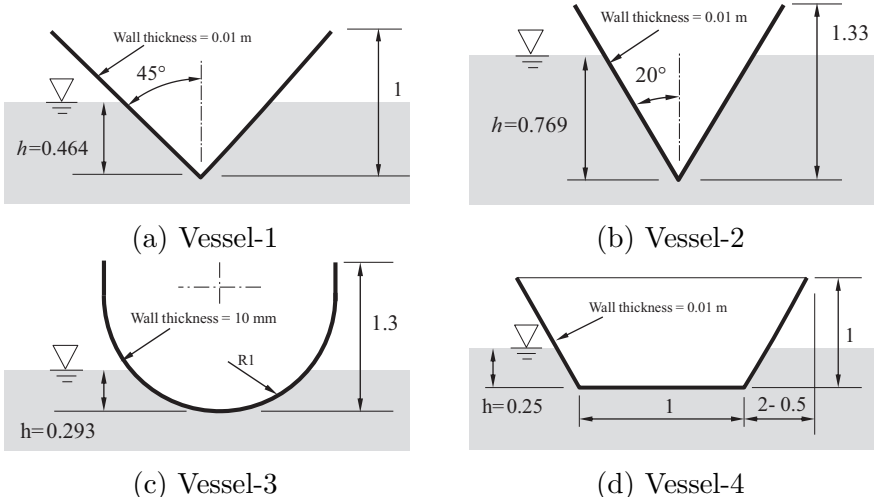
(c) Vessel-3

(d) Vessel-4

Figure 8.2 Transverse section of vessels 1 to 4 (all dimensions in m and drawn not to scale

Results for Vessel-1 to 4

Parameters and results of vertical deflection for the configurations shown in Fig. 8.2 are presented in the following Tables 8.1 to 8.4 and Figs. 8.3 to Fig. 8.6.

Table 8.1 Parameters and results for vessel-1

Vessel mass			=	1545.2	kg
Vessel length			=	7	m
Area, A_T			=	0.215	m^2
Area, A_w			=	3.2484	m^2
Results					
Displacement obtained analytically	h		=	-0.464	m
Displacement using CW model, Fig. 8.3	W_max	=	-0.4638	m
	W_min		=	-0.4678	m
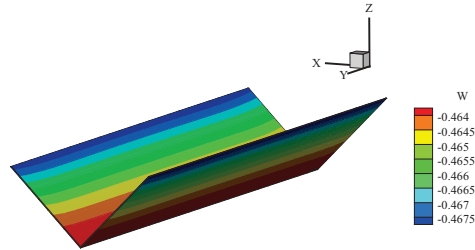
Figure 8.3 Vertical deflection of vessel-1 using CW model

Table 8.2 Parameters and results for vessel-2

Vessel mass			=	1545.2	kg
Vessel length			=	7	m
Area, A_T			=	0.215	m^2
Area, A_w			=	1.959	m^2
Results					
Displacement obtained analytically	h		=	-0.7692	m
Displacement using CW model, Fig. 8.4	W_max	=	-0.7662	m
	W_min		=	-0.7667	m
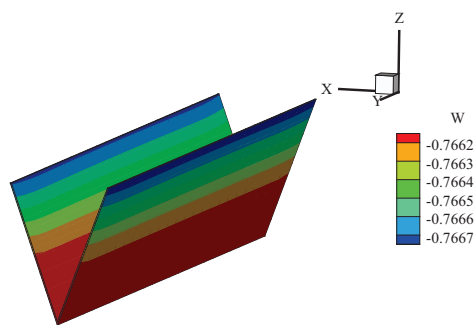
Figure 8.4 Vertical deflection of vessel-2 using CW model

Table 8.3 Parameters and results for vessel-3

Vessel mass		$=$	2047	kg
Vessel length		$=$	7	m
Area, A_{T}		$=$	6.818	m^2
Area, A_{w}		$=$	0.2853	m^2
Results				
Displacement obtained analytically	h	$=$	-0.2929	m
Displacement using CW model, Fig. 8.5	$W_{\max}$	$=$	-0.2912	m
	$W_{\min}$	$=$	-0.2919	m
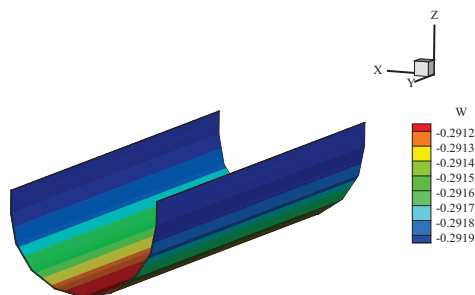
Figure 8.5 Vertical deflection of vessel-3 using CW model

Table 8.4 Parameters and results for vessel-4

Vessel mass		$=$	2001.67	kg
Vessel length		$=$	7	m
Area, A_T		$=$	0.2813	m^2
Area, A_w		$=$	7.875	m^2
Results				
Displacement obtained analytically	h	$=$	-0.2500	m
Displacement using CW model, Fig. 8.6	W_max	$=$	-0.2467	m
	W_min	$=$	-0.2522	m
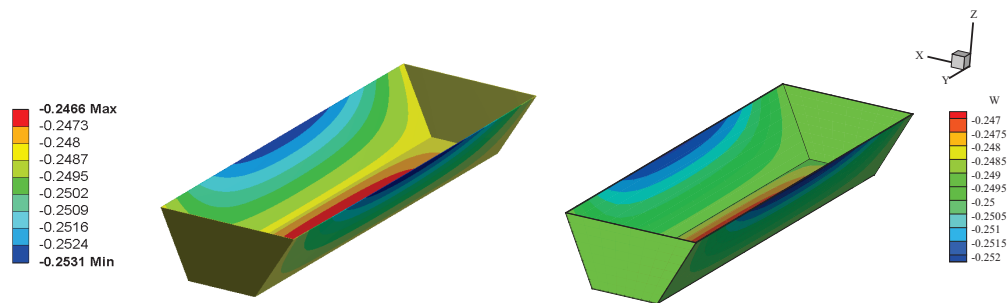
(a) Displacement plot in m from ANSYS solid mesh (DOF=105786) (b) Displacement plot in m from CW beam mesh (DOF=11332)

Figure 8.6 Vertical displacements plot of vessel-4 using ANSYS and CW model

8.1.2 Conclusion

The results discussed above for hulls with slanted faces are significantly close to the analytical ones. The four configurations analysed involve the flat as well as curved surfaces immersed in sea water. Moreover, since the structures are thin-walled, they exhibit localised deflections that are additional to the gross vertical deflection in water. Hence, the less stiffened regions are deflected downward due to weight or upward due to buoyancy. This is also in line with the fact that localised deflection is based on the net force balance of local weight and local buoyancy. It is clear from all the results that the average displacement from CW models is always the analytically obtained displacement for a rigid body. The results also indicate that the CW model of the floating body undergoes a pure vertical displacement as long as the center of buoyancy and center of gravity of the body are collinear. The cases with the points not collinear result in trim or list of the floating body which will be shown in the following chapter.

The results of Fig.8.6 show that the 1D CW model requires much less DOFs (11332) compared to ANSYS model (105786) with displacements close to within 1 percent of

difference. This way, the efficacy of CW models with buoyancy springs is sufficiently established and various scenarios of marine vessels will now be presented.

Chapter 9

Validation Cases: Trim in Still Water

9.1   Parameters

The discussion in this chapter involves rigid body positions acquired by a floating body under static equilibrium. The position of the floating body can be defined in terms of *parameters of equilibrium* and they are displacement, angle of heel and angle of trim. These parameters will be analytically calculated through relations given in any book on Hydrostatics such as Ref [4]. The hydrostatic behaviour for simplified geometries is also simulated using CW models with buoyancy springs and the obtained results are compared to analytical values. Following assumptions hold during the treatment of the problem:

   a. the water is incompressible;

   b. viscosity plays no role;

   c. surface tension plays no role;

   d. the water surface is plane;

   e. the floating bodies are perfectly rigid.

   Referring to Fig.9.1, the coordinate system, x_o-y_o-z_o, is global while the other is local and attached to the floating vessel. If the vessel inclines statically around x-axis,

it is termed as *trim*, denoted as θ in Fig.9.1a, and under dynamic (varying with time) as *pitch*. Similarly, a static inclination around y-axis, denoted as Φ in Fig.9.1b, is termed as *heel* if it is temporary and *list* if is permanent. The vessel, otherwise, is said to float at **even keel** if its y-axis is parallel to free water surface.

(a) Trim or pitch   (b) List or heel
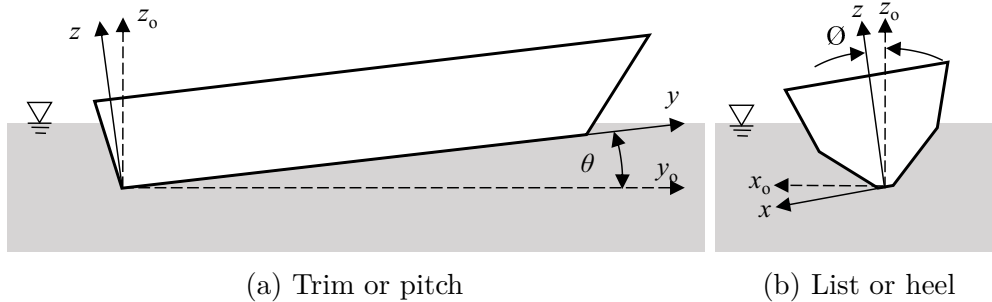
Figure 9.1 Ship inclinations under static equilibrium

9.2 Trim Calculation

A ship may undergo small angle of trim under the following conditions:

a. when the center of buoyancy and center of mass of the vessel do not lie in a vertical transverse plane (parallel to xz-plane);

b. an external load acts on the ship causing to disturb the equilibrium at even keel;

For present analysis, only the first of the above conditions is considered. This condition may arise due to shifting of cargo weight along the length. Referring to Fig.9.2, the trim calculations are given as follows. The objective is to find trim and two draughts, T_F and T_A at the two perpendiculars and the angle θ. These values will be compared to those from CW models for an example problem.
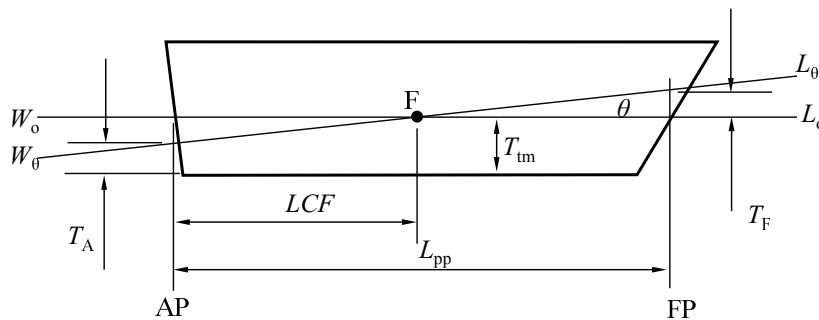
Figure 9.2 Forward and Aft draughts

Under the trim condition, the original water line denoted as W_oL_o now assumes a new position $W_\theta L_\theta$. The two lines intersect at Center of Floatation, F, located at a distance LCF (Longitudinal Center of Floatation) from AP. The mid-ship draught at even keel is denoted as T_m and is found from the hydrostatic curves for actual ship hulls. For simplified geometry such as box-like vessels, $T_m = \Delta/A_w$ where Δ=displaced volume of water and A_w=Water plan area. The trim is given through the following Eq.9.1:

$$trim = T_F - T_A = \frac{\Delta(LCG - LCB)}{MCT} \tag{9.1}$$

and the trim angle θ as :

$$\tan\theta = \frac{T_F - T_A}{L_{pp}} \tag{9.2}$$

where

LCG	:	Longitudinal Center of Gravity		
LCB	:	Longitudinal Center of Buoyancy		
MCT	:	Moment to change trim by 1 m	$=$	$\Delta GM_L/L_{pp}$
GM_L	:	Longitudinal Metacentric Height	$=$	I_L/Δ
I_L	:	Longitudinal Moment of Inertia of water plan area, A_w		

The ship trims around a horizontal transverse axis that passes through the center of floatation, F. The point F is the centroid of the water plan area A_w and can be geometrically calculated. Hence LCF is known and using the Fig.9.2 we can find the draughts at perpendiculars as:

$$T_A = T_m - LCF.\tan\theta = T_m - LCF.\tan\left(\frac{trim}{L_{pp}}\right) \tag{9.3}$$

and

$$T_F = trim + T_A = T_m + trim\left(1 - \frac{LCF}{L_{pp}}\right) \tag{9.4}$$

9.3 Numerical Example-1: Box-like beam

A simplified box-like solid beam is considered whose trim is calculated analytically using Eq.9.1 and CW model. The box has length l=100m, breadth, b=10m and

depth, d=10m. The solid model comprises of two dissimilar materials M1 and M2 with different densities ρ_1=0.7 gm/cm^3 and ρ_2=0.512 gm/cm^3. The two materials occupy the beam geometry as shown in the Fig.9.3. Various parameters defined above have the following values for present problem.
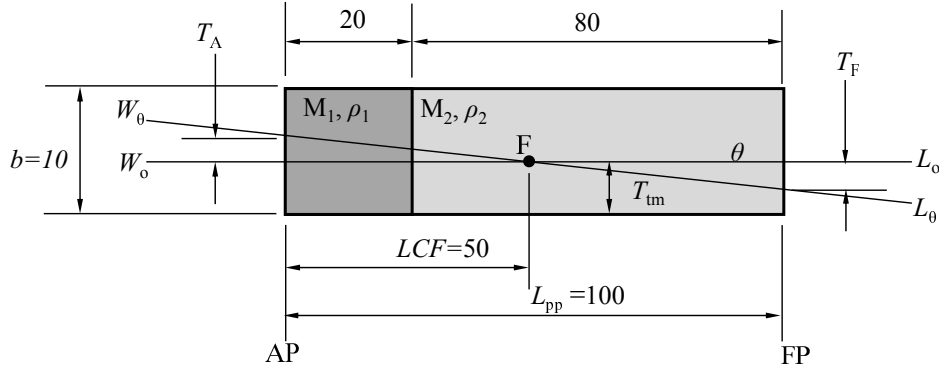
Figure 9.3 Box-like vessel parameters (drawn not to scale and all dimensions in meters)

$$
\begin{aligned}
LCG &= 47.263 \text{ m} \\
LCB &= 50 \text{ m} \\
LCF &= 50 \text{ m} \\
MCT &= 8333.333 \text{ m} \\
GM_{\text{L}} &= 155.415 \text{ m} \\
I_{\text{L}} &= 833333.333 \\
\Delta &= 5362 \text{ m}^3 \\
T_{\text{m}} &= 5.362 \text{ m}
\end{aligned}
$$

And putting all the above values in Eq.9.1,9.3 and 9.4, we get the following values of the two draughts as follows:

$$T_{\text{A}} = 6.2425 \text{ m}, \qquad T_{\text{F}} = 4.4814 \text{ m}$$

9.4   Numerical Example-2: Simple Boat

A 3D boat is modelled using CW approach with realistic features such as floor and walls contoured along the floor edges as shown in Fig.12.1. The material is aluminum and all wall thicknesses are 50 mm. Various parameters discussed above were obtained for the boat and are given in the following:
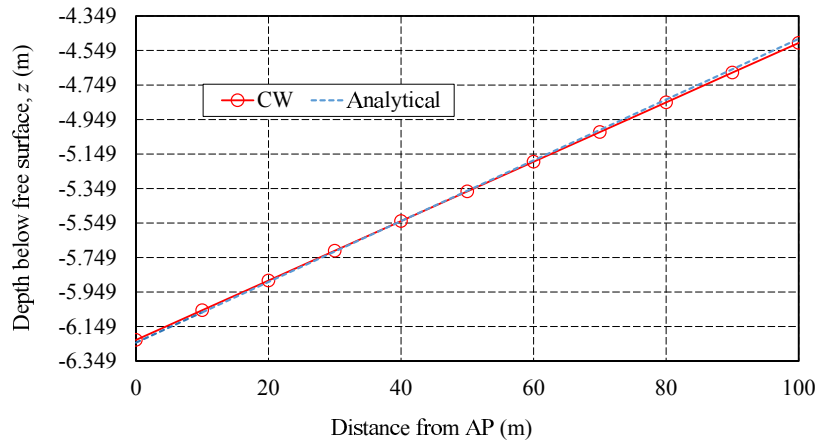
Figure 9.4 Comparison of box-like beam deflection from CW and analytical methods

$$LCG = 4.2364 \text{ m}$$
$$LCB = 4.0186 \text{ m}$$
$$LCF = 4.0186 \text{ m}$$
$$MCT = 11.1262 \text{ m}$$
$$GM_{\text{L}} = 20.5443 \text{ m}$$
$$I_{\text{L}} = 106.7 \text{ m-N/m}$$
$$\Delta = 5.1937 \text{ m}^3$$
$$T_{\text{m}} = 0.2767 \text{ m}$$
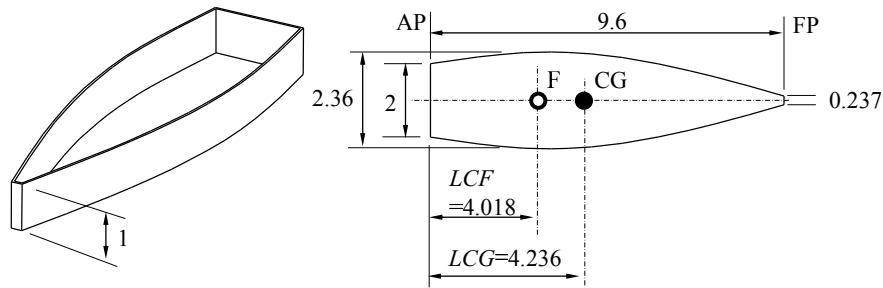
Figure 9.5 Boat parameters in meters (Left: Isometric view and Right: Plan view)

And putting all the above values for boat in Eq.9.1,9.3 and 9.4, we get the following analytical values of the two draughts as follows:

$$T_{\text{A}} = 0.3358 \text{ m}, \qquad T_{\text{F}} = 0.2341 \text{ m}$$

Figures 9.6 and 9.4 are the plots of deflection curves obtained using analytical method and the CW model for the beam and the boat models respectively. In each figure, the two curves are in fairly close implying the correctness of the presented

approach of employing Buoyancy Springs in CW Models. Figure 9.7 shows the vertical deflection V in isometric view.
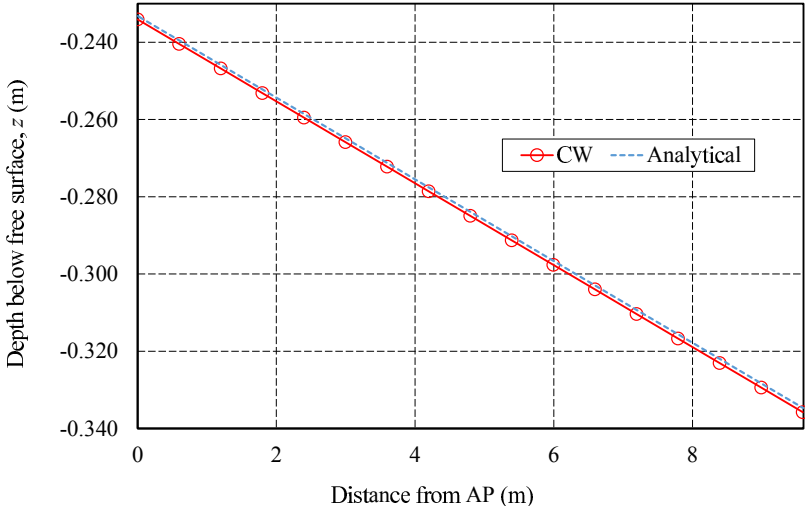
Figure 9.6 Comparison of boat deflection from CW and analytical methods
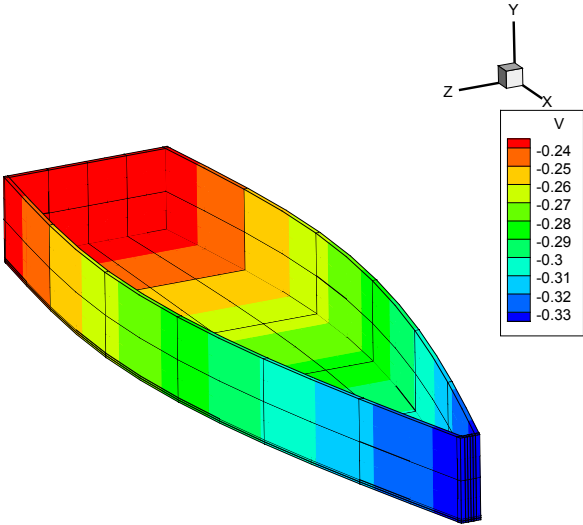
Figure 9.7 Deflection of CW Model of the boat

9.5   Conclusion

The trimming behaviour of a floating beam and a boat were discussed. The objective was to determine the trim parameters for the two structures analytically and compare the values obtained through CW models. The results from CW model were in close

agreement with the analytical ones. The CW models were deliberately rigidized employing solid section for the beam and thick walls for the boat model, so that the rigid body behaviour is clearly evident and comparable with analytical results.

Although the examples discussed involved only the trimming which was a 2D scenario, the rigid body deflections of a real ship are 3D in nature and final deflection can have both the trim and heel component. The present CW model with buoyancy springs involves realistic vessel geometry and the buoyancy distribution. Thus, a CW model with CG and CF not sharing any plane, will render the model to include trimming and heeling deflections simultaneously. For the purpose of brevity and similarity of treatment, the heeling is not discussed here.

Chapter 10

Validation Cases: Flexible Ship Deflections in Still Water

10.1 Analytical Procedure

This chapter discusses the case of a container ship deflections in a still sea water environment. A reference example has been considered from Ref.[63] for which the results from analytical and CW models are compared. A simplified container ship has been modelled as a single beam and has the mid-ship section as the beam cross section through out the beam length. Referring to Fig.10.1, a typical container ship structure is acted upon by the still water buoyancy force and mass distribution acting in the form of weight. The difference of the two loading curves gives the differential loading that acts on the ship which is idealised as a beam. Like any beam problem, the deflections are analysed through the ability of cross section geometry to resist the loads. Similarly, the flexural stresses thus arisen are also obtained employing classical beam models such as Euler Beam Theory.
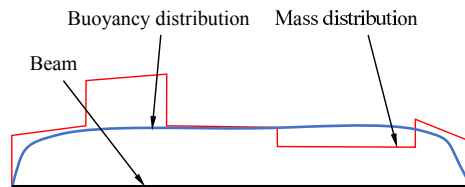
Figure 10.1 Buoyancy and mass distribution loading curves on a ship idealised as a beam

Since to this point, the efficacy of CW models involving buoyancy springs is well established, the container ship with important realistic scantlings is considered here as a CW 1D beam model with buoyancy springs attached. Fig.10.2 shows a simplified loading scenario for a container ship for which the mid-ship scantlings are shown in Fig.10.3. The material is steel with young's modulus E=210 GPa and poisson's ratio, ν=0.3. The problem is given as a numerical example in Ref.[63] at page 160.
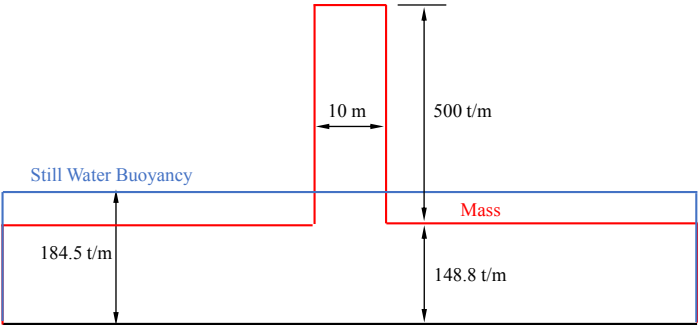
Figure 10.2 Buoyancy and mass distribution curves on a ship
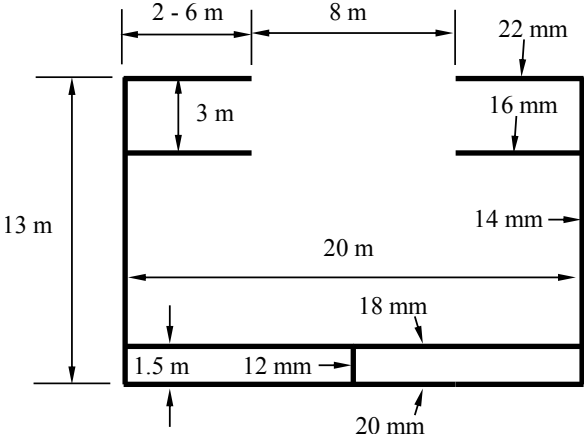
Figure 10.3 Mid-ship section scantlings

In the analytical procedure adopted in Ref. [63] for the ship of length 140 m, 20 m breadth and 13 m height, following parameters are calculated:

Buoyancy moment at mid-ship	=	4434.365 MN m
Mass moment at mid-ship	=	3637.302 MN m
Net Still water bending moment	=	797.062 MN m
Section modulus at base	=	8.16 m³
Normal stress at base	=	97.7 N/m²

10.2   CW Results

The container ship was analysed using CW model with 11 and 27 B3 elements along beam length and 59 and 39 L9 Lagrange elements for the respective cross sections of the three bulkheads and remaining beam section. The weight distribution over the beam length has been modelled in the form of assigning appropriate densities to the beam elements. Figure 10.4a shows the deflected plot which very closely resembles the deformed configuration of a generic ship illustrated in Fig. 10.4b from Ref. [63]. This indicates the correctness of the procedure adopted to model the buoyancy in CW model.

(a) Deformed container ship from CW model

(b) Deformed container ship (generic) from Ref. [63]
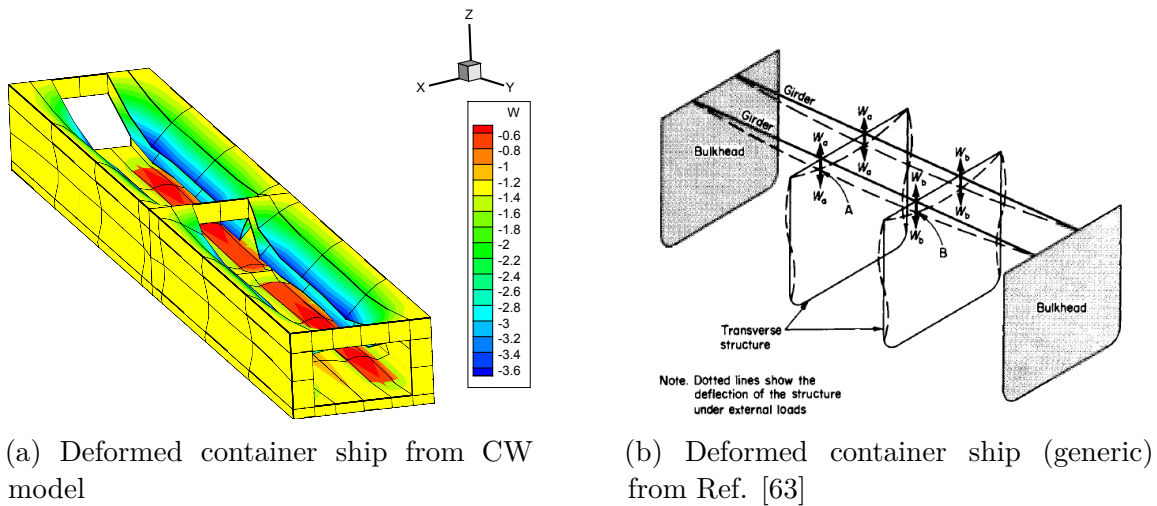
Figure 10.4 Comparison of 3D deformed configuration of a container ship

The stiffening effect of bulkheads is clearly evident in the results and un-stiffened hull walls and floors are seen deflected inwards due to the effect of external forces. The self weight has caused the top plates in CW model, to sag which realistically corresponds to the reference configuration shown in Fig. 10.4b.

Figure 10.5 shows the stress plots along a path located at the middle of the bottom most surface along length of the beam. As shown, the maximum stress is 98.56 MPa for CW model with 27 B3 elements which is very close to the analytically obtained value of 97.7 MPa. The stress discontinuity at the element interface is seen and is because of the discontinuous second derivatives.
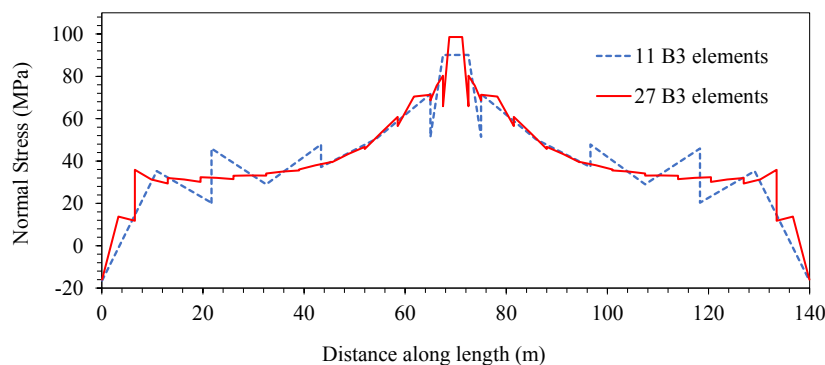
Figure 10.5 Mid-ship section scantlings

10.3   Rigidization of the Ship Model

The previous analysis considered a flexible model of the ship. The same model may be rigidized by increasing the young's modulus in order to manifest a rigid body immersed configuration. For present model, all the points such as center of buoyancy, center of gravity and center of floatation lie in the same longitudinal vertical plane and thus there is no inclination angles involved. Figure 10.6 shows the results of this study whereby deflections of a path are compared as the structure is rigidized. The path is a straight line which is an intersection of a transverse plane and the base surface. The transverse plane is chosen mid-way along the length between the two bulkheads. At such location, the in-plane deflections of the cross section are more pronounced.
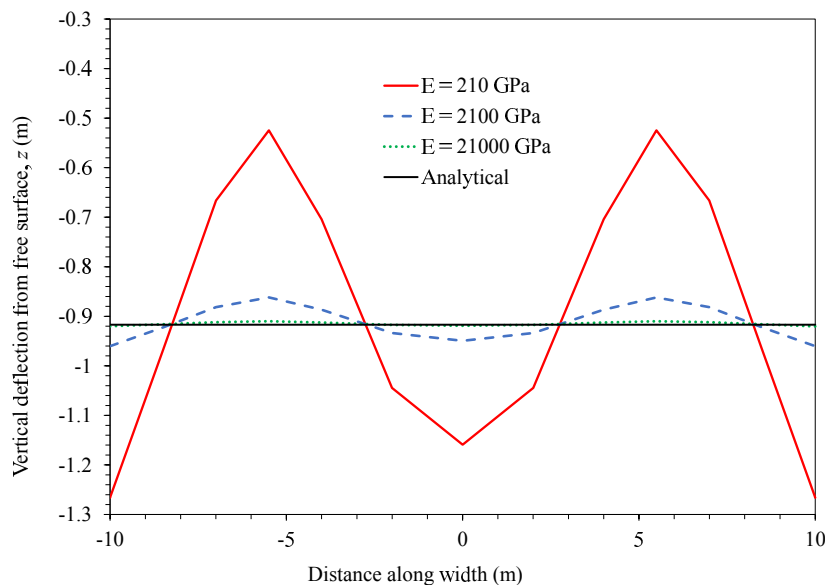
Figure 10.6 Deflection plot as the ship is rigidized

The results clearly show that, as the young's modulus is considerably increased, the deflection curve converges to a final value that is obtained analytially as z=-0.917 m. Also, it is observed that the less stiffened regions of the floor are lifted upwards due to buoyancy forces and the stiffened regions such as corners are pushed downward. All the curves mutually intersect at common point which is the analytical immersion depth.

Present rigidised CW models on buoyancy springs produce very accurate results and do not require calculation parameters such as Metacentric Height or Center of Floatation and various other hydrostatic parameters.

Chapter 11

Ship Poised over Wave Loads

11.1 Buoyancy in Waves

The forces acting on a ship moving through a seaway are very different from those in still water. The static buoyancy is greatly altered both in space and time which was previously assumed a constant for still water. The pressure in a sea wave differs from normal static pressure under still water. The heave and pitch motions involve inertia of both the ship and the surrounding water. The problem thus becomes a dynamic one. In traditional practice (See Ref. [63], [61]), the problem is reduced to an equivalent static problem and the ship is considered as statically poised on a wave.
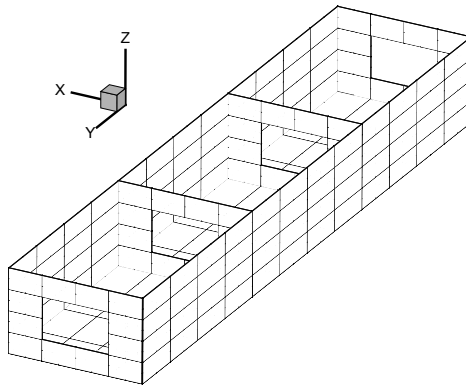
Figure 11.1 Isometric view of container ship meshed with 1D CW beam elements (all dimensions in meters)

A brief discussion on waves is required in order to model the buoyancy forces associated with them. Sea waves can broadly be classified into regular and irregular

waves. In this thesis, only the regular waves are considered. Out of many wave forms trochoidal waves most closely represent the regular sea waves. The trochoidal wave theory was proposed by Gerstner [35]. A trochoid is characterised by crest relatively being sharp compared to the troughs which are flatter. The so-called *Trochoidal Wave Theory* is based on the mathematical description of the free surface of an ocean wave by representing it through a Trochoid. A trochoid is a path traced by a point P lying within a circle which is rolling under a straight line (as shown in Fig.11.2). As shown in Fig. 11.3, the still water line is located at a distance $\zeta = \pi r_o{}^2 / \lambda$ below the orbit center line. Thus, the still water line divides the area under the curve of trochoid in two equal halves. The coordinates of point P travelling along a trochoid are given through the following Eq. 11.1:
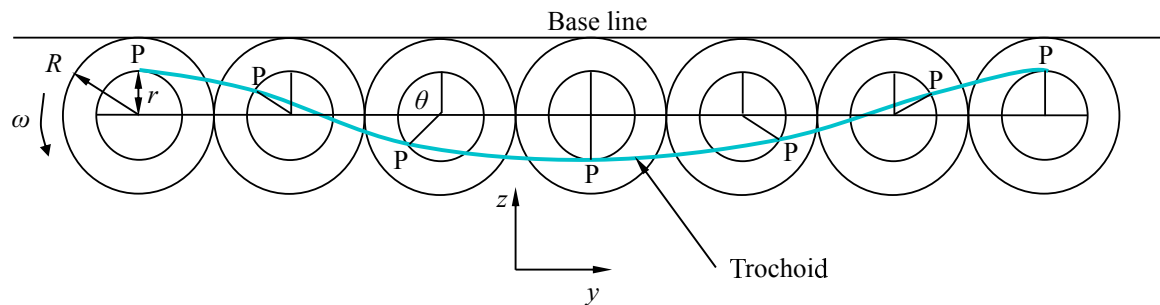
Figure 11.2 Trochoid

$$
\begin{aligned}
y &= R\theta - r\sin\theta \\
z &= R - r\cos\theta
\end{aligned}
\tag{11.1}
$$

The nature of trochoidal waves is stationary and the particles under the wave do not get transported along the wave. Instead, they undergo a circular motion in the plane of wave. The circle geometry varies horizontally as well as vertically . Travelling from deep sea towards sea shore, the circles tend to become ellipses whereas travelling along the depth the circles tend to shrink through a function that is hyperbolic in depth, z. Very near the sea shore, at shallow water depths, the waves tend to break. This behaviour is illustrated in Fig.11.4.
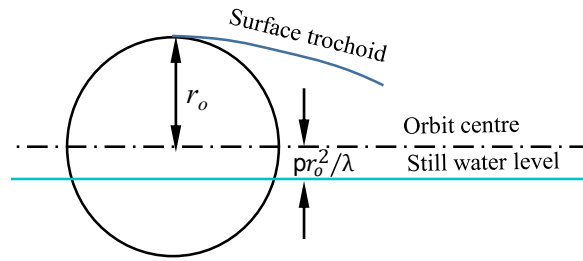
Figure 11.3 Section showing the wave changes approaching shore
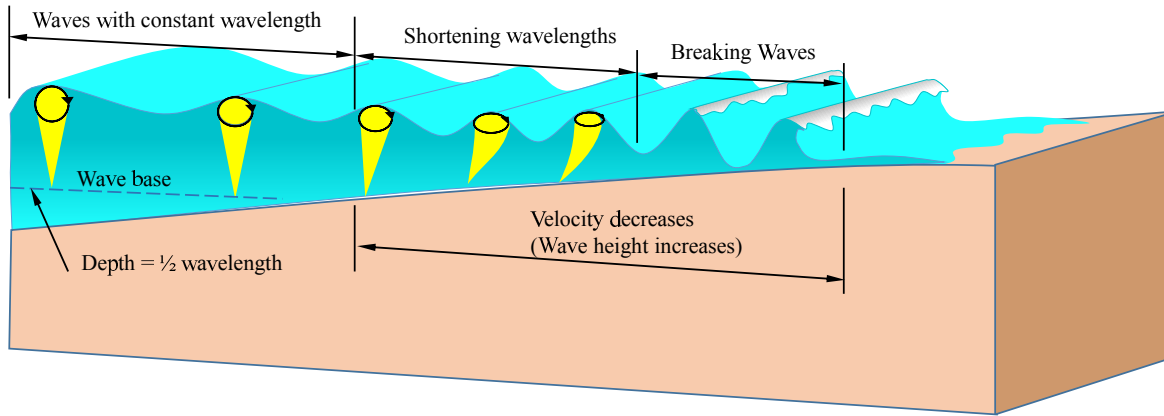
Figure 11.4 Section showing the wave changes approaching shore

11.2   CW Model of a Container Ship

In order to model buoyancy forces due to waves, a container ship is modelled as a single beam with multiple sections using CW approach. Each beam element is assigned a cross section out of the two sections types i.e. the bulkheads and the simple channel shaped section. As seen in Fig. 11.1, in all there are 16 B3 elements out of which 4 are bulkheads and the rest of them are channel section. The material is steel and wall thicknesses at all places is 50 mm. There are no external loads applied to the structure and the only loads are the self-weight of the ship and the buoyancy forces. The ship length is 120 m, width is 26 and height is 16.2 m.

For present study, the ship is assumed to poised statically over a trochoidal wave. Thus, at crest the buoyancy is higher than the still water buoyancy and lower at the other region. The results of the study are presented in the form of contour plots for vertical deflection of vessel floor. The Fig.11.5 and Fig.11.6 show the weight and buoyancy loading on the CW model of container ship along with the contours of vertical deflection. In Fig.11.5, the wave has crests at two ends while the middle of wave has the trough. The wave orbital center line is positioned at distance $\zeta = \pi r_\mathrm{o}^2/\lambda$ = 0.026 m above the still water line which is 1.014 m from keel. Here, $r_\mathrm{o} = 1$ m and

λ = length of the ship = 120 m. In the second Fig.11.6, the same wave is modelled with crest in the middle and two troughs at the ends.
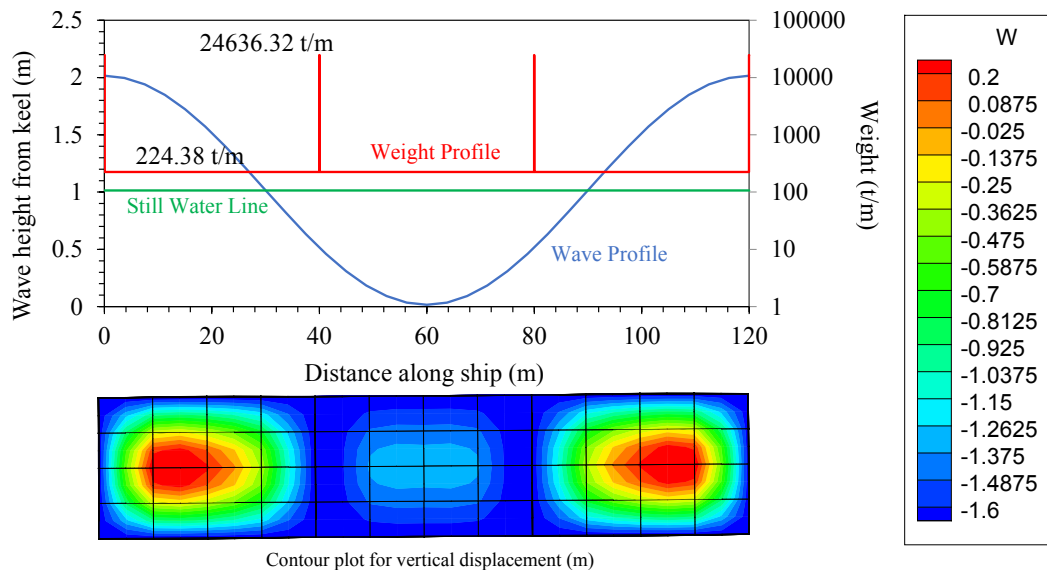
Figure 11.5 Wave loading with crest at ends and displacement contour plot from CW model

11.3   CW Model of a Realistic Boat Geometry

In previous section, the ship exhibited a non-uniform deflection owing to the non-uniform buoyancy. In this section, it is shown that a non-uniform weight distribution in the presence of a uniform buoyancy distribution causes a non-uniform deflection. For this purpose, the boat discussed in Sec. 9.4 is considered again but with less stiff material with Young's modulus, E being 0.1 GPa. Figure 11.7 shows the deflection plot from the static analysis of the boat. The plot shows that downward deflection due to weight is dominant in frontal region whereas the lower region of the floor experiences an upward lift due to buoyancy force.

11.4   Conclusion

The effect of changing buoyancy and weight distribution is convincingly demonstrated in a realistic manner for CW models of a container and a boat vessel. The buoyancy springs have produced the realistic and flexible static deflections in structure. It is seen that each section is acted upon by the net sum of weight and buoyancy loads on
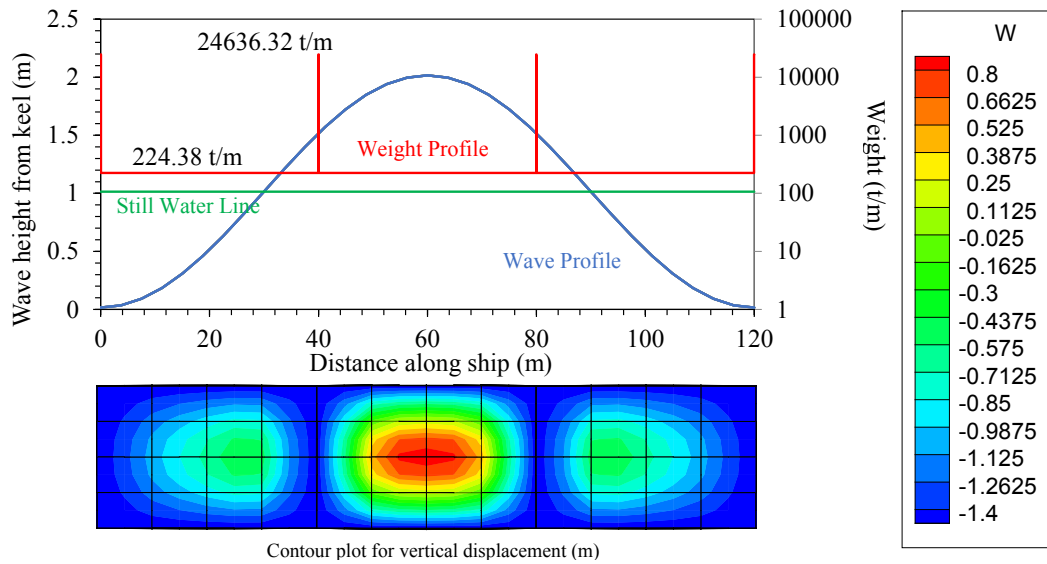
Figure 11.6 Wave loading with crest in middle and displacement contour plot from CW model
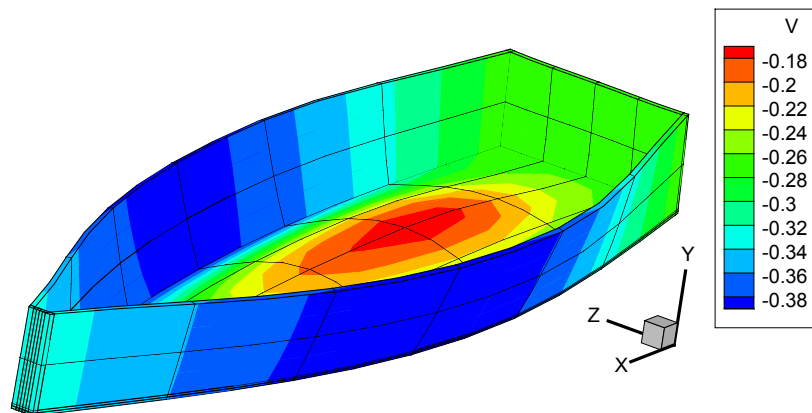
Figure 11.7 Flexible behaviour of a boat under still water buoyancy

the ship. A section is pushed upward by buoyancy in places where buoyancy is higher whereas it is lowered where weight is higher than the buoyancy.

Chapter 12

Dynamic Structural Analysis of Ship on Buoyancy Springs

12.1 Free Vibration Analysis

The efficacy of present beam model has been well demonstrated for the static loading conditions in previous chapters. In this chapter, the beam models representing realistic ship hulls are analysed for free vibration and transient response. The free vibration problem is reduced to an Eigenvalue or Modal Analysis which gives natural frequencies and mode shapes and is given by Eq. 12.1:

$$(\mathbf{K} - \omega^2 \mathbf{M})\mathbf{Q}e^{i\omega t} = 0; \tag{12.1}$$

where $\mathbf{K}$ and $\mathbf{M}$ are respectively the global assembled stiffness and mass matrices and $\mathbf{Q}$ is the amplitude of the assumed harmonic solution $\mathbf{q}$ with ω being the angular frequency in rad/sec. The first six lowest frequencies correspond to rigid body modes that comprise of three translations and three rotations. The three motions of heave, pitch and roll are among these six modes arranged interspersed in ascending order. Subsequent mode 7 and onward are flexible structural modes exactly the same as would have been obtained for a boat in vacuo. For the validation requirement a realistic boat geometry has been chosen for the free vibration analysis under still water conditions.

The dynamic analyses in this chapter do not involve so called *Added Mass* and *Hydrodynamic Damping* effects for the sake of simplicity. The added mass has the effect of added inertia due to the fluid motion of the oscillating body and similarly

damping is the energy dissipation mechanism of waves generated in the fluid around the hull. Given the geometrical form of the vessel and particular mode of motion, the corresponding added mass and hydrodynamic coefficients are added to the overall mass of the vessel finally leading to correct results. This study is presented in next chapter.

Next, the accuracy of present model with buoyancy springs is further demonstrated by simulating the dynamic response of ship due to moving loads on its deck. The governing equation for this case is the most general form of equation of motion and its is re-written here from chapter 3.

$$\mathbf{M}\ddot{\mathbf{q}}(t) + \mathbf{K}\mathbf{q}(t) = \mathbf{P}(y, t) \tag{12.2}$$

where quantities $\ddot{\mathbf{q}}$ and $\mathbf{q}(t)$ are time-dependent responses due to time and position dependent loading $\mathbf{P}$. Well known "Newmark" direct time integration scheme has been employed to solve the equation of motion. The scheme is termed as "direct" since it does not require the equation of motion be transformed into any other form prior to time-integration. In direct numerical integration, the Eq. 12.3 is satisfied at discrete time steps. Thus the equation of motion for an undamped system at time $t + \Delta t$ is:

$$\mathbf{M}\ddot{\mathbf{q}}_{t+\Delta t} + \mathbf{K}\mathbf{q}_{t+\Delta t} = \mathbf{P}_{t+\Delta t} \tag{12.3}$$

The time domain is divided into time steps of interval ΔT. Objective is to obtain the displacement vector $\mathbf{q}$ at each time step. The total time span T is the interval over which the response of the system is evaluated and is subdivided into N_T time steps. The Newmark scheme [64] is an implicit time integration procedure meaning that the displacement vector calculated at time instant $t + \Delta t$ depends on known displacements, velocities, accelerations computed at previous time instant and the unknown velocities, accelerations calculated at time instant $t + \Delta t$. The displacement $\mathbf{q}_{t+\Delta t}$ at time $t + \Delta t$ is found from the following Eq.:

$$\bar{\mathbf{K}}\mathbf{q}_{t+\Delta t} = \bar{\mathbf{F}}_{t+\Delta t} \tag{12.4}$$

where $\bar{\mathbf{K}}$ is the *effective Stiffness Matrix* and $\bar{\mathbf{F}}_{t+\Delta t}$ is the *effective Vector of Equivalent Nodal Forces* at time $t + \Delta t$. The matrix $\bar{\mathbf{K}}$ is related to the original stiffness matrix $\mathbf{K}$ and mass matrix $\mathbf{M}$ as:

$$\bar{\mathbf{K}} = \mathbf{K} + \frac{1}{\alpha \Delta t^2}\mathbf{M} \tag{12.5}$$

and the vector $\bar{\mathbf{F}}_{t+\Delta t}$ is found from $\mathbf{F}_{t+\Delta t}$ and initial quantities of $\mathbf{q}_t$, $\dot{\mathbf{q}}_t$ and $\ddot{\mathbf{q}}_t$ through the following Eq.:

$$\bar{\mathbf{F}}_{t+\Delta t} = \mathbf{F}_{t+\Delta t} + \frac{1}{\alpha\Delta t^2}\mathbf{M}\mathbf{q}_t + \frac{1}{\alpha\Delta t}\mathbf{M}\dot{\mathbf{q}}_t + \left(\frac{1}{2\alpha} - 1\right)\mathbf{M}\ddot{\mathbf{q}}_t \qquad (12.6)$$

Once the new displacement $\mathbf{q}_{t+\Delta t}$ is known from Eq. 12.5, the new velocities and accelerations are obtained as follows:

$$\dot{\mathbf{q}}_{t+\Delta t} = \dot{\mathbf{q}}_t + [(1-\delta)\ddot{\mathbf{q}}_t + \delta\ddot{\mathbf{q}}_{t+\Delta t}]\Delta t \qquad (12.7)$$

and

$$\ddot{\mathbf{q}}_{t+\Delta t} = \frac{1}{\alpha\Delta t^2}\mathbf{q}_{t+\Delta t} - \frac{1}{\alpha\Delta t^2}\mathbf{q}_t - \frac{1}{\alpha\Delta t}\dot{\mathbf{q}}_t - \left(\frac{1}{2\alpha} - 1\right)\ddot{\mathbf{q}}_t \qquad (12.8)$$

where the constants δ and α have the values 0.5 and 0.25 respectively. The procedure is repeated as the new displacements, velocities and accelerations become current ones and effective force vector is updated through Eq. 12.6 and all quantities calculated for the subsequent time step.

Employing the Newmark time-integration scheme, a dynamic response analysis of an aircraft carrier subjected to moving load of an aircraft has been performed. The aircraft carrier is assumed to be rigid body floating over still water. The problem has been referenced from a well cited paper [82] and results are validated. Presently, the effect of damping has not been included.

12.2   Free Oscillations of a Boat in Still Water

A boat of geometry shown in Fig 12.1 was analysed for its free vibration response using the present CW model supported on buoyancy springs. The problem has well established analytical procedure in textbooks on Fluid Dynamics whereby the boat is assumed rigid. The boat exhibits vertical oscillations termed as *heave*, rotational oscillations about transverse axis termed as *pitch* and rotational oscillations about longitudinal axis termed as *roll*. An important aspect to consider is that the boat has at least one plane about which the geometry is not symmetric (e.g. the vertical transverse plane, z-plane in Fig 12.1). This leads to the coupling of heave and pitch oscillations which otherwise remain uncoupled for bodies perfectly symmetric about all three axes.
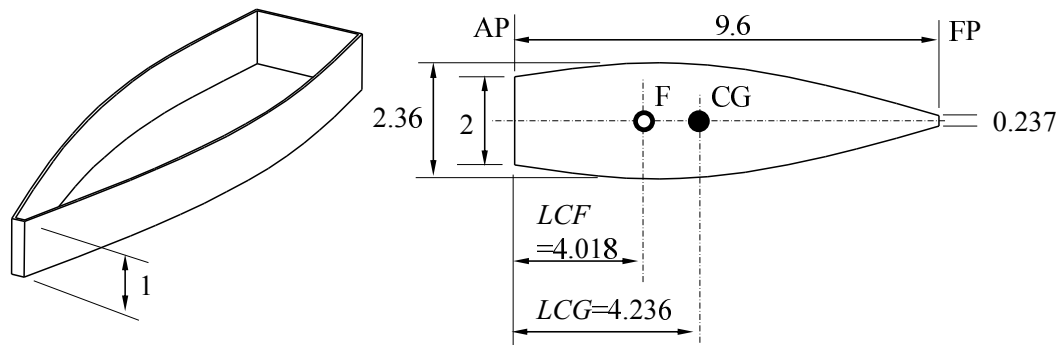
Figure 12.1 Boat parameters in meters (Left: Isometric view, Right: Plan view)

12.2.1 Analytical Model

Heave

From any good reference book on vibrations such as [100], the heave frequency is obtained in Hz through the following Eq. 12.9.

$$f_{\text{heave}} = \frac{1}{2\pi}\sqrt{\frac{\rho_{\text{w}} g A_{\text{w}}}{m}} \tag{12.9}$$

where for the boat in Fig. 12.1

ρ_{w} = 1025   : Density of sea water [kg/m³]
g = 9.81   : Gravity constant [N/m²]
A_{w} = 18.7914 : Water plane area [m²]
m = 5303   : Mass of the boat [Kg]

which gives

$f_{\text{heave}} = 0.950027$ Hz

Pitch

The pitch frequency is obtained in Hz through the following Eq. 12.10.

$$f_{\text{pitch}} = \frac{1}{2\pi}\sqrt{\frac{W h_{\text{pitch}}}{I_{\text{pitch}}}} \tag{12.10}$$

where for the boat in Fig. 12.1

W =   52022.43   :   Weight of the boat [N]

h_{pitch} =   20.342   :   Meta centric height [100] measured from center of gravity [m]

I_{pitch} =   40191.035   :   Pitch Moment of Inertia [kg-m^2]

which gives

$f_{\text{pitch}} = 0.8163\text{Hz}$

Pitch

The roll frequency is obtained in Hz through the following Eq. 12.11.

$$f_{\text{roll}} = \frac{1}{2\pi}\sqrt{\frac{W h_{\text{roll}}}{I_{\text{roll}}}} \qquad (12.11)$$

where for the boat in Fig. 12.1

W =   52022.43   :   Weight of the boat [N]

h_{roll} =   1.3912   :   Meta centric height [100] measured from center of gravity [m]

I_{roll} =   4262.511   :   Roll Moment of Inertia [kg-m^2]

which gives

$f_{\text{roll}} = 0.65704\text{Hz}$

12.2.2   Numerical Results

The present CW model with buoyancy springs has 4 B3 beam elements which are along y-axis (along the boat height). The first two beam elements used to model the floor while the remaining two for the hull walls. These elements have the cross sections lying along $x - z$ planes. Thus, there are two cross section types assigned to 4 beam elements. The floor has been modelled with 48 L9 elements with 221 nodes and the

walls have been modelled with 24 L9 elements with 144 nodes. The complete model has 1681 nodes with 5043 DOFs. The boat material is Aluminum with $E = 72$ GPa and $\nu = 0.3$.

The results of the modal analysis (Natural frequencies and mode shapes) are presented in the following. The natural frequencies obtained are listed in Table 12.1 which do not include the first three translational frequencies. The table also lists the analytical values for the rigid body modes for the purpose of comparison. Ignoring the first three translation modes, the remaining initial six mode shapes are plotted in Fig. 12.2. The coupling effect between the heave and pitch modes is clearly evident owing to the asymmetric geometry across the vertical transverse plane.

Table 12.1 Natural frequencies obtained from numerical (CW) and analytical models

Mode	CW Model (Hz)	Analytical Model (Hz)
Roll	0.6995	0.6570
Pitch	0.8173	0.8163
Heave	0.9608	0.9500
Mode 1	18.1712	–
Mode 2	18.6957	–
Mode 3	28.7631	–
Mode 4	35.3432	–
Mode 5	40.4544	–
Mode 6	43.7889	–
Mode 7	44.5117	–
Mode 8	56.8689	–
Mode 9	58.9391	–

(a) Heave mode

(b) First flexible mode

(c) Pitch mode

(d) Second flexible mode

(e) Roll mode

(f) Third flexible mode
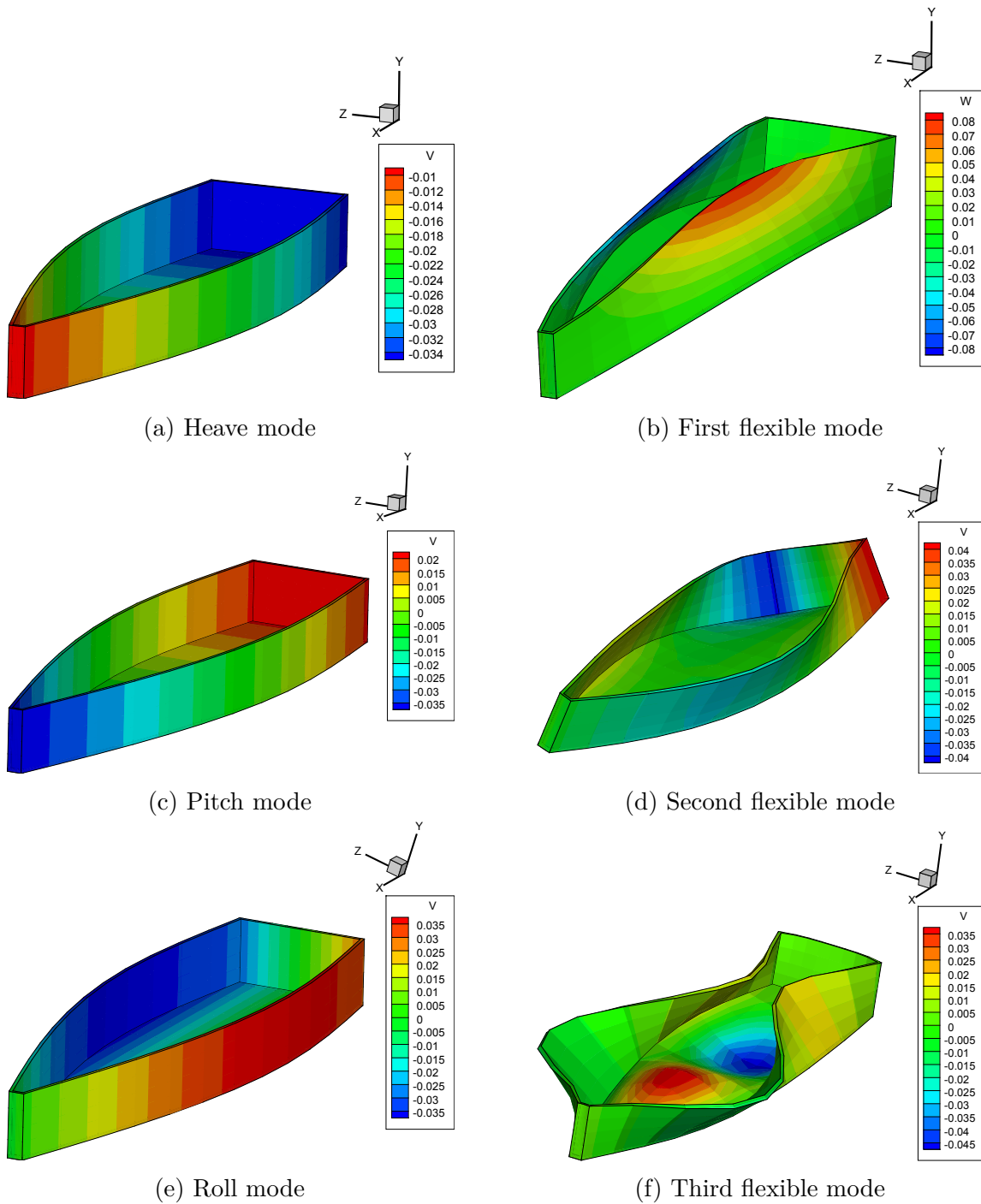
Figure 12.2 Free vibration modes of the boat shown in Fig. 12.1

12.3   Dynamic Response of an Aircraft Carrier due to a Moving Load on Deck

The accuracy of the present model in capturing a dynamic problem is further highlighted through simulation of an aircraft carrier in sea water subjected to a moving load exerted by an aircraft on her deck. The problem has been referenced from an article [82] with which the results of CW model have been compared. In the analysis, the ship has been assumed as a rigid body floating in still sea water. The aircraft exerts 150 kN downward force. The ship is symmetric from all sides except across a vertically transverse plane owing to the tapper at bow. The ship geometry is shown in Fig. 12.3. The ship mass used in the problem is 358.3741×10^5 kg which includes the added mass in addition to its original mass of 132×10^5 kg.
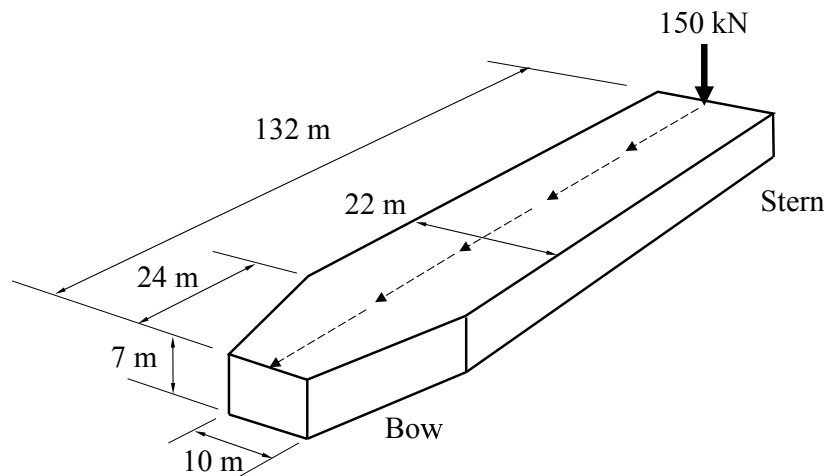
Figure 12.3 Simplified model of aircraft carrier with moving load (shown in perspective view)

The problem has been modelled in the Ref [82] analytically and numerically with the effect of damping included. The effect of added mass is only to contribute towards inertia and hence affects the time period of the vibrations. The present CW analysis involves all the same parameters except damping. It may be noted that the damping only alleviates the response amplitudes therefore in the Ref [82], the oscillations are seen decaying down as the time progresses. As shown in Fig. 12.3, the aircraft travels from stern toward bow with a constant velocity represented as V_p.

12.3.1 Numerical Results

The CW model for the present problem has been modelled using 3 B3 beam elements aligned with y-axis. Gravity is along negative y-axis. The beam cross sections are large areas lying parallel to $x - z$ plane. Each cross section has 20 L9 elements with 105 nodes and the complete model has 2205 DOFs. The lowest cross section (keel surface) has all the nodes connected to vertical springs simulating the effect of buoyancy.

The results of the analysis are the plots of vertical oscillations of center of gravity of the ship (W_{cg}) versus the travelled distance of the aircraft represented as x_p. Figure 12.4 shows the deflected position of the ship at an arbitrarily chosen time instance for which the distance $x_p = 33$ m. Each of the plots for the response in the following comprise of two phases, I and II. Phase-I refers to the condition when $x_p < L$ that is when the aircraft is on the ship and phase-II refers to the condition $x_p > L$ that is when the aircraft has left the ship.
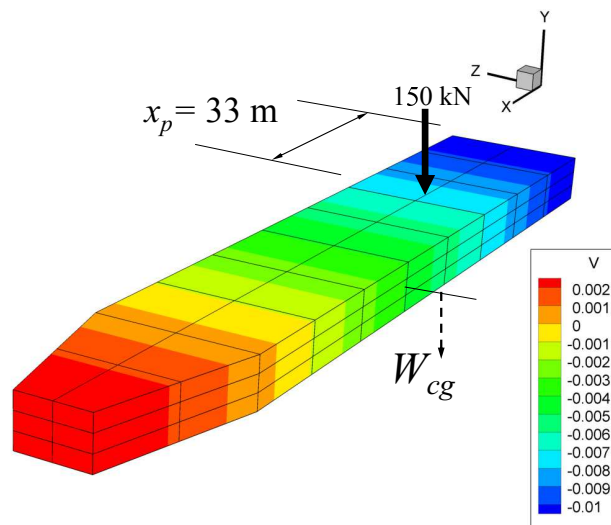
Figure 12.4 Deflected position of aircraft carrier due to moving load

The first result is for the case of aircraft moving with constant velocity of 11 m/s in the direction from stern to bow. The distance travelled from the initial position is denoted as x_p. Figure 12.5 shows the plot of vertical deflection of center of gravity of the ship (denoted as W_{cg}) vs the distance x_p. The figure also shows the plot from exact solution from Ref. [82] for the comparison purpose. In addition to the response during time when aircraft remains on the ship ($x_p < L$), the vertical CG oscillations are continued to be monitored while $x_p > L$ till $x_p = 2L$ as the aircraft leaves the ship oscillating freely. The curve from CW model (shown in Red) is seen closely

approaching the exact solution (shown in blue). As expected, the absence of damping manifests in the form of unchanging amplitude of oscillations.
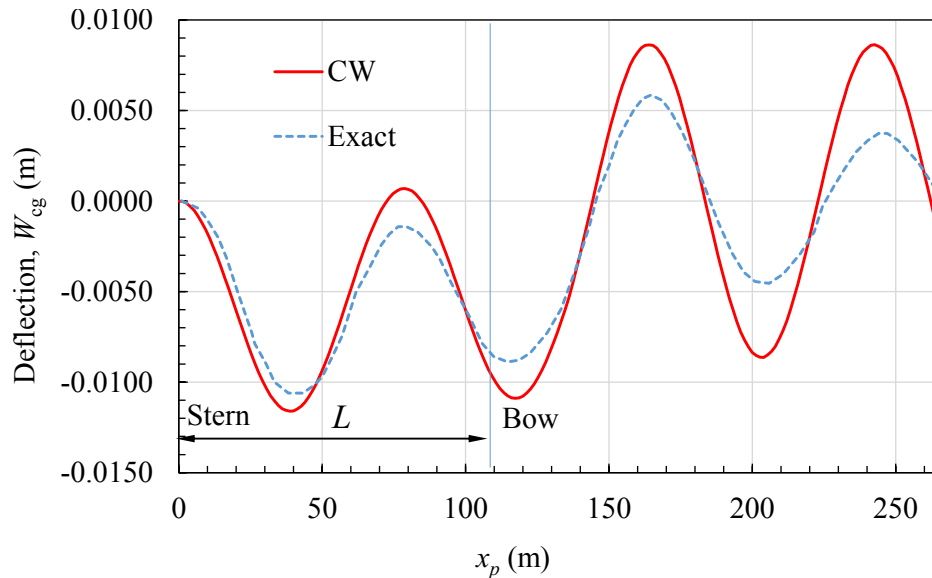
Figure 12.5 Comparison of vertical response of CG of Aircraft Carrier at $V_p = 11$ m/s

For further comparison, two more cases have been plotted for the aircraft velocities $V_p = 22$ m/s and $V_p = 6$ m/s in Figs. 12.6 and 12.7 respectively. The forced and free frequencies of oscillations of CW model are closely approaching the exact solution with the undamped amplitude remaining higher than the damped response. In Fig. 12.7, a noticeable time lag is observed in the free response regime where $x_p > L$. The reason for this lag is the change of initial conditions for this free response part of the curve. For the damped response curve, the amplitude is considerably reduced at location $x_p = L$ resulting in an early start of the free oscillations that follow in phase-II.
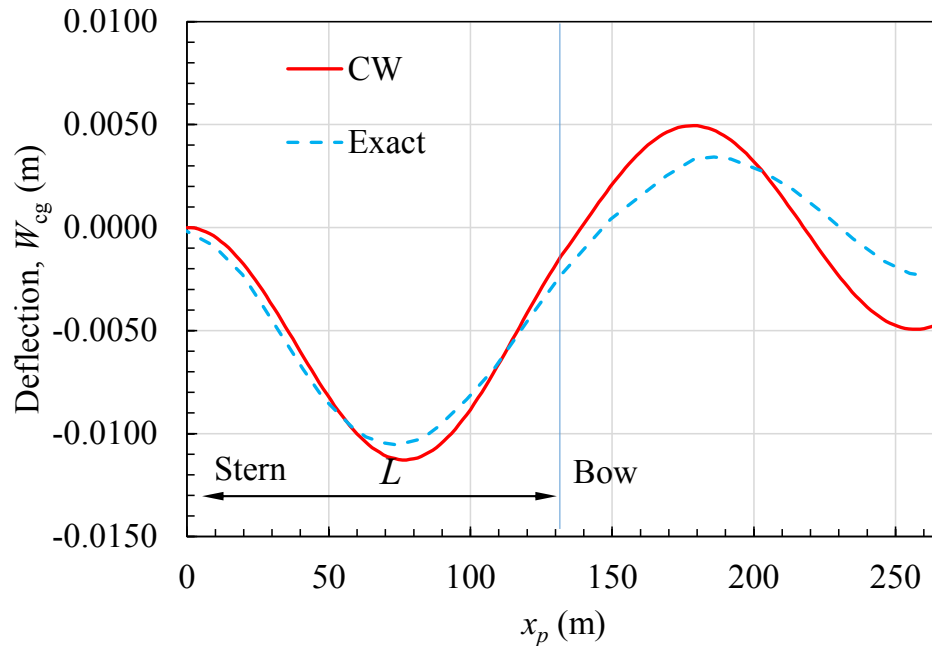
Figure 12.6 Comparison of vertical response of CG of Aircraft Carrier at $V_p = 22$ m/s
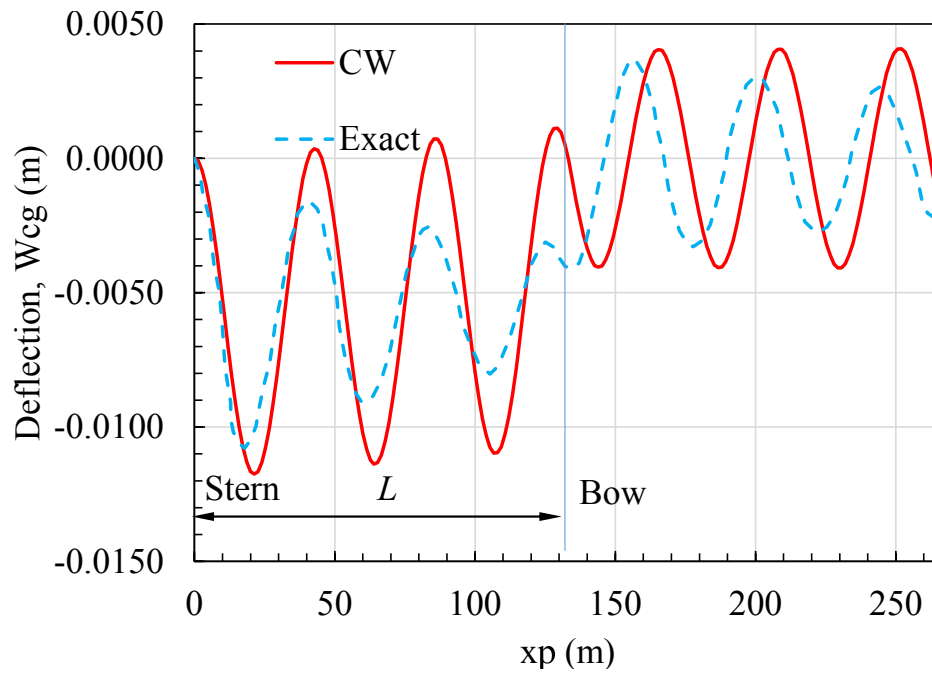
Figure 12.7 Comparison of vertical response of CG of Aircraft Carrier at $V_p = 6$ m/s

12.4   Conclusion

Some marine vessels with realistic geometries were chosen for demonstrating the capability of present CW model with buoyancy springs for the dynamic response analysis. A simple boat hull entailing realistic geometrical features was chosen for modal analysis. It was observed that the initial rigid body modes include the oscillation modes of the boat whose analytical solutions were available. The natural frequencies and mode shapes from CW model were accurately close to the analytical solution validating the idea of employing buoyancy springs. The analysis of the boat was followed by the dynamic response analysis of an aircraft carrier subjected to the moving load of an aircraft. The problem was referenced from an article and the results were compared. The analysis was performed for different velocities which affected the ship response differently. All the results were found closely matching the exact solution.

Chapter 13

Dynamic Sea Loads on Ships

13.1 Introduction

The effect of loads such as weight and buoyancy under the static hydrodynamics was studied in previous chapters. Buoyancy Springs were introduced that accurately captured the hydrostatic restoring forces which are all time present for the case of a floating vessel. This chapter will introduce the bigger picture whereby the dynamics of floating vessels will be studied. It will be seen that previously introduced buoyancy spring model constitutes a part of the complete governing equation of motion for a sea vessel.

13.2 Equation of Motion of a Ship

The dynamic model of a floating ship in sea can be expressed in the most general way through equation of motion as follows:

$$\mathbf{M}\ddot{\mathbf{q}}(t) + \mathbf{C}\dot{\mathbf{q}}(t) + \mathbf{K}\mathbf{q}(t) = \mathbf{P}(t) \tag{13.1}$$

where $\mathbf{M}$, $\mathbf{C}$ and $\mathbf{K}$ are respectively the global assembled matrices of mass, hydrodynamic damping and stiffness and $\mathbf{q}$, $\dot{\mathbf{q}}$ and $\ddot{\mathbf{q}}$ are respectively the generalised displacement, velocity and acceleration vectors. This is the familiar form of equation of motion for a typical spring-mass-damper system.

For the case of ships, Eq.13.1 is modified where some additional terms are added to the terms for mass, damping and stiffness. This is because an oscillating ship

in water generates additional forces of which some forces are in-phase with the vessel's acceleration namely the *Added Mass* and forces in-phase with velocity namely *Hyrdynamic Damping*. The coefficient for the displacement is stiffness matrix which is the stiffness of the whole system comprising of the structural stiffness of the vessel and the hydrostatic stiffness (See Lewis [59]). The RHS of Eq.13.1 involves generalized force vectors due to the presence of waves. They are categorized into *Incident* and *Diffraction* Waves and will be discussed later. Hence the equation of motion can be written as:

$$[\mathbf{M+A}]\ddot{\mathbf{q}}(t) + [\mathbf{C}_{\mathrm{HD}}]\dot{\mathbf{q}}(t) + [\mathbf{K}_{\mathrm{S}} + \mathbf{K}_{\mathrm{HS}}]\mathbf{q}(t) = \mathbf{F}_{\mathrm{I}}(t) + \mathbf{F}_{\mathrm{D}}(t) \qquad (13.2)$$

where the matrices are:

M	:	Mass of vessel or Displacement denoted as Δ
A	:	Hydrodynamic Added mass
C$_{\mathrm{HD}}$	:	Hydro-Dynamic damping
K$_{\mathrm{S}}$	:	Structural stiffness
K$_{\mathrm{HS}}$	:	Hydro-Static stiffness
F$_{\mathrm{I}}$	:	Incident Wave Force
F$_{\mathrm{D}}$	:	Diffraction Wave Force

13.3   Forces on a Ship

Forces acting on the hull of a moving and oscillating ship are explained in many books such as Refs. [76], [47] and [32]. The procedure adopted here has been referenced from Lewis [59] whereby the coefficient matrices in Eq.13.2 have been obtained for 6-DOF rigid body motions of a ship. Thus, there are three translational and three rotational DOFs. The coordinate system adopted for the present discussion is shown in Fig. 13.1. The three translations along x, y and z axes are respectively called as surge, heave and sway and the three rotations about these axes are respectively termed as roll, yaw and pitch.

Coordinate System

As can be noticed from Fig.13.1 that the present coordinate system is different from the one considered in previous chapters. In earlier models, the ship's longitudinal axis was along the beam axis and the transverse hull sections were contained by planes parallel to the $x - z$-plane. Such beam orientation could produce only prismatic hulls
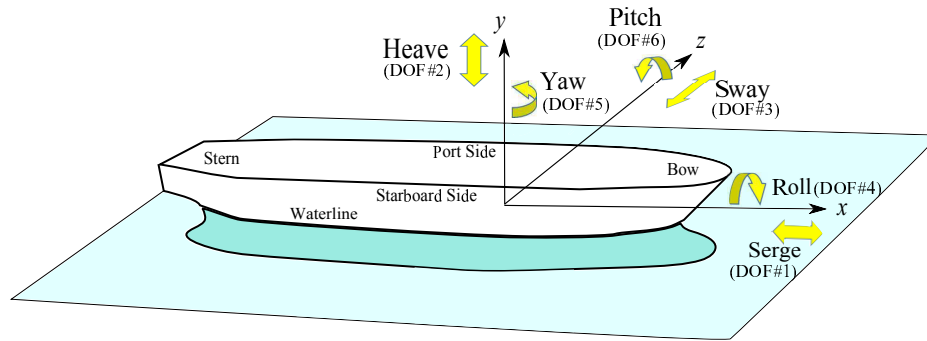
Figure 13.1 Six DOFs of a ship in seaway

with no variation along the length. Changes in transverse section along the length have significant impact on pitch-heave coupling.

In this chapter, the planform area of the vessel has been taken as the beam cross section and the vessel's height is along the beam axis. Thus, the length-wise variations in planform can be accommodated in the beam cross sections. In these models, each transverse section of hull is a rectangle with width equal to the "Beam" [1], $B = B(x)$ and draught $T(x)$.
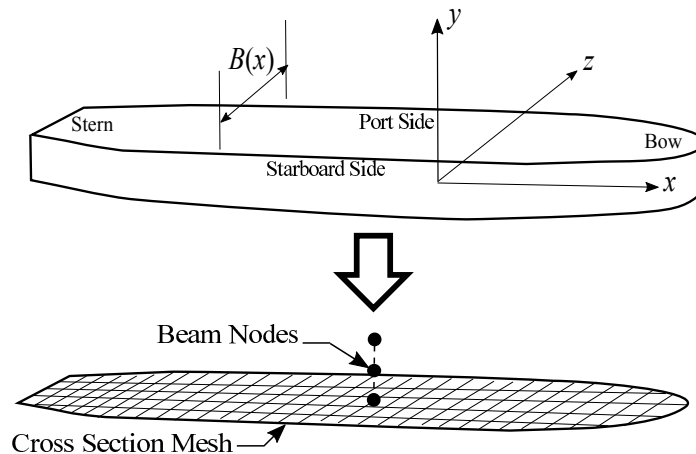
Figure 13.2 Beam meshing scheme for ships with varying width $(B = B(x))$

13.3.1   Simplifications and Assumptions

The ship is assumed to travel at velocity U_o and an angle μ to the sea waves that have the frequency of ω. Thus, the *Frequency of Encounter*, ω_e is given as follows:

---

[1]Width of the ship is called Beam

$$\omega_e = \omega + \frac{\omega^2 g}{U_{\mathrm{o}}} \cos \mu \tag{13.3}$$

The waves are assumed to be linear whereby the wave height is assumed to be smaller compared to wave length. The following discussion on the wave forces is based on this assumption and is well known as *Airy Wave Theory.* The Airy theory assumes the fluid properties as inviscid, incompressible and irrotational and hence the fluid particle kinematics can be described through a velocity potential Φ. The forces in fluid-hull interaction problem result from solving these velocity potential functions under appropriate boundary conditions.

In general, the ship geometry may have starboard-port side symmetry. That is, a vertical plane of symmetry passing through center line of the vessel. The ship, however, may not be For-Aft Symmetric (as seen in Figs.13.1 and 13.2). That is, the bow and stern may be different when looked in top view. Such asymmetries result in coupling of some DOFs. For example, for the ship with For-Aft asymmetry, the heave DOF is coupled with the pitch DOF. As a result we find coupling coefficients in mass, damping and stiffness matrices. In general, a force acting in ith direction exciting motion in jth direction will have subscripts ij. Thus the mass, damping and stiffness matrices will have terms M_{ij}, C_{ij} and K_{ij} where $i, j = 1, 2, ..., 6$. For the case of no coupling the corresponding coefficient is zero. Following the aforesaid, the mass, damping and stiffness matrices for the present 6-DOF system are written in the following. Here, referring to the coordinate system shown in Figs.13.1 and 13.2, the serge, heave and sway are numbered 1,2 and 3 and roll, yaw and pitch are numbered 4,5 and 6.

Writing Euler's equation of motion for the six rigid body generalised displacements and generalized forces, we get:

$$\sum_{k=1}^{6} \mathbf{M}_{jk} \ddot{\mathbf{q}}_k(t) \;=\; \mathbf{F}_j(t) \qquad j = 1, 2, ..., 6 \tag{13.4}$$

where $\mathbf{M}$ is the generalised inertia matrix with terms M_{jk}. The subscripts j, k correspond to the six DOFs and the matrix $\mathbf{M}$ includes three mass terms $M_{11} = M_{22} = M_{33} = \Delta$, three principle inertia terms and coupling inertia terms when $j \neq k$. Both the displacements and forces are harmonic in time. For the ship with Star-Port side symmetry, many of the terms become zero and the generalised force in each of the six DOF is given as follows:

$$
\begin{aligned}
\Delta(\ddot{q}_1 + y\ddot{q}_6) &= \mathbf{F}_1 & \text{(serge)} \\
\Delta(\ddot{q}_2 - x\ddot{q}_6) &= \mathbf{F}_2 & \text{(heave)} \\
\Delta(\ddot{q}_3 - y\ddot{q}_4 + x\ddot{q}_5) &= \mathbf{F}_3 & \text{(sway)} \\
I_{44}\ddot{q}_4 - I_{45}\ddot{q}_5 - \Delta y\ddot{q}_3 &= \mathbf{F}_4 & \text{(roll)} \\
I_{55}\ddot{q}_5 - I_{54}\ddot{q}_4 + \Delta x\ddot{q}_3 &= \mathbf{F}_5 & \text{(yaw)} \\
I_{66}\ddot{q}_6 + \Delta[y\ddot{q}_1 - x\ddot{q}_2] &= \mathbf{F}_6 & \text{(pitch)}
\end{aligned}
\tag{13.5}
$$

where

$\mathbf{F}_j, j = 1, 2, 3$:   Total forces in x,y and z directions

$\mathbf{F}_j, j = 4, 5, 6$:   Total moments about x,y and z axes

Δ :   Total mass of the ship

$I_{jj}, j = 4, 5, 6$:   Moment of inertia about x,y and z axes

$I_{45} = I_{54}$:   Roll-yaw coupled product of inertia

x, y :   Coordinates of Center of Gravity in ship coordinate system

$\ddot{\mathbf{q}}_j, j = 1, 2, ..., 6$:   Generalized acceleration in jth DOF

$$
\mathbf{M_{ij}} =
\begin{bmatrix}
\Delta & 0 & 0 & 0 & 0 & \Delta y \\
0 & \Delta & 0 & 0 & 0 & -\Delta x \\
0 & 0 & \Delta & -\Delta y & \Delta x & 0 \\
0 & 0 & -\Delta y & I_{44} & -I_{45} & 0 \\
0 & 0 & \Delta x & -I_{54} & I_{55} & 0 \\
\Delta y & -\Delta x & 0 & 0 & 0 & I_{66}
\end{bmatrix}
\tag{13.6}
$$

Recognizing the two kind of forces as being the weight of the ship and the fluid forces, Eq.13.4 can be written as:

$$
\sum_{k=1}^{6} \mathbf{M}_{jk}\ddot{\mathbf{q}}_k(t) = \mathbf{F}_j(t) = F_{Gj} + F_{Fj} \qquad j = 1, 2, ..., 6
\tag{13.7}
$$

where

F_{Gj} :   Gravity component of force which is the weight of ship

F_{Fj} :   Fluid component of force

$\mathbf{M}_{jk}$:   Inertia matrix given by Eq.13.6

The gravitational forces are simply the weight acting at center of gravity of ship while the fluid forces are further divided into *Hydrostatic* and *Hydrodynamic* forces.

In general, the fluid forces $F_{\text{F}j}$ are obtained by integrating the fluid pressure over the hull surface which can written as:

$$F_{\text{F}j} = \iint_S P \ n_j \ ds, \qquad j = 1, 2, ..., 6 \qquad (13.8)$$

where

n_j : Unit normal in direction of generalized force
P : Fluid pressure
S : Surface area of submerged portion of ship

The fluid pressure on the hull is obtained using Bernoulli's equation. Under the assumption of an incompressible, inviscid and irrotational flow, the equation for the pressure is:

$$P = \tfrac{1}{2}\rho U_{\text{o}}^2 + \rho\frac{\partial \Phi}{\partial t} - \tfrac{1}{2}\rho(\nabla\Phi \times \nabla\Phi) - \rho g y \qquad (13.9)$$

where ρ is the density of water. The first three terms in Eq.13.9 are hydrodynamic pressure and the last term is hydrostatic pressure. Thus we can write.

$$\begin{array}{ccccc} \mathbf{F}_{\text{F}} & = & \mathbf{F}_{\text{HS}} & + & \mathbf{F}_{\text{HD}} \\ & & \text{(Hydrostatic)} & + & \text{(Hydrodynamic)} \end{array} \qquad (13.10)$$

where

$$\mathbf{F}_{\text{HS}j} = \rho g \iint_S y \ n_j \ ds, \qquad j = 1, 2, ..., 6 \qquad (13.11)$$

and

$$\mathbf{F}_{\text{HD}j} = \rho g \iint_S \left(\frac{1}{2}U_{\text{o}}^2 + \frac{\partial \Phi}{\partial x} - \frac{1}{2}(\nabla\Phi.\nabla\Phi)\right) ds, \qquad j = 1, 2, ..., 6 \qquad (13.12)$$

The total fluid forces represented as $\mathbf{F}_{\text{HD}}$ are written as the sum of *Incident Wave Forces (Froude-Krylov Forces)*, *Diffraction Wave Forces* and *Radiation Wave Forces* each of which is explained in the following. That is,

$$\mathbf{F}_{\text{HD}} = \mathbf{F}_{\text{I}} + \mathbf{F}_{\text{D}} + \mathbf{F}_{\text{R}}$$

where

$\mathbf{F}_\mathrm{I}$	:	Incident Wave Forces (ship is assumed absent)
$\mathbf{F}_\mathrm{D}$	:	Diffraction Wave Forces (ship is assumed fixed)
$\mathbf{F}_\mathrm{R}$	:	Radiation Wave Forces (ship is assumed oscillating)

13.4 Hydrostatic Forces

These are the forces due to the weight of water at a given point on the hull surface. Since the hydrostatic pressure acts normal to the surface therefore, only the vertical components of the hydrostatic pressure is balanced by weight of the structure. The Hull on Buoyancy Spring model was introduced in Chapter 7 to 11 which accurately simulates the hydrostatic stiffness where each buoyancy spring has upper end connected to the wetted surface of hull and the lower end is fixed to the ground. As the buoyancy linearly increases with depth, there is a constant of linearity which acts as a spring constant. That spring constant is Buoyancy Stiffness. These hydrostatic forces are in-phase with displacement and hence the quotient with the generalised displacement vector $\mathbf{q}$ is termed as *Hydrostatic Stiffness* matrix appearing together with *Structural Stiffness* with dimensions as much as the DOFs of the model at hand.

For the purpose of completeness, the expressions for the hydrostatic stiffness components for a Star-port symmetric ship are explained in the following ([59]). For the problem with 6-DOFs, the hydrostatic stiffness matrix $\mathbf{K}_\mathrm{HS}$ is a 6×6 matrix whose each term, K_{ij}, is the hydrostatic generalized restoring force in ith direction due to unit generalized displacement in jth direction. All the terms of $\mathbf{K}_\mathrm{HS}$ matrix are zero except the following:

$$
\begin{aligned}
K_{22} &= \rho g \int B(x)\ dx \\
K_{26} &= K_{62} = -\rho g \int x B(x)\ dx \\
K_{44} &= \rho g \nabla \overline{GM}_T \\
K_{66} &= \rho g \nabla \left(\overline{GM}_L + \frac{\overline{LCF}^2}{\nabla} S \right)
\end{aligned}
\tag{13.13}
$$

where

$\overline{GM}_T$	:	Transverse metacentric height		
$\overline{GM}_L$	:	Longitudinal metacentric height		
S	:	Waterplane area	$=$	$\displaystyle\int_L B(x)dx$

13.5   Hydrodynamic Forces

The aforementioned coefficients for hydrostatic force, K_{jk} and mass matrix, Δ_{jk} are easily obtained. The hydrodynamic forces are unsteady complex forces and *Strip Theories* (Ref [76]) are employed to reduce the complexity of three dimensional problem to 2D. The ship is considered divided through transversal planes resulting in strips of length dx and sectional area A. Use of strip theory entails certain assumption; for instance, the ship is assumed as a slender body whereby the breadth B and draught T are assumed much smaller than the length. Within a strip, the fluid flow is assumed to be two dimensional. Various coefficients are obtained for the strip and their total effect is obtained by integration over all strips along the length. The fluid forces have three main components which are explained in the following.

13.5.1   Radiation Wave Forces

These are the forces due to the motion of the ship when it generates outgoing waves in otherwise calm water. The waves take away the energy and hence the motion dampens out. They result in two additional terms as seen in equation of motion (Eq.13.2). Thus the force $\mathbf{F}_\mathrm{R}$ has two components as shown in Eq.14.1. One is proportional and in-phase with acceleration and the other is proportional and in-phase to velocity.

$$\mathbf{F}_{\mathrm{r}j} = \sum_{k=1}^{6} (\omega_e^2 A_{jk} - i\omega_e C_{jk})\overline{\mathbf{q}}_k e^{i\omega_e t} \qquad\qquad j = 1, 2, ..., 6 \qquad\qquad (13.14)$$

where, $\overline{\mathbf{q}}_k$ is the response amplitude for the kth DOF.

A_{jk} :   Added mass in the jth DOF due to unit motion in the kth direction
C_{jk} :   Damping in the jth DOF due to unit velocity in the kth direction
$\overline{\mathbf{q}}_k$:   Response amplitude for the kth DOF

Determination of Radiation Coefficients

For the rigid body with 6-DOFs, there are 36 coefficients for the 6×6 matrices of A_{jk} and C_{jk}. Because of symmetries many of the coupling terms are zero. A complete list of non-zero terms is given in Ref [59] from where for the heave motion i.e. $j = 2$, we have:

$$A_{22} = \int a_{22}dx \qquad C_{22} = \int c_{22}dx \qquad\qquad (13.15)$$

where

A_{22} : Added mass coefficient for entire ship for unit acceleration in vertical direction

a_{22} : Added mass coefficient for section of length dx for unit acceleration in vertical direction

C_{22} : Damping coefficient for entire ship for unit velocity in vertical direction

c_{22} : Damping coefficient for section of length dx for unit velocity in vertical direction

In each term, the integration is carried over the ship length l along x direction. The integrands come from 2D sectional properties for which well known *2D Strip Theory* Ref [76]. In strip theory the sectional forces are calculated using 2D *Velocity Potentials* i.e. along $y - z$ plane.

13.5.2   Incident Wave Forces

These forces are also known as *Froude-Krylov* forces. They are the forces due to fluid particle motions acting over the hull surface but considering hull to be absent. Hence, the fluid is undisturbed by the presence of ship. The Froude-Krylov excitation force can be found by integrating the pressure given by Eq.13.9 in which the potential function Φ is Φ_I, the Incident Wave Potential. Since the flow is assumed linear, the term with $\nabla\Phi$ is dropped and the Eq. 13.8 for the force on the hull due to Incident waves becomes:

$$F_{FK} = -\rho \iint_S n_j \left(i\omega_e - U_o \frac{\partial}{\partial x} \right) \Phi_I \, ds \tag{13.16}$$

where for deep water conditions, Φ_I is:

$$\Phi_I = \frac{i\,g\,\zeta_a}{\omega_o} e^{-ik(x\cos\mu + z\sin\mu)} e^{ky} \tag{13.17}$$

Thus, the Eq.13.16 becomes:

$$F_{FK}j = -\rho \iint_S n_j \left(i\omega_e - U_o \frac{\partial}{\partial x} \right) \left(\frac{i\,g\,\zeta_a}{\omega_o} e^{-ik(x\cos\mu + z\sin\mu)} e^{ky} \right) ds$$

$$\approx +\rho\,g\,\zeta_a \int_L dx\, e^{-ik\,x\cos\mu} + \int_{Cx} \hat{n}_j\, e^{-kz\sin\mu} e^{ky}\, dl \tag{13.18}$$

In Eq.13.18, the line integral gives the sectional Froude-Krylov force. Representing it by $f_j(x)$ where j is the DOF number:

$$f_j(x) = -\rho\,g\,\zeta_a \int_{Cx} N_j\, e^{-kz\sin\mu} e^{ky}\, dl \qquad j = 1, 2, 3, 4 \tag{13.19}$$

Hence,

$$F_{FKj} = \int_L e^{-ik\,x\cos\mu}\, f_j(x)\, dx \qquad j = 1, 2, 3, 4$$

$$F_{FK5} = -\int_L e^{-ik\,x\cos\mu}\, x f_3(x)\, dx \tag{13.20}$$

$$F_{FK6} = \int_L e^{-ik\,x\cos\mu}\, x f_2(x)\, dx$$

In the above equations the term e^{ky} indicates the hyperbolic variation of amplitudes along the depth (along y-axis). At any given depth from free surface, the force is

function of time t as well as the wave period k. The wave amplitude is represented as ζ_a. The term N_j are the unit normals for sections for the jth force in DOF. The expressions for unit normals for modes along the six DOF are given as follows:

$$N_1 = \partial b/\partial x \Big/ \sqrt{1 + (\partial b/\partial y)^2}$$

$$N_2 = \partial b/\partial y \Big/ \sqrt{1 + (\partial b/\partial y)^2}$$

$$N_3 = \pm 1 \Big/ \sqrt{1 + (\partial b/\partial y)^2}$$

$$N_4 = \left(z\frac{b}{y} + y \right) \Big/ \sqrt{1 + (\partial b/\partial y)^2}$$

$$N_5 = +x\, N_3$$

$$N_6 = -x\, N_2$$

(13.21)

where $z = \pm b$ is the equation of hull section contour and $b = b(x,y)$ is half beam with $x - y$ plane being the plane of Star-Port symmetry.

13.5.3 Diffraction Wave Force

These are the wave forces that result from the diffraction of waves that strike the ship. They complement the Froude-Krylov forces as together the pair of these forces are called *Excitation Forces*. For large vessels, or small wave lengths, the diffraction component constitutes significant proportion of the excitation forces. The velocity potential is represented by Φ_D and requires boundary conditions similar to those of radiation potential Φ_R. Although, the potential Φ_D is difficult to solve, the diffraction excitation forces are determined employing only the potentials Φ_R and Φ_j and this method is known as *Haskind Relations*. Like Froude-Krylov force problem, the expressions are reduced to 2D sectional equations involving sectional potential functions ψ_j and unit normals N_j (given above in Eq. 13.21). Defining sectional diffraction force function as $h_j(x)$ as:

$$h_j(x) = \rho\, \zeta_a\, \omega_o \int_{Cx} (iN_2 \,+\, N_1 \cos\mu \,+\, N_3 \sin\mu) \times\, e^{ikz\sin\mu}\, e^{ky}\, \psi_j(y,z)\, dl \qquad j = 1,2,3,4$$

(13.22)

Total diffraction force is obtained by integrating the sectional diffraction force over the ship length. Thus for each of the six DOF modes, we have:

$$F_j^D = \int_L e^{-ikx\cos\mu}\, h_j(x)dx \qquad\qquad j = 1, 2, 3, 4$$

$$F_5^D = +\int_L e^{-ikx\cos\mu}\left(x + \frac{U_o}{i\omega_e}\right) h_3(x)dx$$

$$F_6^D = +\int_L e^{-ikx\cos\mu}\left(x + \frac{U_o}{i\omega_e}\right) h_2(x)dx$$

(13.23)

For the case of head seas (i.e. $\mu = 180\,\mathrm{deg}$), the sectional diffraction force for heave (DOF=j=2) becomes

$$h_3(x) = \rho\,\zeta_a\,\omega_o \int_{Cx} (iN_2 + N_1)\, e^{kz}\, \psi_2(y, z)\, dl$$

(13.24)

Chapter 14

Verification Model for Dynamic Sea Loads

14.1   Introduction

The dynamics of ship motion are governed by Equation of Motion 13.1 as given in previous chapter. As stated earlier, the fluid forces due to motion are of three types; *Incident Wave* Forces, *Diffraction Wave* Forces and *Radiation Wave* Forces. These forces for a simplified geometry are obtained and applied onto the submerged part of the hull as external forces. The response of the vessel will be the main outcome of the analyses. All the analyses involve ship modelled as a rigid body and hence serge, sway, heave, roll, pitch and yaw are the only DOFs.

   As an example a box-like vessel has been chosen to study the dynamic characteristics involving hydrodynamic damping and added mass. The vessel has been referenced from [94] and is of prismatic shape with a rectangular transverse section of size 0.4 m × 0.4 m. The vessel length is 4.19 m.

   Unlike typical spring-mass-damper system where the damping and mass coefficients can be constant, for oscillating vessel, the added mass and damping are functions of oscillation frequency. Ref [94] gives frequency dependent variation of added mass and hydrodynamic damping coefficients for various cylinders with circular, rectangular, wedge shaped sections. Figure 14.4 shows the plot sectional added mass a_{22} and sectional damping c_{22} for the chosen box-like vessel studied by Vught [94]. The two plots are normalized and denoted by a_{33} for sectional added mass and sectional damping b_{33} respectively. The plots consider the damping and added mass forces only in a

2D plane transverse to the vessel's longitudinal axis. Strip theory is then required to integrate all the sectional forces to obtain the total damping and added mass force.

14.1.1   Hydrodynamic Damping and Added Mass

Radiation wave loads on a floating structure are result of waves that radiate radially outwards from the structure owing to the oscillatory motions of platform in otherwise still water. As explained in section 13.5.1 the wave radiation forces typically comprise of those acting in phase with acceleration $\ddot{\mathbf{q}}$ namely the *Added Mass* and others out-of-phase with velocity $\dot{\mathbf{q}}$ namely the *Hydrodynamic Damping*. They are written as follows:

$$\mathbf{F}_{\mathrm{r}j} = \sum_{k=1}^{6} (\omega_e^2 A_{jk} - i\omega_e C_{jk})\overline{\mathbf{q}}_k e^{i\omega_e t} \qquad j = 1, 2, ..., 6 \qquad (14.1)$$

where,

A_{jk} : Added mass in the jth DOF due to unit motion in the kth direction

C_{jk} : Damping in the jth DOF due to unit velocity in the kth direction

$\overline{\mathbf{q}}_k$: Response amplitude for the kth DOF

For the present box-like model, the values of added mass and damping coefficients have been obtained using the plots provided by Vught [94] and ANSYS AQWA Workbench. The problem is solved in frequency domain after which frequency dependent plots of damping and added mass coefficients are obtained against frequency of oscillations. The values depend on the transverse section geometry and Vught [94] gives similar plots for other sectional forms.

The curves for radiation coefficients are obtained by solving the dynamic problem in frequency domain. For present analysis, the problem was required to be solved in time domain. Therefore, the radiation coefficients from Fig.14.4 need be transformed into time dependent values. Equation of motion in time dependent coefficients is obtained from Cummins [29] and is written as follows:

$$(M + A)\ddot{x} + \int_0^t k(\tau)\dot{x}(t - \tau)d\tau + K(t)x = F(t) \qquad (14.2)$$

where K is the hydrostatic spring constant. The terms $A\ddot{x}$ and $\int_0^t k(\tau)\dot{x}(t - \tau)d\tau$ in the above equation can be combined and called Radiation Force F_{Rad}:

$$F_{Rad} = -A(\omega)\ddot{x}(t) - B(\omega)\dot{x}(t) = -M_A\ddot{x}(t) - \int_0^t k(\tau)\dot{x}(t-\tau)d\tau \qquad (14.3)$$

where $A(\omega)$ and $B(\omega)$ are the respectively the added mass and damping coefficients in frequency domain. The term M_A is $A(\omega)$ at $\omega = \infty$. The term $k(t)$ is defined as *Retardation Function* or *Kernel* of the wave radiation. Retardation function $k(t)$ can be obtained by integrating $B(\omega)$ over entire frequency range as follows:

$$k(t) = \frac{2}{\pi} \int_0^\infty B(\omega) \cos(\omega t)d\omega \qquad (14.4)$$

This means that at any time (t), the function $k(t)$ is the integral of all frequencies in range. For the box-like vessel for which damping function $B(\omega)$ comes from Fig.14.1, the retardation function is plotted in Fig.14.2.

The damping force comes from the convolution integral that is the product of retardation function and system's velocity. The use of convolution results in so-called memory effect. Mathematically, we can write damping force as memory Force that *remembers* history of oscillations till the current time τ.
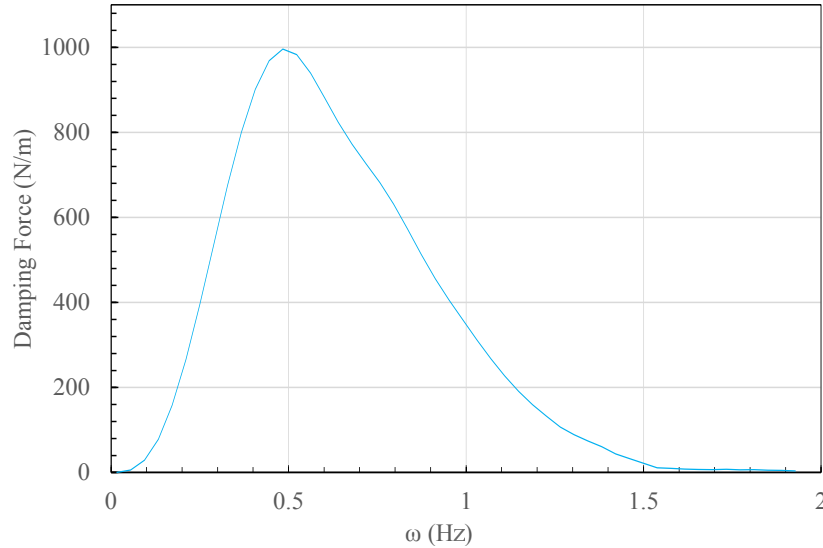
Figure 14.1 Heave damping force vs heave oscillation frequency for 4.19 m long vessel (Plot obtained after removing non-dimensionalization of Fig.14.4a)

14.1.2   Mass Properties of the Model

The model details are mentioned in Ref.[94] which has the following properties:
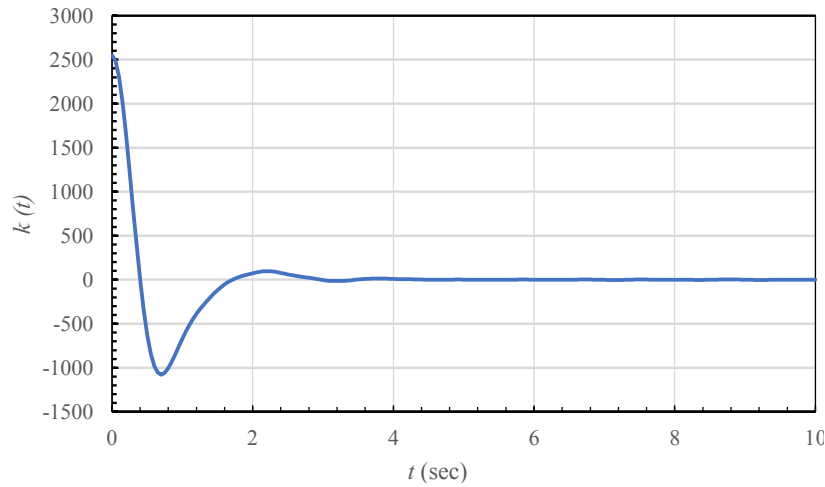
Figure 14.2 Retardation function $k(t)$ for the box-like vessel for heave DOF

Length,	$L =$	4.19 m
Breadth,	$B =$	0.4 m
Draught,	$T =$	0.2 m
B/T ratio,	$L =$	2 m
Immersed sectional area,	$A =$	0.08 m ^{2}
Displacement,	$\Delta =$	343.26 kg

14.2   Results and Discussion

The hydrostatic and hydrodynamic analysis of the vessel model of [94] were performed using present CUF and ANSYS Workbench models. In both the models, the vessel was assumed as rigid body with 6-DOFs. For the hydrodynamic analysis, only vertical (Heave) DOF was analysed and results are presented in the following. The present CUF model is oriented in a way that vertical axis perpendicular to the water surface is global y-axis while the x-z plane is parallel to the water plan area. Thus, the vessel is modelled as a beam with beam length along y-axis.

14.2.1   Hydrostatic Results

Table 14.1 Hydrostatic Results of the box-like model

	ANSYS AQWA WB	Present (CUF)	Units
Hydrostatic Stiffness in Heave DOF	16846.883	16852.599	N/m
Waterplan Area	1.676	1.676	m^2
Center of Gravity	0,0,0	0,0,0	m
Center of Buoyancy	0,0,-0.1	0,-0.1,0	m
Draught	-0.2	-0.2	m

14.2.2 Hydrodynamic Results

Hydrodynamic results presented in this section include the effect of Radiation Coefficients of Added Mass and Hydrodynamic Damping. The scope was limited only to vertical DOF (Heave) oscillations. The Added Mass is the addition of mass to the mass matrix. The additional mass taken here was value of $A(\omega)$ at $\omega = \infty$ which was obtained from Fig.14.4a ($A_\infty = 400$ kg).

Hydrodynamic damping was considered like an external force regarded here as $\mathbf{F}_{Rad}$. The force is obtained through a convolution integral introduced earlier in Eq.14.3. For a time step of size dt and frequency step size of $d\omega$, the integrals in Eqs.14.2 and 14.4 are written as summation as follows:

$$k(t) = \frac{2}{\pi} \sum_{j=1}^{N} B(\omega_j) \cos(\omega_j t)(\omega_{j+1} - \omega_j) \tag{14.5}$$

$$F_{Memory} = \sum_{i=1}^{M} \sum_{j=1}^{i} k(\tau_j)\dot{x}_j(t_i - \tau_j)(\tau_{j+1} - \tau_j) \tag{14.6}$$

The time integration in the above Eq.14.6 is implemented through Newmark time integration scheme. At each time step, current damping force includes contribution from previous time steps by employing all previous velocities. This contribution spans only for the time for which the retardation function $k(t)$ lasts. Hence, the Eq.14.6 has two summation loops; outer one ranging from t=0 to total simulation time and the inner one spanning for the length of retardation function.
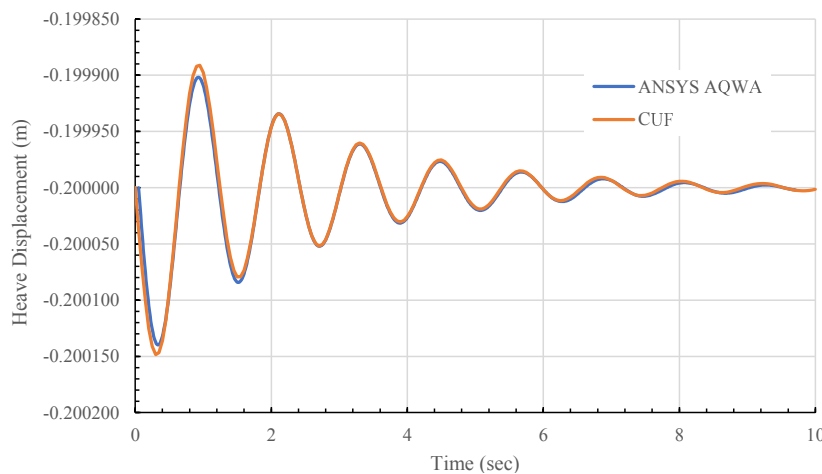
Figure 14.3 Time decaying heave oscillations obtained through ANSYS AQWA and CUF Model

Figure 14.3 is the result of the two simulations run in ANSYS AQWA Worbench and CUF model. The plots are the heave responses triggered by imparting an initial velocity (=-0.0075 m/s) to the vessel. The vessel was initially in equilibrium depth of -0.2 m from still water line. The two plots sufficiently match implying the correctness of the procedure adopted using CUF model. The total damping force is distributed on all keel nodes by applying per unit area damping force on the area of the 9-noded panels and distributing the panel force among nodes.
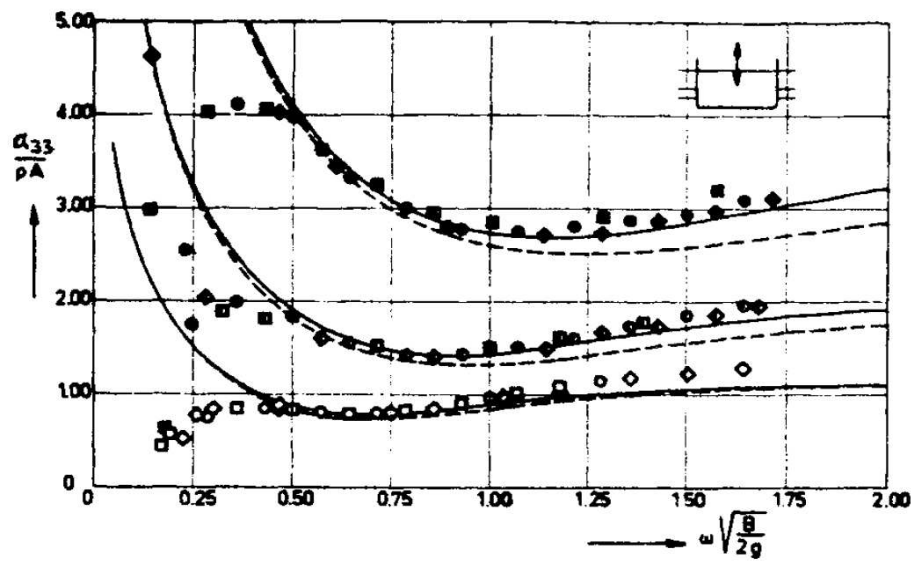
(a) Added mass versus frequency
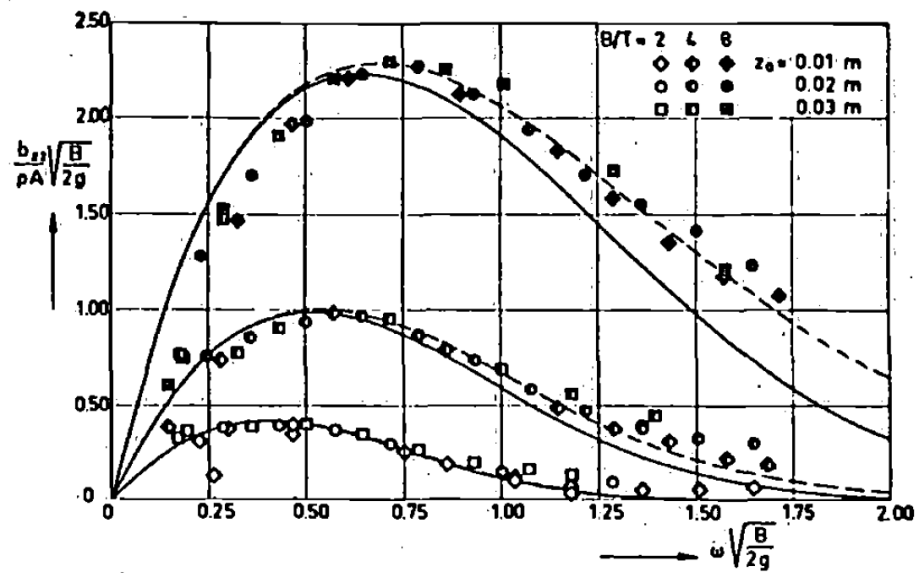
(b) Hydrodynamic damping versus frequency

Figure 14.4 Rectangular sectional added mass and damping coefficients in heave [94]

Chapter 15

CW Model for a Composite Boat

15.1   Introduction

This chapter demonstrates the capability of present CW model to capture the deflections in a composite boat under mechanical loading. For this purpose, a simplified boat has been modelled as a beam and a static analysis was performed with beam length aligned vertically to the waterplan area. Figure 15.1 shows the basic geometric configuration.
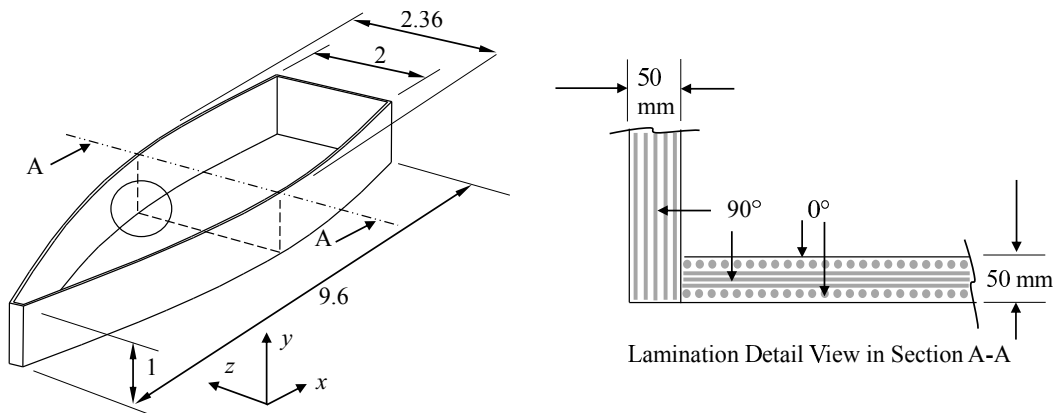
Figure 15.1 Boat dimensions in meters and composite lamination scheme

15.1.1   Material Properties and Lamination Details

The lamination details as shown in schematic Fig.15.1 are given in detail in Table 15.1 and the orthotropic material properties of Unidirectional Carbon/Epoxy layers are given in Table 15.2:

Table 15.1 Lamination details

	Lamination	Thickness per layer	Material
Floor	[0/90/0]	16.6667 mm	Unidirectional Carbon/Epoxy
All walls	[90]	50 mm	Unidirectional Carbon/Epoxy

Table 15.2 Material properties of Unidirectional Carbon/Epoxy layer

$E_{11} = 138$ GPa	$E_{22} = 8.28$ GPa	$E_{33} = 8.28$ GPa
$\nu_{12} = 0.33$ GPa	$\nu_{23} = 0.0198$	$\nu_{13} = 0.33$
$G_{12} = 6.9$ GPa	$G_{23} = 6.9$ GPa	$G_{13} = 6.9$ GPa
	Density $= 1900$ kg/m^2	

15.1.2   Meshing Details

The 3D configuration of the boat comprises of 8 B3 Lagrange beam elements aligned along y-axis. Utilizing Component-Wise Model, two types of cross sections have been employed. Both section types are meshed with L9 Lagrange elements. Starting from bottom, the floor has been meshed with 48 L9 elements. This section type holds for first 6 B3 beam elements. Next 2 Beam elements comprise of 24 L9 elements. The first section type has 221 Lagrange nodes and second one has 144 nodes. Total DOFs are 3449.

The ANSYS mesh is comprised of Shell-99 elements which are 9 noded and each node has 6 DOFs. The DOFs of the ANSYS model are 42783.

15.1.3   Boundary Conditions and Loading

The boat is assumed to be simply supported on four bottom corners. The loading is only through the self weight which is 36624.04 N.

15.2 Results and Discussion

The first results presented are the vertical deflection plots. For CW model, the vertical deflection is along y-axis and for ANSYS model, it is along z-axis. The origin for the CW model lies at mid point of rear edge of floor. x-axis is along the length of the boat. The two deflections are shown in Fig.15.2. It is seen that the two deflections closely match validating the procedure adopted using CW model.
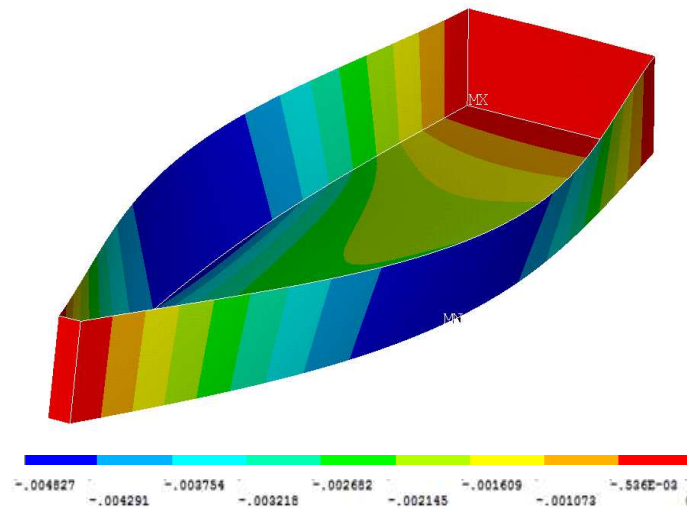
(a) ANSYS Model
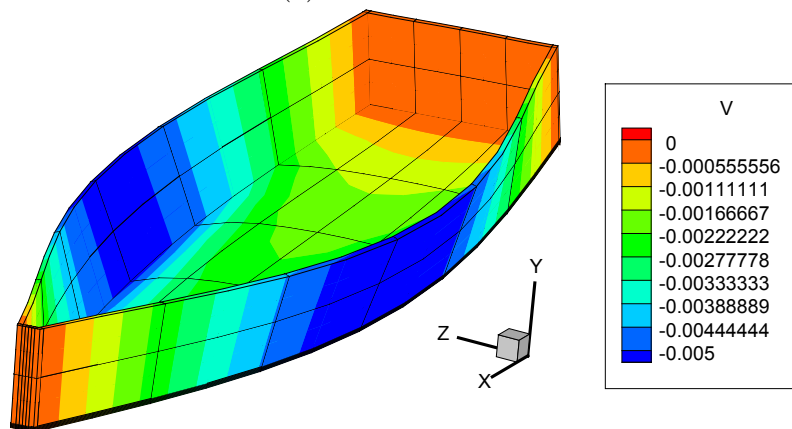
(b) CW Model

Figure 15.2 Vertical deflection plots of composite boat

Next, the stress components in top and bottom surfaces of the floor are listed in Table 15.3 for both the ANSYS and CW models at location $X = 3.17634$ m, $Y = Z = 0$ (bottom) and $X = 3.17634$ m, $Y = 0.05$ m and $Z = 0$ (top). It is noted

that the displacements are continuous across element interfaces but stresses are not and ANSYS takes the average values at nodes.

Table 15.3 Stress components at locations bottom and top on the floor (Components written for ANSYS are along CW model coordinate axes)

	Model (DOFs)	Stresses (MPa)					
		σ_{xx}	σ_{yy}	σ_{zz}	σ_{xy}	σ_{xz}	σ_{yz}
Bottom	CW (3449)	0.5371	0.0734	-0.3208	0.0219	0.0000	0.0000
	ANSYS (42783)	0.4208	0.0000	-0.3032	0.0000	0.0000	0.0000
Top	CW (3449)	0.4015	-0.07168	0.3653	0.02353	0.0000	0.0000
	ANSYS (42783)	0.2255	0.0000	0.3356	0.0000	0.0000	0.0000

Chapter 16

Conclusions

The main advantage of Carrera Unified Formulation (CUF) manifested itself through the Component Wise approach and this paved the way for the advancements such as present work. The CW models have displacements DOFs of nodes that are spatially distributed in the entire structure much like a 3D solid mesh. The global structural behaviour of marine vessels required special boundary conditions to afford us with accurate and realistic results. The buoyancy springs are attached to particular DOFs on the structural mesh. Corresponding to those DOFs, a nodal hydrostatic stiffness is obtained by multiplying foundation modulus of water with the nodal share of the area over which it acts. Finally, a global hydrostatic stiffness matrix is obtained.

Present work included two approaches to model hull. In the first approach, the hull is considered a horizontal beam with beam sections representing transverse hull sections. This model is length-wise prismatic and the transverse sections can take any arbitrary shape. These models were termed as *Hull Beam Model*. Through the results it was demonstrated that the approach captured displacements with sufficient accuracy in its comparison with both analytical and commercial codes.

In the second approach, the hull is modelled as a vertical beam, that is, beam length is along ship height. The first beam section is the submerged keel area which can take an arbitrary shape. The model is prismatic height-wise. These models are termed as *Hull Planform Model*. The thesis includes the validated results for these models through comparison with published work and commercial codes.

Attaching buoyancy springs have had previously been employed with 3D solid element meshes. Those FEM meshes have always been computationally heavy and therefore the computational advantage of CUF was needed to be exploited involving complex geometries such as realistic ship hulls. The CW approach allows attachment

of 1D springs to the physical nodes distributed three dimensionally much like the way one would attach them to a mesh of solid elements.

The buoyancy springs act like elastic foundations which are dealt in problems of beams on elastic foundation. One such problem was chosen from literature as the first validation case for the present approach of attaching numerous 1D linear spring. The beam displacements closely matched the analytical results with a well rounded convergence behaviour.

Having gained the confidence, various submerged cross section geometries were considered as validation cases. Those shapes involved inclined and curved hull surfaces. It was observed that the simply using the graphical projection of the submerged faces onto the free water surface does not give correct solution. A special procedure was employed whereby an equivalent transverse rectangle was introduced which had the same area as that of the actual submerged transverse geometry. This provided a new Water Plan Area which lead to the correct buoyancy spring constant and thereby a correct solution for hulls with slanted or curved faces.

The procedure to determine the spring constant of buoyancy springs involved an iteration loop which starts by an assumed draught depth. This approach resembles the way a typical vessel is physically lowered into the water until it stabilizes at equilibrium. The converged final equilibrium position of the vessel obtained through the CW model was accurately close to the analytical solution and thus the present approach was validated.

It was learnt from the literature that a vessel under the global equilibrium of buoyancy and weight experiences a net load distribution spread across the vessel area. Considering vessel divided into sections, the buoyancy and weight are not necessarily balanced section-wise and the local net force varyingly may act upward or downward. Modeled by classic beam theories, this variation is considered only length-wise. However, in present CW model, the variation is addressed over the entire area of the submerged geometry. This results in less stiffened regions displacing upward owing to the buoyancy in contrast to the stiffened and the heavy portions which displace downward. Thus, the final result is a three dimensional and realistic deformed shape of a hull which otherwise was possible only through the heavy mesh of 3D solid elements of a commercial software.

The accuracy of present model has also been demonstrated for the dynamic analyses. A structural modal analysis of a realistic boat geometry was performed and rigid body modes of heave, pitch and roll were obtained which closely matched the analytical solutions. Using present model, the dynamic response of an aircraft carrier

subjected to moving load of an aircraft was analysed. The analyses were performed for different aircraft velocities which resulted in the different response frequencies. In all cases, the results closely matched the published ones.

The hydrodynamic behaviour of a floating vessel was also analysed. The hydrodynamic loads comprised of Radiation Loads which have two components, viz. hydrodynamic damping and added mass. The hydrodynamic damping force was obtained in time domain with *memory effect*. The force in time domain was obtained after its conversion from frequency domain which was obtained from damping vs frequency plots. The decaying oscillation plot was compared with that of commercial software.

The capability of present model is fairly established through the above mentioned scenarios that cover both the static and dynamic regimes for hull structures.

16.1 Further Work

Having obtained confidence in the efficacy of present model in capturing structural response of hulls, certain areas are foreseen as further work. In Part-I of the thesis, complex hull geometries were modelled having walls inclined at 3D angles. Those hulls were analysed *in vacuo*. The Part-II where hulls were analysed with hydrostatic and hydrodynamic loads, included hulls that were prismatic in configuration. As an extension of the work, hulls with three dimensionally oriented walls may be analysed in presence of hydrostatic and hydrodynamic loads.

Another area for future work can be the extension of work in chapter 13. Present study was limited to the ship modelled as rigid body with vertical oscillations in which all the bottom submerged nodes had an *in-phase* vertical motion. In the extended study, the ship may be considered divided into slices called *strips*. The ship may be considered as a rigid body and pitching or rolling oscillatory behaviour be captured. In that case, the vertical motion of submerged nodes will be $out-of-phase$ along the length. Each strip will observe a gross vertical deflection with a local vertical velocity. This local velocity will produce local damping contribution. Similarly, the same strip approach can be extended to the more general case of flexible vessels. In any deflected configuration, the strips will have their local velocity component and hence the *strip wise* damping force acting corresponding to the velocity of the strip.

Bibliography

[1] American Bureau of Shipping (2014). Guidance notes on safehull finite element analysis of hull structures. Technical report.

[2] Association, J. S. R. (1999). Investigation into structural safety of aged ships, report of no. 74 rule and regulation panel. Technical Report 74.

[3] Bathe, K. J. (1996). *Finite element procedure*. Prentice hall, United States of America.

[4] Biran, A. and López-Pulido, R. (2013). *Ship Hydrostatics and Stability*. Butterworth-Heinemann, 2nd edition.

[5] Bishop, R. E. D.; Price, W. G. T. P. (1980). Antisymmetric vibration of ship hulls. *Transactions, Royal Institution of Naval Architecture*, 122:209–226.

[6] Budynas, W. C. Y. R. G. (2002). *Roark's Formulas for Stress and Strain*. McGraw-Hill, United States of America.

[7] Carrera, E. (2002). Theories and finite elements for multilayered, anisotropic, composite plates and shells. *Archives of Computational Methods in Engineering*, 9:87–140.

[8] Carrera, E. (2003). Theories and finite elements for multilayered plates and shells:a unified compact formulation with numerical assessment and benchmarking. *Archives of Computational Methods in Engineering*, 10:215–296.

[9] Carrera, E., Cinefra, M., Petrolo, M., and Zappino, E. (2014). *Finite Element Analysis of Structures through Unified Formulation*. John Wiley & Sons, United Kingdom.

[10] Carrera, E. and Giunta, G. (2010). Refined beam theories based on a unified formulation. *International Journal of Applied Mechanics*, 02:117–143.

[11] Carrera, E., Giunta, G., Nali, P., and Petrolo, M. (2010). Refined beam elements with arbitrary cross-section geometries. *Computers & Structures*, 88:283–293.

[12] Carrera, E., Giunta, G., and Petrolo, M. (2011a). *Beam Structures: Classical and Advanced Theories*. John Wiley & Sons, United Kingdom. DOI: 10.1002/9781119978565.

[13] Carrera, E. and Pagani, A. (2014). Free vibration analysis of civil engineering structures by component-wise models. *Journal of Sound and Vibration*, 333:4597–4620.

[14] Carrera, E., Pagani, A., and Jamshed, R. (2015a). Refined beam finite element to analyse hull structures. In *International Conference on Lightweight Design of Marine Structures, LIMAS-2015*, Glasgow, United Kingdom.

[15] Carrera, E., Pagani, A., and Jamshed, R. (2016). Refined beam finite elements for static and dynamic analysis of hull structures. *Computers & Structures*, 167:37–49.

[16] Carrera, E., Pagani, A., and Petrolo, M. (2013a). Classical, refined and component-wise theories for static analysis of reinforced-shell wing structures. *AIAA Journal*, 51:1255–1268.

[17] Carrera, E., Pagani, A., and Petrolo, M. (2013b). Component-wise method applied to vibration of wing structures. *Journal of Applied Mechanics*, 80:041012.

[18] Carrera, E., Pagani, A., and Petrolo, M. (2015b). Refined 1d finite elements for the analysis of secondary, primary, and complete civil engineering structures. *Journal of Structural Engineering*, 141:04014123.

[19] Carrera, E., Pagani, A., Petrolo, M., and Zappino, E. (2012). A component-wise approach in structural analysis. *Computational Methods for Engineering Science*, pages 75–115.

[20] Carrera, E. and Petrolo, M. (2012a). Refined beam elements with only displacement variables and plate/shell capabilities. *Meccanica*, 47:537–556.

[21] Carrera, E. and Petrolo, M. (2012b). Refined one-dimensional formulations for laminated structure analysis. *AIAA Journal*, 50:176–189.

[22] Carrera, E., Petrolo, M., and Nali, P. (2011b). Unified formulation applied to free vibrations finite element analysis of beams with arbitrary section. *Shock and Vibrations*, 18:485–502.

[23] Carrera, E. and Zappino, E. (2015). Carrera unified formulation for free-vibration analysis of aircraft structures. *AIAA Journal*, pages 1–13. DOI: 10.2514/1.J054265.

[24] Catapano, A., Giunta, G., Belouettar, S., and Carrera, E. (2011). Static analysis of laminated beams via a unified formulation. *Composite Structures*, 94:75–83.

[25] Chakrabarti, P., Joshi, S. P., and Maiti, M. K. (2000). Pull-down analysis of jack-up rigs. *ASME 2007 26th International Conference on Offshore Mechanics and Arctic Engineering*, 1:77–83.

[26] chao Qiu, L. (2007). Numerical simulation of transient hydroelastic response of a floating beam induced by landing loads. *Applied Ocean Research*, 29(3):91–98. DOI: 10.1016/j.apor.2007.11.001.

[27] Cowper, G. R. (1966). The shear coefficient in timoshenko's beam theory. *Journal of Applied Mechanics*, 33:335–340.

[28] CS, S. (1977). Influence of local compressive failure on ultimate longitudinal strength of a ship's hull. In *Proc. int. symp. on practical design in shipbuilding*, pages 73–9.

[29] Cummins, W. (1962). The impulse response function and ship motions.

[30] Dong, S. B., Alpdongan, C., and Taciroglu, E. (2010). Much ado about shear correction factors in timoshenko beam theory. *International Journal of Solids and Structures*, 47:1651–1665.

[31] Euler, L. (1744). *De curvis elasticis*. Lausanne and Geneva: Bousquet. (English translation: W. A. Oldfather, C. A. Elvis, D. M. Brown, Leonhard Euler's elastic curves, Isis 20 (1933) 72–160).

[32] Faltinsen, O. (1993). *Sea Loads on Ships and Offshore Structures (Cambridge Ocean Technology Series)*. Cambridge University Press.

[33] Fatmi, R. E. (2007a). Non-uniform warping including the effects of torsion and shear forces. part i: A general beam theory. *International Journal of Solids and Structures*, 44:5912–5929.

[34] Fatmi, R. E. (2007b). Non-uniform warping including the effects of torsion and shear forces. part ii: Analytical and numerical applications. *International Journal of Solids and Structures*, 44:5930–5952.

[35] FJ, G. (1809). Theorien der wellen. *Ann. Phys.*, 32:412–440.

[36] Giunta, G., Biscani, F., Belouettar, S., and Carrera, E. (2011). Analysis of thin-walled beams via a one-dimensional unified formulation through a navier-type solution. *International Journal of Applied Mechanics*, 03:407–434.

[37] Gunnlaugsson, A. G. and Pedersen, P. T. (1982). A finite element formulation for beams with thin-walled cross-sections. *Computers & Structures*, 15:691–699.

[38] Hetenyi, M. (1946). *Beams on Elastic Foundation: Theory with Applications in the Fields of Civil and Mechanical Engineering*. University of Michigan Press.

[39] Hutchinson, J. R. (2001). Shear coefficients for Timoshenko beam theory. *Journal of Applied Mechanics*, 68:87–92.

[40] I., S. (1990). *Ship Vibrations. Part 2*. University of Zagreb.

[41] I., S. and Grubisic, R. (1979). Coupled horizontal and torsional vibration of ship hull with large openings. In *Proceedings, Euromech Col. 122, Numerical Analysis of the Dynamics of Ship Structures, ATMA*, Paris.

[42] I., S., I, C., and S., T. (2007). Coupled flexural and torsional vibrations of ship-like girders. *Thin-Walled Structures*, 45:1002–1021.

[43] I., S. and Y., F. (1993). A finite element formulation of initial ship cross-section properties. *Brodogradnja*, 41:27–36.

[44] J, V. (1958). Lessons learnt from full-scale ship structural test. *SNAME Trans*, 66:165–243.

[45] JB, C. (1965). Ultimate longitudinal strength. *Trans Roy Inst Naval Architect*, 107:411–30.

[46] Jensen, J. (1983). On the shear coefficient in timoshenko's beam theory. *Journal of Sound and Vibration*, 87:621–635.

[47] Jensen, J. (2001). *Load and Global Response of Ships*. Elsevier, United Kingdom.

[48] Jer-Fang, W., Wang, S., Liao, M., and Basu, R. (2006). On the vibration analysis of large commercial vessels. In *The Sixteenth International Offshore and Polar Engineering Conference*, San Francisco, California, USA. International Society of Offshore and Polar Engineers. ID ISOPE-I-06-196.

[49] jun Chen, X., sheng Wu, Y., cheng Cui, W., and Jensen, J. J. (1961). Thin-walled elastic beams. *National Science Foundation*.

[50] Kaneko, T. (1975). On Timoshenko's correction for shear in vibrating beams. *Journal of Physics D: Applied Physics*, 8:1927–1936.

[51] Kapania, K. and Raciti, S. (1989a). Recent advances in analysis of laminated beams and plates, part I: Shear effects and buckling. *AIAA Journal*, 27(7):923–935.

[52] Kapania, K. and Raciti, S. (1989b). Recent advances in analysis of laminated beams and plates, part II: Vibrations and wave propagation. *AIAA Journal*, 27(7):935–946.

[53] Kashiwagi, M. (2000). A time-domain mode-expansion method for calculating transient elastic responses of a pontoon-type vlfs. *Journal of Marine Science and Technology*, 5:89–100.

[54] Kennard, E. (1955). Forced vibrations of beams and the effect of sprung masses. Technical report.

[55] Kurrer, K.-E. (2008). *The History of the Theory of Structures: From Arch Analysis to Computational Mechanics*. Wiley-VCH.

[56] Lang DW, W. W. (1952). Structural strength investigation of destroyer albuera. *Trans Inst Naval Arch*, 94:243–86.

[57] Lee, G.-H., Lee, H.-W., and Yoo, S.-W. (2004). An analysis of steel fender system for vessel collision. In *European Congress on Computational Methods in Applied Sciences and Engineering*.

[58] Lewis, E. V. (1988). *Principles of Naval Architecture (Second Revision), Volume II - Resistance, Propulsion and Vibration*. Society of Naval Architects and Marine Engineers (SNAME).

[59] Lewis, E. V. (1989). *Principles of Naval Architecture (Second Revision), Volume III - Motions in Waves and Controllability*. Society of Naval Architects and Marine Engineers (SNAME).

[60] Lubbad, R. and Løset, S. (2011). A numerical model for real-time simulation of ship–ice interaction. *Cold Regions Science and Technology*, 65(2):111–127. DOI: 10.1016/j.coldregions.2010.09.004.

[61] Misra, S. C. (2016). *Design principles of ships and marine structures.* CRC Press.

[62] MP., C. K. K. L. P. C. B. (1983). Ultimate strength of ship structures. *SNAME Trans*, 91:149–68.

[63] Muckle, W. (1975). *Naval Architecture for Marine Engineers.* Butterworth-Heinemann.

[64] Newmark, N. (1959). A Method of Computation for Structural Dynamics. *Journal of the Engineering Mechanics*, 85(7):67–94.

[65] Nguyen, T. K., Vo, T. P., , and Thai, H. T. (2013). Static and free vibration of axially loaded functionally graded beams based on the first-order shear deformation theory. *Composites Part B: Engineering*, 55:147–157.

[66] Novozhilov, V. V. (1961). *Theory of elasticity.* Pergamon, Elmsford.

[67] O, K. C. (1931). Investigation of structural characteristics of destroyers "preston" and "bruce". part i—description. *SNAME Trans*, 39:35–64.

[68] O, K. C. (1940). Investigation of structural characteristics of destroyers "preston" and "bruce". part ii—analysis of data and results. *SNAME Trans*, 48:125–72.

[69] Pagani, A., Carrera, E., , and Jamshed, R. (2016). Application of aerospace structural models to marine engineering. *Advances in Aircraft and Spacecraft Science.* In Press.

[70] Patev, D. J. G. M. T. D. G. R. C. . R. C. (2015). Determination of hurricane-induced barge impact loads on floodwalls using dynamic finite element analysis. *Engineering Structures*, 104:95–106.

[71] Pedersen, P. T. (1983). A beam model for the torsional-bending response of ship hulls. *Transactions, Royal Institution of Naval Architecture*, 125:171–182.

[72] Pedersen, P. T. (1985). Torsional response of containerships. *Journal of Ship Research*, 29:194–205.

[73] Pittaluga, A. (1978). Recent developments in the theory of thin-walled beams. *Computers & Structures*, 9:69–79.

[74] Price, R. E. D. B. W. G. (1974). On modal analysis of ship strength. *Proceedings of Royal Society of London A*, 341(1624):121–134.

[75] Price, R. E. D. B. W. G. (1975). Ship strength as a problem of structural dynamics. *The Naval Architect*, 2:61–63.

[76] Price, R. E. D. B. W. G. (1979). *Hydroelasticity of Ships.* Cambridge University Press.

[77] Reddy, J. N. (2004). *Mechanics of laminated composite plates and shells. Theory and Analysis.* CRC Press, 2nd edition.

[78] SE, R. and JB., C. (1990). Ultimate longitudinal strength of ships: a case study. *SNAME Trans*, 98:441–71.

[79] Senjanović, I., S., T., and N., V. (2009). An advanced theory of thin-walled girders with application to ship vibrations. *Marine Structures*, 22:387–437.

[80] Senjanović I, G. R. (1991). Coupled horizontal and torsional vibration of a ship hull with large hatch openings. *Computers & Structures*, 41(2):213–226.

[81] Shama, M. (2010). *Torsion and Stresses in Ships.* Springer, Germany.

[82] Sheu, J.-S. W. J.-J. (1996). An exact solution for a simplified model of the heave and pitch motions of a ship hull due to a moving load and a comparison with some experimental results. *Journal of Sound and Vibration*, 192:495–520.

[83] Sokolnikoff, I. S. (1956). *Mathematical theory of elasticity.* McGraw-Hill.

[84] Stephen, N. G. (1980). Timoshenko's shear coefficient from a beam subjected to gravity loading. *Journal of Applied Mechanics*, 47:121–127.

[85] Szabo, B. A. and Babuska, I. (1991). *Finite element analysis.* John Wiley & Sons.

[86] T., K. (1973). The application of finite element methods to ship structures. *Computers & Structures*, 3:117–594.

[87] Takabatake, H. (2015). A simplified analysis of rectangular floating plates subjected to moving loads. *Ocean Engineering*, 97(2):37–47. DOI: 10.1016/j.apor.2007.11.001.

[88] Timoshenk and P., S. (1953). *History of Strength of Materials - With a Brief Account of the History of Theory of Elasticity and Theory of Structures.* Dover Publications.

[89] Timoshenko, S. P. (1922a). On the corrections for shear of the differential equation for transverse vibrations of prismatic bars. *Philosophical Magazine*, 41:744–746.

[90] Timoshenko, S. P. (1922b). On the transverse vibrations of bars of uniform cross section. *Philosophical Magazine*, 43:125–131.

[91] Timoshenko, S. P. and Goodier, J. N. (1970). *Theory of elasticity.* McGraw-Hill.

[92] Todd, F. H. (1961). *Ship Hull Vibration.* Edward Arnold, London.

[93] Varello, A. (2013). *Advanced higher-order one-dimensional models for fuid-structure interaction analysis.* PhD Thesis, Politecnico Di Torino, Italy.

[94] Vughts, J. (1968). The Hydrodynamic Coefficients for Swaying, Heaving and Rolling Cylinders in a Free Surface. *Computers and Structures*, 15.

[95] W.G., J. (1874). On the strength of iron ship. *Trans. Inst. Naval Arch.*, 15:74–93.

[96] Wu, J.-S. and Ho, C.-S. (1987). Analysis of wave-induced horizontal-and-torsion-coupled vibrations of a ship hull. *Journal of Ship Research*, 31:235–252.

[97] Wu, J.-S. and Sheu, J.-J. (1996). An exact solution for a simplified model of the heave and pitch motions of a ship hull due to a moving load and a comparison with some experimental results. *Journal of Sound and Vibration*, 192(2):495–520. DOI: 10.1006/jsvi.1996.0200.

[98] Wu, J.-S. and Shih, P.-Y. (1998). Moving-load-induced vibrations of a moored floating bridge. *Computers & Structures*, 66(4):435–461. DOI: 10.1016/S0045-7949(97)00072-2.

[99] Y., S. I. F. (1992). A higher-order theory of thin-walled girders with application to ship structures. *Computers & Structures*, 43:31–52.

[100] Zachmanoglou, E. V. E. C. (1965). *Dynamics of vibrations*, volume 1. C.E. Merrill Books.

[101] Zhang, J., ping Miao, G., xun Liu, J., and jun Sun, W. (2008). Analytical models of floating bridges subjected by moving loads for different water depths. *Journal of Hydrodynamics Ser. B*, 20(5):537–546. DOI: 10.1016/S1001-6058(08)60092-X.

Appendix A

Component-Wise Model

What are the 'Components'

The 1D beam models in this thesis utilize the Component-Wise (CW) approach [20]. Each structural feature of a hull such as hull Walls, bulkheads, floors etc. are modeled as components. The CW models have the advantage that displacements are the only unknown variables over the beam cross section. The displacement kinematics over the cross section is approximated through 2D Lagrange Polynomials. Cross section is thus meshed with 2D Lagrange elements. CW beam mesh has solid-like appearance and thus has physical nodes much similar to 3D solid element mesh.

The given complex geometry is broken down into simpler components, each component is prismatic in nature. That is, it has a planar area of arbitrary geometry which is extruded to some height. In terms of beam model, this area is beam cross section and the height is beam length. For a component, such as hull wall, the area is the large planar area of wall and beam length is wall thickness. In other words, we have a plate modeled through 1D beam formulation. This is well visualized through Fig. A.1.

Lagrange Expansion

The CUF model in present work is referred to as Lagrange Expansion (LE) class. The beam is considered aligned with y-axis. At each beam node, the cross section is meshed with 2D elements that can have a 3-noded (L3), 4-noded (L4) or 9-noded (L9). The shape functions describing the displacements of these nodes are Lagrange func-
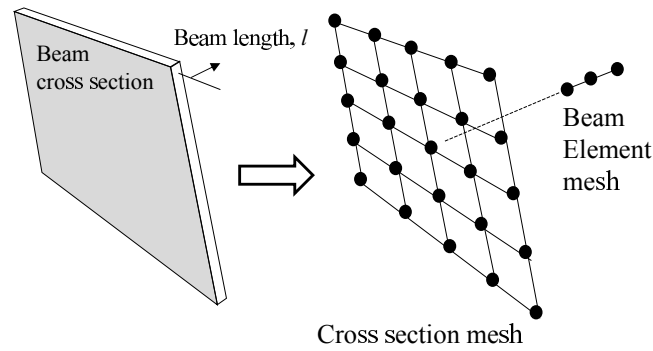
Figure A.1 A wall modelled with CW approach

tions which are isoparametric functions. These functions are interpolation functions represented as F_τ and are written in terms of cross section coordinates x and z.

An L9 element, for example, has the interpolation function as given in Eq.A.1:

$$F_\tau = \frac{1}{4}(\alpha^2 + \alpha\alpha_\tau)(\beta^2 + \beta\beta_\tau), \qquad\qquad \tau = 1, 3, 5, 7$$

$$F_\tau = \frac{1}{2}\beta_\tau{}^2(\beta^2 + \beta\beta_\tau)(1 - \alpha^2) + \frac{1}{2}\alpha_\tau{}^2(\alpha^2 + \alpha\alpha_\tau)(1 - \beta^2), \quad \tau = 2, 4, 6, 8 \qquad \text{(A.1)}$$

$$F_\tau = (1 - \alpha^2)(1 - \beta^2), \qquad\qquad \tau = 9$$

where α and β range from -1 to +1, whereas α_τ and β_τ are the coordinates of the nine points whose numbering and location in the natural coordinate frame are shown in Fig.A.2. The 3D displacement field of the beam model based on L9 polynomial is
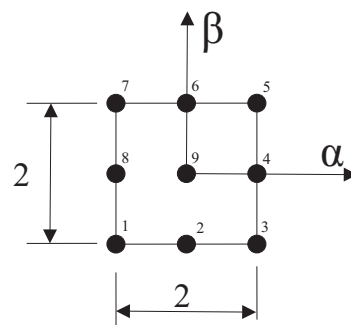

Figure A.2 L9 element in natural coordinates

given as:

$$u_x = F_1 u_{x_1} + F_2 u_{x_2} + F_3 u_{x_3} + F_4 u_{x_4} + F_5 u_{x_5} + F_6 u_{x_6} + F_7 u_{x_7} + F_8 u_{x_8} + F_9 u_{x_9}$$
$$u_y = F_1 u_{y_1} + F_2 u_{y_2} + F_3 u_{y_3} + F_4 u_{y_4} + F_5 u_{y_5} + F_6 u_{y_6} + F_7 u_{y_7} + F_8 u_{y_8} + F_9 u_{y_9}$$
$$u_z = F_1 u_{z_1} + F_2 u_{z_2} + F_3 u_{z_3} + F_4 u_{z_4} + F_5 u_{z_5} + F_6 u_{z_6} + F_7 u_{z_7} + F_8 u_{z_8} + F_9 u_{z_9}$$

$$(\text{A.2})$$

Illustrative Example

The working of CW model is explained with the help of box-like geometry as follows. Consider the box-like configuration as shown in Fig. A.4a. The given geometry is 3D with considerable complexity rendering it to be not feasible for 1D beam models employing classical beam theories. However, this configuration will be easily handled using CW 1D beam model. For the sake of clarity, Fig. A.4b shows the cross section mesh and 1D beam mesh separately. The 1D beam mesh has all elements aligned with y-axis. There are two section types assigned to the beam nodes. Each of these sections comprises of 2D Lagrange elements. These sections are shown separately in Fig. A.4. Starting with the first beam node (towards left in Fig A.4b), the beam element has the cross section in the shape of the wall (Section-1). Each node of this element has the same cross section mesh associated with it. The length of this element is the thickness of the wall. Proceeding further toward right, the second beam element has the new cross section that is assigned to all of its beam nodes. In the similar fashion, the meshing continues and every changed section manifests in the form of a new cross section mesh.
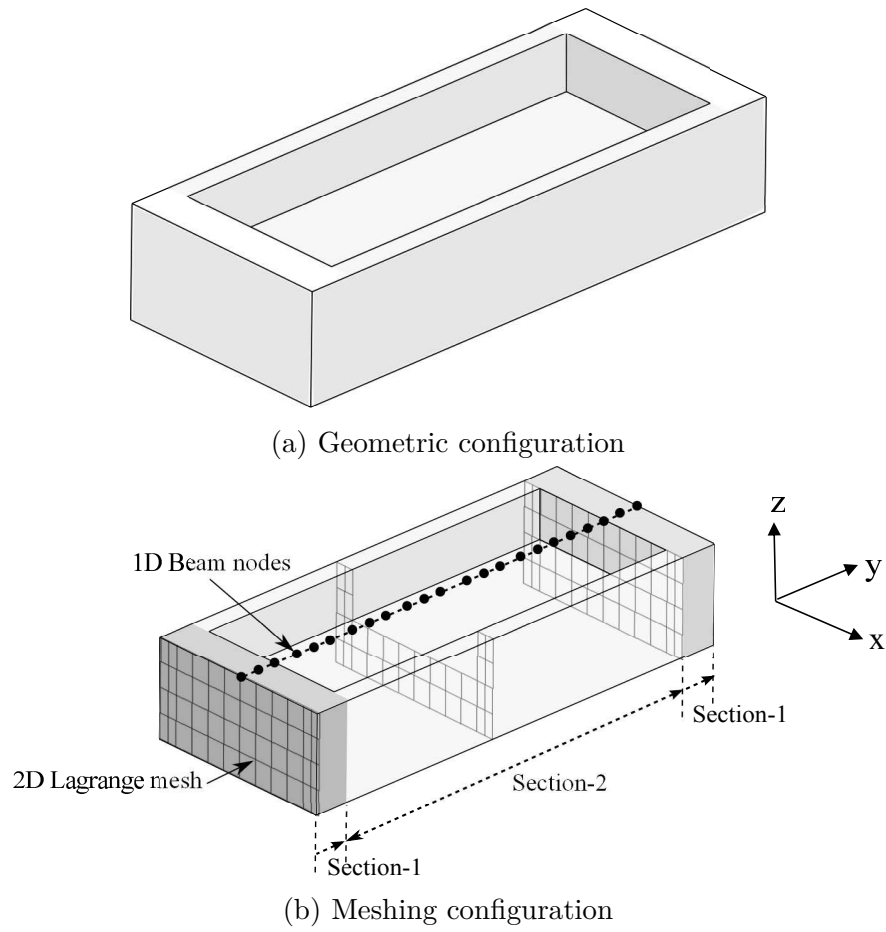
(a) Geometric configuration

(b) Meshing configuration

Figure A.3 Box-like shape for illustrative example of CW Model
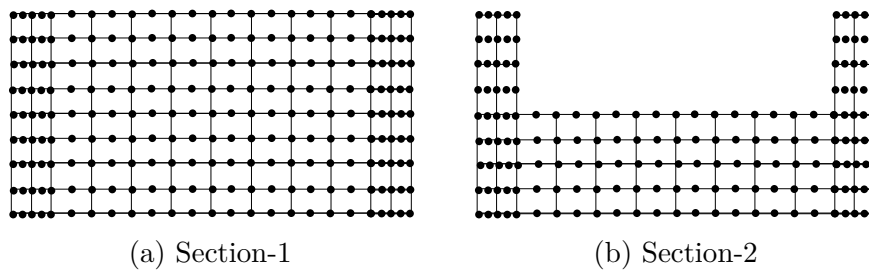

(a) Section-1   (b) Section-2

Figure A.4 2D Lagrange element mesh with two section types